Investigating the Role of Sestrin 1 and Sestrin 2 in Preclinical Models of Tuberculosis Disease

Saiyukthi Naidoo

NDXSAI009

For the Degree of Doctor of Philosophy

In Clinical Sciences and Immunology,

Department of Pathology, Faculty of Health Sciences, University of Cape Town

June 2025

Supervisor: Associate Professor Suraj P. Parihar
Co-supervisors: Dr Mumin Ozturk and Professor Frank Brombacher

Divisions of Medical Microbiology and Immunology, Institute of Infectious Diseases and Molecular Medicine (IDM), Faculty of Health Sciences, University of Cape Town, Cape Town, South Africa

DECLARATION

I, Saiyukthi Naidoo, hereby declare that the work on which this thesis is based, is my original work (except where acknowledgements indicate otherwise) and that neither the whole work nor any part of it has been, is being, or is to be submitted for another degree in this or any other university.

I empower the university to reproduce for the purpose of research either the whole or any portion of the contents in any manner whatsoever.

Date: 27 June 2025

ACKNOWLEDGMENTS

Out of all my chapters I've had to write, this has perhaps been the most difficult. How to put into words, my gratitude to every person who has played a part, not just in this PhD thesis, but in my decade long journey of arriving here. Looking back over the last 10 years, has been a roller-coaster ride, with challenges I've had to overcome and learn to live with that has shaped me not only into the scientist I am, but the person I've become.

First and foremost, I extend my sincere gratitude to my supervisors. Assoc. Prof. Suraj Parihar, thank you for providing me with the tools and environment in which to grow and learn, and for all your advice and contributions to the completion of this thesis. To Prof. Frank Brombacher, thank you for the opportunity to be a part of your lab, I will always be grateful for the skills I have learned.

To Dr. Mumin Ozturk, I have yet to meet a more insightful, patient, compassionate mentor. I am so grateful that you were part of my scholarly journey, and your constant encouragement is deeply appreciated. Thank you for teaching me everything I know, and for being such an inspiring scientist, enriching everyone around you. Your efforts do not go unnoticed, and you have been instrumental in shaping the scientist I am today. I also know that these sentiments are shared by everyone who knows you, and that's a testament to your character.

I am also indebted to my lab colleagues and friends, who showed the real meaning of teamwork. Rudy, Sibo, Shandre, Shelby, Rob, your comradery, encouragement and support are deeply appreciated, and has made the journey more memorable. I would also like to acknowledge the entire Brombacher lab for their expertise.

To Hlumani and Jackson, thank you for sparking my passion in research during my Honors program. I'm grateful for your mentorship, and continued support through my career and hold you both in high regard.

Finally, to my family and friends, thank you for your boundless love and support, I always acknowledge that this was a team effort. Your unwavering belief in my abilities has kept the fire burning in my darkest moments, through the ups and downs of this academic journey.

To Kai and Ley, my brothers, thank you for always making me laugh through everything, you have always had my back when I've needed you. You've seen me at my worst and best and love me the same regardless. So, here's to a good time and a long time, and family we would choose as friends, I am blessed with you both.

Shnee, my best friend, aunt, cousin and sister, you have been my role model since before I knew it myself. Thank you for inspiring me to reach for the the stars by living it yourself, and for always wanting the best life has to offer for me, you are enlightening. To Sabash, Uncle K, Atha and Mama, it really takes a village to raise a child, you have been a constant in my life, and you've always loved me as your own daughter.

To Akhil and Dhaval, you both have kept me sane through my struggles. Dhaval thank you for painstakingly listening and supporting me through this PhD journey. In return you have learnt about TB. Akhil, you have been the most loyal, supportive, friend I could ask for, you always know how to brighten my day, and I'm so glad I convinced you to be my friend on our very first day at UCT together 10 years ago.

Last but not least, to my parents, thank you for supporting the path I chose in life. You've given me the freedom to be exactly who I am, unapologetically, and I am so grateful for that. Dad, you've taught me how the world can be tough, and opportunities are not just given, they need to be earned. You have raised the strong charactered woman you see today. Ma, you have shown me the meaning of unconditional love. Thank you for being my sounding board, my rock, and my biggest cheerleader. Today you get to see the fruits of all your sacrifices. Everything I am I owe to you.

Thank you all for being a part of this milestone in my life.

ABBREVIATIONS

5-LOX	5-lipoxygenase
AhpD	Alkyl hydroperoxide reductase
AICAR	5-aminoimidazole-4-carboxamide ribonucleotide
ALI	Acute lung injury
ALT	Alanine transaminase
AM	Alveolar Macrophages
AMPK	Adenosine monophosphate-activated protein kinase
AP-1	Activating Protein-1
APC	Antigen Presenting Cell
ARDS	Acute respiratory distress syndrome
AST	Aspartate aminotransferase
ATP	Adenosine triphosphate
BCG	Bacillus Calmette-Guerin
BMDM	Bone Marrow-Derived Macrophages
CAGE	Cap Analysis of Gene Expression
cDNA	Complementary Deoxyribonucleic Acid
DC	Dendritic Cells
DMEM	Dulbecco's Modified Eagle Medium
DNA	Deoxyribonucleic Acid
DOTS	Directly Observed Therapy Short Course
EDTA	Ethylenediamine tetra acetic acid
ELISA	Enzyme-Linked Immunosorbent Assay
ENCODE	Encyclopedia of DNA Elements
ER	Endoplasmic reticulum
ESAT	Early Secretory Antigenic Target
FANTOM	Functional Annotation of the Mammalian genome
FBS	Fetal Bovine Serum
FDA	Food and Drug Administration
Foxo	Forkhead box, subgroup O
H&E	Hematoxylin and Eosin
HDT	Host-Directed Therapy
HIF-1α	Hypoxia-inducible factor-1α
HIV	Human Immunodeficiency Virus
HPRT	Hypoxanthine Phosphoribosyl transferase

HUVECs	Human umbilical vein endothelial cells
ICA	Icariin
IFN	Interferon
IL-	Interleukin
JNK	c-Jun N-terminal kinase
Keap1	Kelch-like ECH-associated protein 1
KO	Knockout
LM	Lipomannan
LPS	Lipopolysaccharide
LTA4H	Leukotriene A4 hydrolase
M-CSF	Macrophage colony stimulating factor
M1	Classically Activated Macrophage
M2	Alternatively Activated Macrophage
ManLAM	Mannosylated Liparabinomannan
MAPk	Mitogen-Activated Protein (MAP) Kinase
MDM	Monocyte-Derived Macrophages
MDR-TB	Multi-Drug Resistant Tuberculosis
Mincle	Macrophage inducible Ca2+-dependent lectin receptor
MMP	Matrix metalloproteinase
MOI	Multiplicity of infection
MR	Mannose Receptor
Mtb	*Mycobacterium tuberculosis*
mTOR	Mammalian target of rapamycin
NAC	N-acetyl cysteine
NADPH	Nicotinamide adenine dinucleotide phosphate
NFκB	Nuclear Factor κB
NLR	NOD-Like Receptor
NO	Nitric Oxide
Nrf2	Nuclear factor erythroid 2-related factor 2
NSAIDs	Non-steroidal anti-inflammatory drugs
OADC	Oleic acid-albumin-dextrose-catalase
PAMP	Pathogen-Associated Molecular Pattern
PBS	Phosphate Buffered Saline
PCR	Polymerase Chain Reaction
PRR	Pattern Recognition Receptors
qRT-PCR	Quantitative Real-Time Polymerase Chain Reaction
RCL	Red cell lysis

RNA	Ribonucleic Acid
ROS	Reactive Oxygen Species
SANS	South African National Standard
Sesn	Sestrin
Sesn1	Sestrin 1
Sesn2	Sestrin 2
Sesn3	Sestrin 3
SOD2	Superoxide Dismutase
SPF	Specific pathogen-free
SQSTM1	Sequestosome-1
TB	Tuberculosis
TDM	Trehalose-6,6-dimycolate
TGFβ	Transforming growth factor-beta
TLR	Toll-Like Receptors
TNF	Tumor Necrosis Factor
TSC2	Tuberous sclerosis complex 2
UCT	University of Cape Town
ULK1	Unc51-like 1
US	United States
WHO	World Health Organization
WT	Wildtype
XDR-TB	Extensive Drug Resistant Tuberculosis

CONTENTS PAGE

TABLE OF FIGURES

Figure 3.6.3:	The macrophage-specific deficiency of *Sesn1* had no effect on lung histology at a naïve state.
Figure 3.7.1:	The macrophage-specific deletion of *Sesn1* showed increased lung cell numbers at 6-weeks post infection
Figure 3.7.2:	The macrophage-specific deletion of *Sesn1* altered immune responses in the lungs after 6-weeks of *Mtb* infection.
Figure 3.7.3:	The macrophage-specific deletion of *Sesn1* showed altered immune cell recruitment in the lungs after 6-weeks of *Mtb* infection.
Figure 3.7.4:	The macrophage-specific deletion of *Sesn1* showed minor changes to immune cell populations in lymph nodes at 6-weeks post *Mtb* infection.
Figure 3.7.5:	The macrophage-specific deletion of *Sesn1* had no effect on lung pathology after 6-weeks of *Mtb* infection.
Figure 3.8.1:	The macrophage-specific *Sesn1*-deficiency showed no significant differences at 12-weeks of *Mtb* infection in mice.
Figure 3.8.2:	The macrophage-specific deletion of *Sesn1* showed altered immune responses in the lungs after 12-weeks of *Mtb* infection.
Figure 3.8.3:	The macrophage-specific deletion of *Sesn1* showed altered immune cell recruitment in the lungs after 12-weeks of *Mtb* infection.
Figure 3.8.4:	The macrophage-specific deletion of *Sesn1* showed minor changes to immune cell populations in lymph nodes after 12-weeks of *Mtb* infection.
Figure 3.8.5:	The macrophage-specific *Sesn1*-deficiency had no effect on lung pathology after 12-weeks of *Mtb* infection.
Figure 3.9.1:	*Sesn1* depletion in macrophages had no effect on mortality during TB disease in mice.
Figure 3.10.1:	*Sesn1*-deficient macrophages showed increased bacterial growth, ROS production and cell death in vitro.
Figure 3.10.2:	*Sesn1*-deficient macrophages showed increased pro-inflammatory responses in vitro.
Figure 3.10.3:	Deletion of *Sesn1* in macrophages increased total ATP production rate and glycolysis in BMDMs post infection.

ABSTRACT

Despite efforts to eradicate Tuberculosis (TB), *Mycobacterium tuberculosis (Mtb)*, a causative agent for TB, can persist, and the emergence of drug resistance, emphasizes a dire need for new effective treatments and vaccine candidates. Recent understanding of TB immunology has shown hyperinflammatory responses causing damage to lung tissue structure and function, increasing pathology and severity of disease. This has sparked a search for anti-inflammatory modulators for Host Directed Therapies (HDT) to attenuate the effects of prolonged inflammation during chronic TB and persist after the completion of the therapy. Using Cap Analysis of Gene Expression (CAGE) transcriptomics, we identified a family of genes, *Sestrins* (*Sesn 1* and *Sesn 2*), which showed differential expression after *Mtb* infection, particularly in *Sesn1* where expression was significantly reduced, alluding to a possible role of Sestrins during TB disease. Sestrins are a family of antioxidant genes that have shown anti-inflammatory and metabolic modulatory roles in various disease models including cardiomyopathy, mitochondrial dysfunction, insulin resistance, and neurodegenerative diseases. However, the potential role of these genes remains unknown in TB, and conducting infection studies would contribute novel information to the TB field. By generating *Sesn2* and macrophage-specific *Sesn1* knockout mouse models, we uncovered the role of these genes for the first time in inflammation and TB disease. Here, we have shown that the deletion of *Sesn1* (macrophage-specific) and *Sesn2* (null) mice were undistinguishable from control animals at a naïve state. During TB disease, we demonstrate that global ablation of *Sesn2* results in a significant increase in inflammation at later stage of *Mtb* infection and increased mortality. The increased inflammation was associated with enhanced total lung and lymph node cells, immune cell recruitment and lung tissue pathology. In contrast, macrophage-specific deletion of *Sesn1* had no effect on the outcome of *Mtb* infection. To understand the mechanism, we found *Sesn1*- and *Sesn2*- deficient macrophages showed increased bacterial growth, pro-inflammatory response, and higher levels of cell death. We found reactive oxygen species, known to potentiate tissue damage, are associated with Sestrin ablation. Moreover, Sestrins are closely linked to metabolic regulation, Seahorse analysis showed that the absence of *Sesn1* or *Sesn2* hinders the ability of macrophages to regulate energy metabolism in the presence of stress, with higher ATP production rate and consistent energetic state, may result in elevated ROS levels. While our findings do not directly establish ROS as the primary driver of pathology in *Sesn2* knockout mice, they suggest modulating inflammatory responses during TB disease.

CHAPTER 1: LITERATURE REVIEW

1.1. Epidemiology of Tuberculosis

Tuberculosis (TB) disease has plagued us for centuries, and barring the advent of COVID-19 remains the leading infectious cause of death globally (1). *Mycobacterium tuberculosis* (*Mtb*) is the bacterial agent responsible for TB disease prevalent in low-to-middle income countries (Figure 1.1) (2). Despite desperate attempts to eradicate TB, our efforts remain modest. Though there is no precise method to measure the latent infection rate of TB, it is estimated that *Mtb* manages to infect roughly a quarter of the world's population (3). In 2022, 10.6 million infections were recorded with 1.3 million people dying from the disease (4). Even with global organizations committing to the End TB goal by 2035, reaching milestones has been tenuous. Furthermore, the current COVID-19 pandemic has reversed the progress made in the fight against TB due to missed diagnoses, untreated cases increasing TB-related deaths and increasing its spread to the community (3). The World Health Organization's most recent report shows the dramatic impact that COVID-19 has had, with the number of TB cases increasing during 2019-2021 as opposed to its previous declining trend, taking the lives of 1.6 million people in 2021 (4)

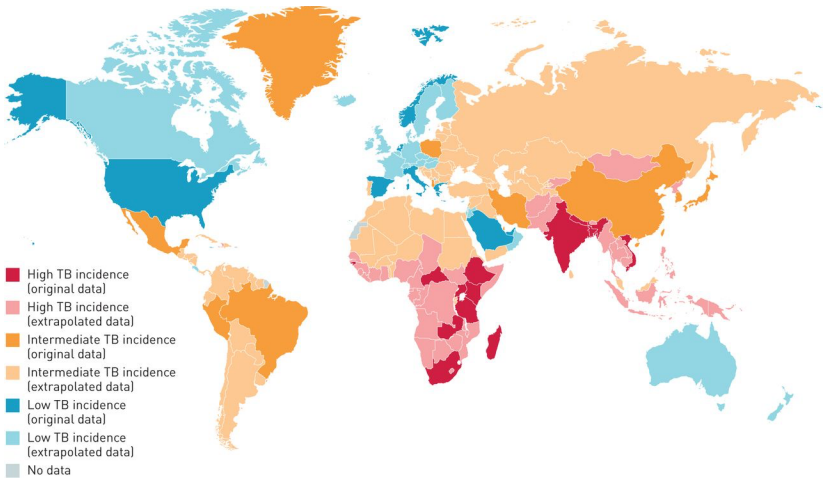

Figure 1.1: **Distribution of TB disease incidence.** Shown globally, emphasizing the burden on low-to-middle income countries and exempting first-world nations (2).

1.2. Problem Statement

Even though TB can be treated and cured with the current antibacterial therapies, there have been multiple factors impeding our efforts to treat the disease effectively. Despite the introduction of directly observed therapy short course (DOTS), treatment strategies are long and still lead to poor adherence which gives rise to drug resistance. The emergence of multidrug-resistant TB (MDR-TB), extensively drug-resistant TB (XDR-TB) and drug-resistant TB (TDR-TB) have rendered our first-line treatments, and therapies ineffective, leaving patients with poor prognoses. Secondly, the TB crisis is exacerbated by co-morbidities and other co-infections, particularly affecting immunocompromised people (Figure 1.2) (3,5). Another cause for concern is that *Mtb* has evolved several immune evasion mechanisms that favor its persistence in the host, facilitating its further spread and contributing to the growing reservoir of TB latency. Research has come a long way in the fight against TB, however, to reach our End TB goal by 2035, we need a multifaceted approach towards this disease. Consequently, there is a call for more efficacious vaccines, drugs and treatment regimens that will result in better disease outcomes and promote cure.

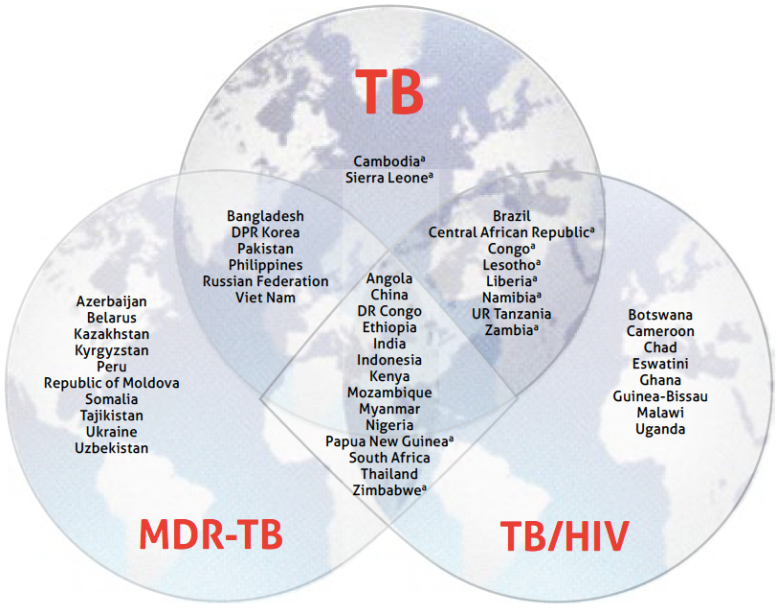

Figure 1.2: **Distribution of TB disease, compounded with HIV and multidrug-resistant TB cases.** South Africa is among 14 countries burdened with MDR and HIV cases, highlighting our country's dire need for more effective treatment strategies (5)

1.3. History of Tuberculosis

Tuberculosis (TB) is characterized as being an ancient disease that dates as far back as 150 million years ago (6). Since then, many advancements have been made in understanding the pathophysiology of this disease in the fight against these bacilli. Throughout history, TB has been described and recorded in many cultures as it transcends across borders and spreads globally.

Human tuberculosis is caused by the infectious agent, *Mtb*, however, the *Mycobacterium* genus includes a range of related species and might explain the introduction of human TB through zoonotic genesis. To support this, traces of TB have been discovered in bone remains of extinct bison in Wyoming from 17,000 years ago (7). The earliest evidence of human tuberculosis was identified in remains from two subjects, where early domestication of animals was evident 9000 years ago, further supporting the theory that *Mtb* spilled over into human hosts from *Mycobacterium bovis*-infected animals (8,9). Another study looking at Peruvian human skeletons revealed genomes distinct from human-human strains and were more like strains adapted to sea lions and seals (10). Dating approaches suggested a *Mtb* common ancestor to under 6000 years, and implicated sea mammals in possibly transmitting TB to humans (10).

Early evidence of TB was found in paleontological samples of ancient Egyptian mummies from the predynastic era (11). During Ancient Greek times in 460 BC, Hippocrates classified pulmonary TB as ‘phthisis’ which he described as the weakness of the lung, associated with fever and a cough (12,13). It was Girolamo Fracastorius who in 1546, implied that TB was a contagious disease, spreading through small particles, and in 1680 Franciscus Sylvius, who studied TB patients with pulmonary lesions and termed them as resembling small knots, or in Latin, ‘tubercula’, a term that gave TB its historical name (12,13).

In the 1700s, Benjamin Martens built on the preliminary idea of TB being contagious by these infectious particles that were believed to be minute living creatures and were hypothesized to spread through the air. After studying tubercula, in 1834, Johann Lukas Schonlein finally termed the elusive disease ‘Tuberculosis’, the globally accepted name. The proof of concept of TB being contagious ensued shortly after in 1865, when Jean-Antoine Villemin proved transmission of TB

from humans to animals and animals to animals, thereby confirming the transmissibility of TB (12,13). This disease soon caused devastating epidemics throughout the 17th and 19th centuries, fast becoming the leading killer amongst microbial pathogens, a title that still holds today (14).

The most notable milestone in the history of TB took place in 1882 by Robert Koch, who discovered the causative agent of pulmonary TB, terming it the 'tuberkel virus' or tubercle bacillus. His method of culturing and microscopy techniques to identify the pathogen later earned him the Nobel Prize in Medicine, in 1905. Paul Ehrlich later improved on Koch's staining method, laying the foundation for the development of the Ziehl-Nielsen staining method. Robert Koch's method of observing the bacillus showed that this pathogen grew in a mould-like fashion and appeared under the microscope as small rods. It was this resemblance to a fungus that encouraged them to name the agent *Mtb*, with the Greek prefix 'myco' meaning fungus (15).

In 1896, Theobald Smith showed the variation of strains within the Mycobacterium genus, observing that bovine TB had a distinct causative agent to human TB, and was termed *Mycobacterium bovis*. This was an important turning point and paved the way for the later discovery of the BCG vaccine. Leon Charles Albert Calmette first extracted a protein, tuberculin, from culturing the bacillus to use as therapy, termed, 'tuberculinisation'. Although efforts of this treatment were unsuccessful, this method was later adopted in 1908 by Charles Mantoux, who used tuberculin to diagnose TB through an intradermal skin test (13).

In the years after 1908, Calmette and Camille Guerin discovered that after 39 passages through a guinea pig, *Mtb* seemed to lose its virulence, and after 231 passages later, it was administered orally for the first time, sparking the era of vaccination studies. It took thirteen years to passage the bacterium to the point where it was first administered to a human and has since been named the Bacille Calmette-Guerin vaccine (BCG) (11). To this day it is the only effective vaccine we have in our ammunition to prevent childhood TB and is administered in its live attenuated form. Our next major advancement was only in 1943 when Albert Schatz and Selman Waksman found that streptomycin had antitubercular properties (16). This catalyzed the discovery of various other chemotherapies such as ethambutol, rifampicin and p-aminosalicylic acid, to name a few.

1.4. Pathogenesis of TB

At the onset of infection, *Mtb* is recognized and phagocytosed by alveolar macrophages resident in the lungs (17). After this, these infected macrophages trigger the recruitment of other immune cells into the infected region by releasing chemotactic signals, ultimately resulting in the formation of a granuloma (18). The granuloma, a hallmark of TB pathology, is comprised of an array of innate and adaptive immune cells that aggregate to contain the bacilli. At the start of innate immunity, immune cells including various macrophages, dendritic cells (DC), giant cells, and neutrophils form an inner cellular sphere. Upon adaptive immune induction, this sphere becomes surrounded by a lymphocytic cuff comprised of B and T cells. In this state, granulomas are in a solid form and can restrict growth and contain the bacteria at their center. However, during disease progression, these granulomas undergo structural changes and accumulate caseum that result in cavitation and necrotic breakdown of the structure. In this state, granulomas are no longer in a solid form, and collapse, releasing the bacilli into the airway and facilitating the cycle of transmission (19,20).

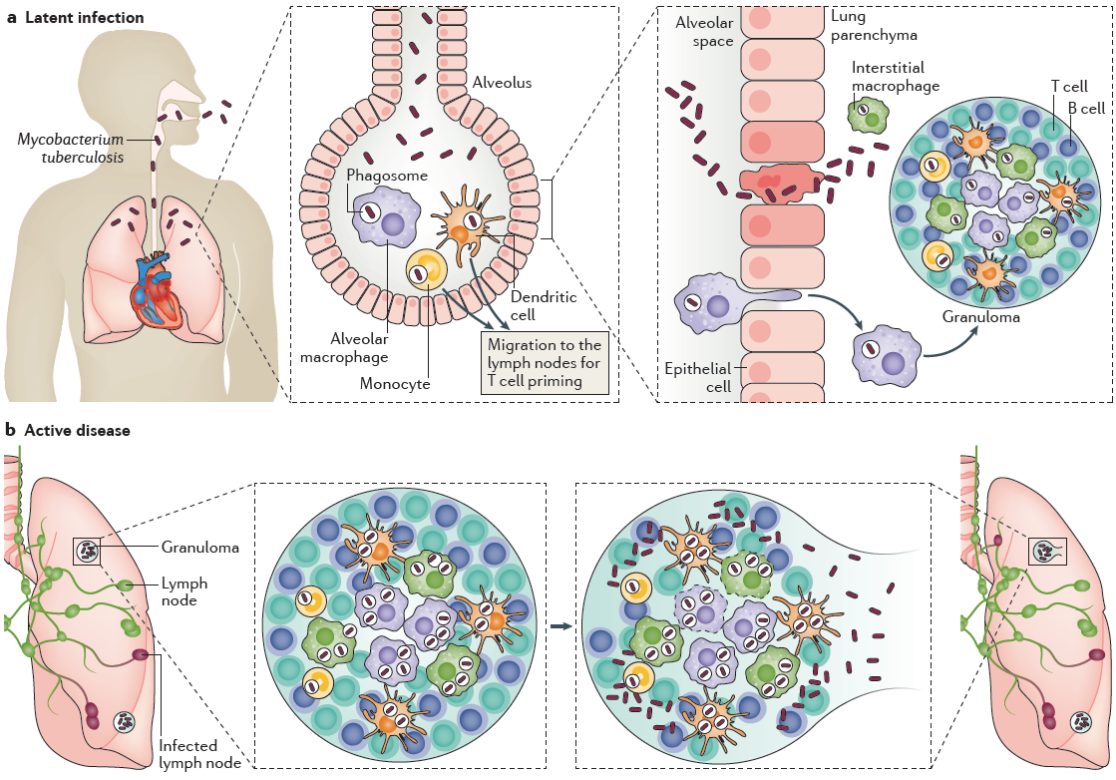

Figure 1.3: **Transmission of airborne *Mtb* and progression of TB disease**. a) *Mtb* is inhaled and reaches the alveolar space in the lungs where it encounters the first line of defense, resident alveolar macrophages. If these macrophages are not capable enough to eliminate the *Mtb,* the bacteria can migrate into the interstitial tissue by two different methods; either by infecting the alveolar epithelium or by infecting the alveolar macrophages which then migrate to the lung parenchyma. Thereafter, dendritic cells or monocytes transport the phagocytosed *Mtb* to the pulmonary lymph nodes to prime T cells. Subsequently, more immune cells are recruited, and T and B cells filter into the lung parenchyma contributing to the formation of a granuloma that will contain the bacilli. b) Within the granuloma, *Mtb* begins to replicate, in some cases, if the bacterial load becomes overwhelming, the granuloma will collapse, and release the bacteria, disseminating the infection to the bloodstream, and other organs, or enabling re-entry to the lungs to be released into the air facilitating the cycle of infection. The host at this stage is infectious, symptomatic and is characterized as having active TB disease (17).

1.5. The role of macrophages in *Mycobacterium tuberculosis* infection

Mycobacterium tuberculosis infection occurs upon inhalation of viable bacteria into the airway of the host. This triggers an intricate interaction between the bacterium and the host through a wide range of activation and stimulation of the immune system signaling cascades. *Mtb* is exquisitely adapted to being an intracellular pathogen of the phagocytic macrophages, with alveolar macrophages (AMs) being the primary channel of infection (21).

The bacilli are recognized by pathogen-associated molecular patterns (PAMPs) and phagocytosed by the first responding resident AMs, triggering a cytokine response. These *Mtb*-infected macrophages can disseminate from the alveolar space into the lung interstitium and further through the lymphatic system to other organs (22). Under certain conditions, the bacilli can grow unimpeded inside these phagocytes, leading to disease or a short period of latency followed by reactivation of the disease (23). Ideally, the growth of the bacilli is controlled and restricted within cellular granulomas, and latent infection is established. Latency can persist for decades in otherwise healthy hosts, until immune control of the bacilli fails, for example in the case of HIV infection (23).

Traditionally in a restrictive environment, *Mtb* is faced with a pro-inflammatory response, with increased phagosomal acidification, lysosomal degradation and release of nitric oxide, reactive oxygen species (ROS) and cytokines that combat the bacilli effectively and further augment

immune responses. However, these protective responses are dependent on the initial recognition, and the pathogen-associated molecular pattern-pathogen recognition receptor (PAMP-PRR) interaction between the bacilli and the host immune cell (24,25).

Macrophages express various receptors on its surface aiding in the recognition, binding and internalization of *Mtb* and consequently, triggering a cascade of events that lead to the release of antimicrobial and innate immune mediators promoting control of the infection. Studies have shown that the initial milieu of inflammatory mediators determines the functionality of these cells, while other studies suggest that macrophages show plasticity toward environmental changes. These findings may explain why the macrophage-*Mtb* interaction varies to such a large degree depending on the microenvironment (26–31).

There are numerous PAMPs that are recognized by PRRs on immune cells and *Mtb* encompasses a wide range of these antigens, thereby facilitating a strong response to *Mtb* preceding the adaptive immune response. The structure of *Mtb* contains distinct antigens such as mannosylated lipoarabinomannan (ManLAM), lipomannan (LM), lipoproteins and mycolic acids. All of which are recognizable by immune cell PRRs namely TLRs, NOD-like, and C-type lectin receptors (24). Additionally, *Mtb* may secrete proteins via its type VII secretion systems, for example the ESX-1 secretion system which includes ESAT-6 (32).

The C-type lectin receptor expressed on AMs, CD206, also known as the mannose receptor, is most commonly expressed in non-activated macrophages and binds with high affinity to mannans (33,34). However, these receptors are also able to interact with and bind mannosylated PAMPs found on pathogens including *Mtb* (35). It is possible that *Mtb* evolved to camouflage as a glycoprotein found within the host itself, using molecular mimicry and its mannosylated PAMPs (21). The MR binds to the mannose caps of ManLAM in *Mtb*, inducing PPARγ, which functions to limit pro-inflammatory responses and instead triggers the release of anti-inflammatory cytokines (36). *Mtb* is also able to block phagosomal acidification and lysosomal fusion (37). However, the interaction between the MR and mannosylated PAMPs still facilitates *Mtb* granuloma formation through the involvement of multinucleated giant cells (37,38).

Macrophage-inducible C-type lectin, or Mincle, is also a C-type lectin receptor and is expressed on myeloid cells at low levels before activation but is upregulated upon exposure to TLR ligands and cytokines. This protein is receptive to trehalose dimycolate (TDM), an antigen of *Mtb,* but is inessential for controlling TB infection in mouse models (39,40).

Perhaps the most critical immune mediators are the family of toll-like receptors (TLR). These receptors are present on lymphocytes, AMs, DCs, neutrophils and even on non-immune alveolar epithelial cells (41–44). TLRs respond to a variety of ligands, and are diverse, with at least twelve known mammalian variants (45–49). These receptors respond to a variety of pathogens, *Mtb* included, and are expressed either on the cell surface (TLR2 and 4) or are expressed intracellularly (TLR8 and 9) (50–52). Once TLRs are bound, an intracellular signalling cascade is initiated, leading to differential activation of inflammatory responses often including NF-κB involvement. Many antigens of *Mtb* are recognized by TLR1, TLR2, TLR4, TLR6 and TLR9, and the expression and functionality of these receptors are influenced by the pulmonary microenvironment (53–57). For example, surfactant protein A (SP-A) upregulates human macrophage expression of TLR2, while simultaneously inhibiting the intracellular TLR2 and TLR4 signaling, resulting in an attenuated pro-inflammatory response (58). To add complexity, TLRs interact with additional cell surface receptors which help to regulate and fine-tune the inflammatory response (59).

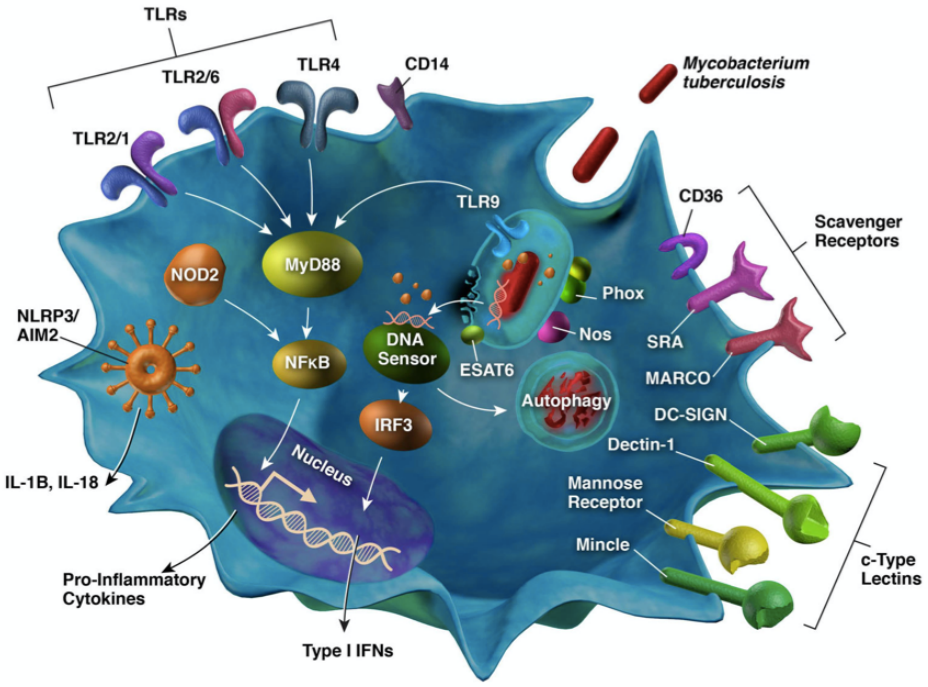

Figure 1.4: **Host cell receptors involved in *Mtb* signaling pathways.** Schematic of a host cell, containing various pattern recognition receptors (PRRs) and their associated mycobacterial PAMPs that are recognized before triggering immune signaling pathways (24).

1.6. Current tools and therapies for tuberculosis

Thus far, ten drugs have been approved by the United States Food and Drug Administration (FDA) federal agency. The first line TB treatment regime consists of rifampicin, isoniazid, ethambutol, pyrazinamide and streptomycin (60,61). The regimen includes an intensive two-month period on pyrazinamide, isoniazid and rifampicin, after which, the treatment course can last as long as six to nine months comprising isoniazid and rifampicin only (60). For patients who develop severe disease, ethambutol and streptomycin are prescribed additionally. In addition, drug resistance has been the biggest hindrance in the eradication of TB. Resistance to the first-line drugs isoniazid and rifampicin is classified as multi-drug resistance (MDR). Patients infected with these strains of *Mtb* have a longer treatment period of 18 months. This regime consists of fluoroquinolones (moxifloxacin, ciprofloxacin, levofloxacin and ofloxacin), aminoglycosides (amikacin, capreomycin, and kanamycin), ethionamide, p-amino salicylic acid and cycloserine (62,63). Strains that have been classified as extensively drug-resistant (XDR) are additionally resistant to

fluoroquinolone and an injectable (amikacin, kanamycin or capreomycin) used for second-line treatment. Treatment of drug-resistant strains is more challenging and needs to be tailored (63).

Even though there has been progress in the last decades, the development of newer, more effective drugs has been modest. Only three new drugs have been approved for the treatment of MDR and XDR anti-TB regimes, these are bedaquiline, delamanid, and pretomanid (60,64). Additionally, TB treatments continue to be lengthy, come with a wide range of side effects, and are a massive economic burden. These challenges emphasize the need for new strategies and treatments and have led the path to a new school of thinking. In more recent years, we have broadened our understanding of host-pathogen interactions, immunology and TB pathogenicity. The leaps in research have paved the way for innovative strategies termed host-directed therapies, which may provide highly rewarding results in TB treatment (65).

1.7. Host-directed therapies targeting the inflammatory balance in TB.

Initially, susceptibility to TB was thought to be caused by an insufficient immune response (66). Since then, recent research has shown that it is both an inadequate immune response and excessive inflammation that contribute to exacerbated TB outcome, the latter of which, by promoting lung tissue injury (67). Adding an adjunctive therapy alongside conventional TB drugs may therefore provide the headway for novel approaches. As a result of this new school of thought, a whole spectrum of clinical trials has been underway examining the effects of repurposed drugs to see whether there is an improvement in disease outcome either through immunomodulation and/or immune augmentation to promote cure (20,68).

The main ways in which these host-directed therapies work are (i) controlling hyperinflammatory responses and the tissue pathology associated with them, (ii) augmenting the efficacy and strengthening of the host immune and memory responses, (iii) promoting host-driven bactericidal mechanisms and reducing the growth of the bacilli, and (iv) rendering the granuloma permeable to anti-TB drugs to increase the exposure to the bacilli. With these concepts in mind, the

approaches to discover HDTs are expansive, exploring a broad spectrum of drug classifications and mechanisms (68).

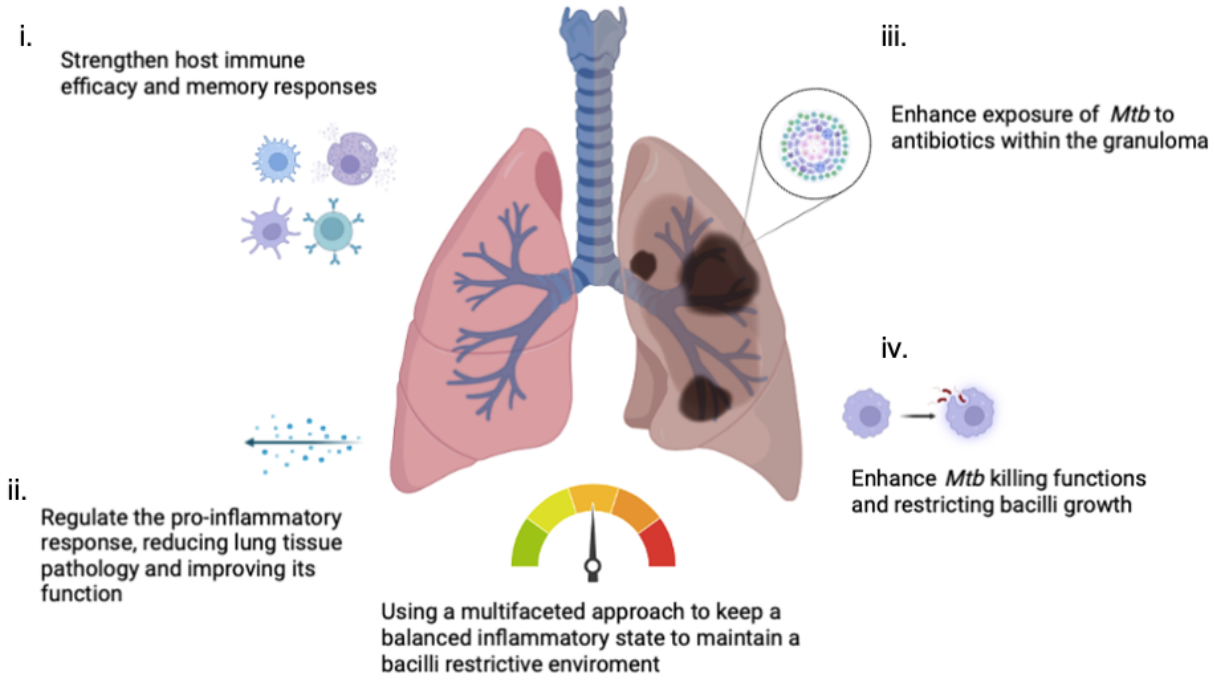

Figure 1.5: **Main strategies of repurposing adjunctive therapies for use in TB alleviation**. i) Strengthening the host immune response to augment efficacy and memory response, ii) modulation of inflammatory mediators to reduce hyper-inflammatory responses and augment lung integrity, iii) penetrating the granuloma to maximize exposure of the bacilli to drugs, iv) promote host bactericidal mechanisms and *Mtb* killing functions ultimately reducing growth of the bacilli. All approaches aim to maintain a balanced inflammatory state within the host while optimizing a bacilli-restrictive environment (68). Figure generated using BioRender.

One of the well-studied HDT candidate drugs is metformin. Metformin is an anti-hyperglycemic drug and has shown immunomodulatory effects. It promotes autophagy of macrophages by activating AMP-activated protein kinase (AMPK) to reduce inflammation. Metformin also reduces hyperglycemia-induced reactive oxygen species (ROS) production and inhibits the growth of the *Mtb* (69). While excessive ROS production can be detrimental to the host, it is still important for *Mtb*-killing functions. ROS is required for the fusion of the phagosome-lysosome complex that aids in the killing of *Mtb*. Metformin has been shown to promote phagosome-lysosome fusion while also reducing chronic inflammation (70,71). Murine *in vitro* and *in vivo* studies using

metformin have also shown the expansion of anti-inflammatory cell types, particularly, the alternatively activated macrophages, promoting tissue repair (72–75). Another promising aspect of this drug is the data from various preclinical trials which showed synergistic effects of metformin and the antimicrobial rifampicin in reducing the intracellular growth of *Mtb.* This occurs by inhibiting the proliferation of pro-inflammatory cell types in an AMPK-dependent manner (71,76). While most studies have been conducted on diabetic participants, recent pre-clinical evidence from healthy subjects showed that metformin was able to modulate cellular metabolism, as well as innate immune response changes at a transcriptomic level (77).

Other examples of possible HDTs include eicosanoid-modulating drugs such as NSAIDs and lipoxygenase inhibitors (68). Zileuton, currently approved for the treatment of asthma, is an interesting, repurposed drug as an HDT. Lipoxygenase inhibitors, specifically 5-LOX inhibitors, were shown to restrict lung pathology, reduce the production of type-I IFN, lower replication of *Mtb* and exhibit a greater percentage of survival in a TB-susceptible murine study (78,79). Another example being explored is statin therapy which is used conventionally to treat hypercholesterolemia but has also shown immunomodulatory and anti-inflammatory effects (68). Statins inhibit β-Hydroxy β-methylglutaryl-CoA reductase enzymes thus preventing important steps in lipid metabolism and inflammation (68). *Mtb* thrives in a lipid-rich intracellular macrophage environment, thus statins' ability to reduce this lipid-rich environment limits bacterial growth instead of favoring persistence. Another study showed that phagosome maturation and autophagy improved by statin therapy, making it a promising HDT (80). Currently, ongoing trials are delineating the safety, tolerability, pharmacokinetics and effectivity of statin therapy in conjunction with standard TB drugs (81–83).

A broader group of HDTs are immune-modulating drugs that include corticosteroids such as dexamethasone. A study looking at optimizing the inflammatory response showed that zebrafish that carried a mutation in the leukotriene A4 hydrolase (*LTA4H*) gene had increased susceptibility to *M. marinum* (84). The *LTA4H* gene plays an essential role in facilitating the balance between pro- and anti-inflammatory eicosanoids through control of the downstream TNF effector molecule. In theory, control of this gene mechanism could balance the hyper-inflammatory TNF response that leads to increased susceptibility. In a Vietnamese clinical trial, dexamethasone was used to

dampen hyperinflammatory immune responses in patients suffering from TB meningitis (84). Dexamethasone is a glucocorticoid with broad anti-inflammatory effects, able to reduce pro-inflammatory eicosanoids, however, not all patients benefited from this treatment, in fact, many had a detrimental outcome. The study showed that those who were homozygous for the high expression variant of *LTA4H* had an improved prognosis from treatment. Conversely, patients homozygous for the low expression of the variant resulted in worsened outcomes and fatalities. The study showed how it can be critical to evaluate the genotype of patients before prescribing a broad anti-inflammatory as an adjunctive therapy. Heterogeneity is a running theme within the scope of TB disease, with *Mtb* itself and the spectrum it presents, as well as between individuals who suffer from the disease highlighting the importance of precision medicine. Genotyping patients to detect the high expression variant of *LTA4H* would identify those who would benefit from the dexamethasone treatment. Personalized medicine may be a high aspiration currently, but what this study highlighted was the importance of balancing the immune response to TB and how it can improve disease outcomes in a targeted manner. Therefore, there may be great value in investigating the role of these genes involved in inflammatory pathways and it may just lead us to our next breakthrough in the fight against TB.

1.8. The Sestrin family of proteins

Sestrins (SESNs) are a family of antioxidant proteins with regulatory and anti-inflammatory roles in immunity (85). Invertebrates possess a single variant of the gene while vertebrates express three paralogues, *Sestrin 1 (Sesn1), Sestrin 2 (Sesn2) and Sestrin 3* (*Sesn3*) (86). Sestrins are conserved proteins that accumulate within cells during stress responses to various stimuli including DNA damage and oxidative stress and have shown anti-inflammatory effects in several ways (87). The role of Sestrins has been overlooked in infectious diseases but they are gaining attention due to their role in aging and other disease models suggesting they may be a key player in reducing and regulating inflammation. The established roles of Sestrins are their ability to reduce cellular damage and protect against age- and diabetes-related pathologies (88). Some of these pathologies include cardiac malfunction, mitochondrial dysfunction, triglyceride accumulation, insulin resistance, muscle degeneration, and neurodegenerative diseases (88,89). There have been

multiple studies looking at its involvement with slowing the progression of carcinomas, and tumorigenesis (89).

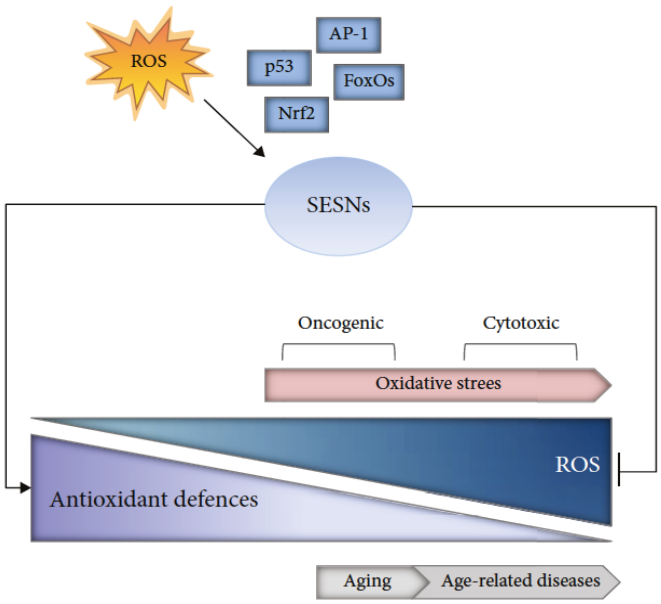

Figure 1.6: **Sestrins as master regulators of antioxidant defenses.** *Sestrin* may be induced during some level of oxidative stress, or ROS, by being stimulated by a host of transcription factors including but not limited to p53, Nrf2, AP-1 and the FoxOs. Once Sestrin is activated it can attenuate oxidative stress and ROS via multiple mechanisms ultimately restoring oxidative homeostasis, therefore playing a functional role in age-related diseases where high ROS is a driving force (89).

Although all three paralogues have sequence homology, and common origin, each of the three genes maps to a different chromosome in the human genome: *Sesn1* to 6q21, *Sesn2* to 1p35.3 and *Sesn3* to 11q21 (89,90). The crystal structure of the human Sesn2 protein showed that there are three subdomains, two of which are structurally similar, SESN-A and SESN-C, connected by SESN-B, a helix-loop-helix domain (89) (See Figure 1.7). Intriguingly, both subdomains share homology with other proteins that belong to the alkyl hydroperoxidase family, with emphasis on AhpD, the *M. tuberculosis* protein (91,92). Analyzing the structure of Sesn2 leads to the identification of three separate functional domains. The first permits the antioxidant properties of Sesn2 and depends on three amino acid residues, catalytic cysteine (C125), Y127 and H132 contained in the oxidoreductase active site within SESN-A (89). Only Sesn2 has been described to have alkyl hydroperoxidase activity, able to reduce peroxiredoxins. The second domain is a GATOR2-interacting plane, with an aspartate-aspartate (DD) motif, crucial for the direct physical interaction between Sesn2 and GATOR2 facilitating its mTORC1-regulating functions (89).

Within this domain is also a leucine-binding site, suggesting the function of Sesn2 to directly sense the cellular level of leucine, a key amino acid involved in the lysosome-mTORC1 system used to sense the overall nutritional level of amino acids (93). The structure of Sesn2 allows it to interact with Kelch-like ECH-associated protein 1 (Keap1), Unc51-like 1 (ULK1) and p62/sequestosome-1 (SQSTM1) and thus contributes to the impact it has in suppressing oxidative damage and its role in autophagy (89,90).

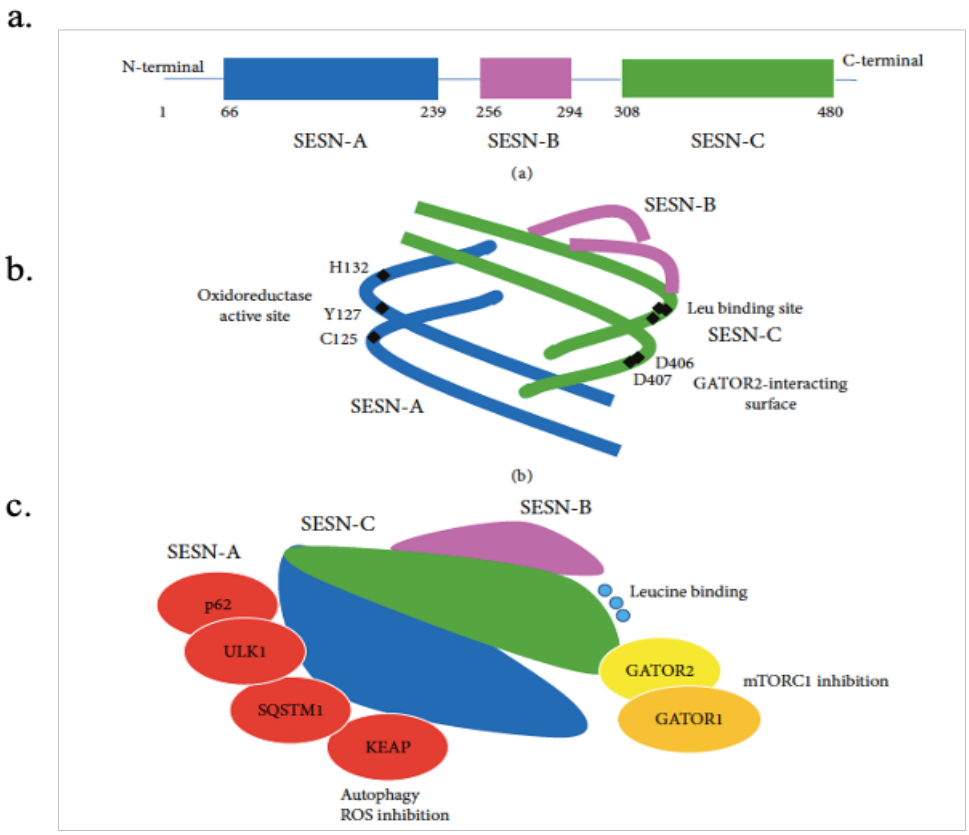

Figure 1.7: **Structure of the Sestrin 2 protein.** a) Shows the full-length protein structure of Sestrin 2 from the N-terminal to the C-terminal, and shows the division into its three functional domains, SESN-A, SESN-B, and SESN-C. b) Representation of Sesn2 based on the structure analysis by Ho et al. The schematic shows the position of the catalytic cysteine (C125) and the conserved Y127 and H132 residues associated with the proton relay system. These three residues are in the SESN-A region, depicted in blue. In the SESN-C domain the characteristic aspartate-aspartate (DD) motif and the leucine binding site depicted in green. c) schematic showing the direct interacting partners of Sestrin 2, and the pathways involved (89).

Sestrin has two well-known functions, these are, a) decreasing oxidative stress levels, and b) regulating the mammalian target of rapamycin (mTOR) (94). Both Sesn1 and Sesn2 have been shown to decrease levels of ROS and suppress the activity of mTORC1 in primary cells and

cultured cell lines, as well as play an important role in autophagy (89,95,96). Silencing all three paralogues of the *Sestrin* gene blunts the antioxidant response when challenged by various oxidative stresses whereas ectopic expression has a protective impact, however, the molecular basis for this occurrence and the extent of Sestrin's anti-inflammatory ability is still not fully understood (97,98).

Sesn1 and *Sesn2* are strongly induced by the upstream p53, whereas *Sesn3* is activated by the *Foxo3* transcription factor (97). Nuclear factor erythroid 2-like 2 (Nrf2), (JNK)/c-Jun pathway, and hypoxia-inducible factor-1α (HIF-1α) are other transcription factors involved in the expression of *Sesn2* (99–101). Sesn2 also contains three conserved phosphorylation sites, promoting its interaction with GATOR2, and repressing mTORC1 thus supporting the role of Sesn2 as a negative regulator of mTOR (102). However, more is to be discovered with Sestrin since its physiological ROS substrate is still unknown. Due to its sequence homology with AhpD, it was thought that maybe Sestrin could reduce AhpD substrates such as peroxiredoxins. As expected Sestrin can reduce peroxiredoxins, but no catalytic activity is required to do so, moreover, it can promote the activity of sulfiredoxin, in turn regenerating peroxiredoxin in positive feedback involving Nrf2 (98,103). In the context of TB, where inflammatory responses lead to increased pathology and bactericidal effector functions such as autophagy are crucial, the roles that Sestrin play in ageing and other disease models become of interest.

1.9. The role of Sestrins in inflammation

1.9.1. AMPK

Sestrin's ability to augment AMPK activity is one mechanism through which Sestrin leads to anti-inflammatory and anti-oxidative effects (104). Knockdown of *Sesn2* in HUVECs, THP-1 cells and aortic tissue from C57BL/6 mice resulted in increased NFκB phosphorylation and pro-inflammatory cytokine secretion when stimulated with LPS (104). *Sesn2* knockdown was also associated with decreased AMPK activation causing atherosclerosis in mice treated with LPS (104). Moreover, knockdown in HUVEC cells displayed elevated levels of LPS-induced ROS, cell

toxicity and endoplasmic reticulum (ER) stress (104). The study showed that the pro-inflammatory effects were nullified upon treatment with an AMPK activator, suggesting that *Sesn2* knockdown aggravates pro-inflammatory responses via an AMPK-dependent pathway and *Sesn2* could provide therapeutic relief in balancing inflammation (104).

A study by Hwang et al. showed a similar result when looking at the role of *Sesn2* in cardiomyopathy. The *Sesn2* knockdown in H9c2 cells resulted in decreased levels of AMPK phosphorylation. Antioxidant genes such as catalase and superoxide dismutase (*SOD2*) were downregulated, and the production of ROS was increased when cells were stimulated with LPS (105). Furthermore, the expression of matrix metalloproteinase (*MMP*) *2* and *MMP9*, which are activated by ROS, were increased in the *Sesn2*-depleted H9c2 cells, and LPS-induced cell death increased. Once again, when treated with an AMPK activator, 5-aminoimidazole-4-carboxamide ribonucleotide (AICAR), these increased patterns vanished, showing a regulatory effect of *Sesn2* in an AMPK-dependent manner (105). An important factor in TB disease progression is lung tissue pathology, where increased fibrosis is associated with a poor prognosis. Additionally, it was shown that the knockdown of *Sesn2* led to the expression of cardiac fibrotic factors, such as collagen type I and II in the heart tissue of C57BL/6 mice (105). These results suggest the *Sesn2* is a potential novel therapeutic target for diseases exacerbated by inflammatory conditions.

1.9.2. NLRP3

A recent study by Min-Ji Kim et al showed that Sestrin 2 enabled the suppression of prolonged NLRP3 inflammasome activation, a key pro-inflammatory pathway, by stimulating mitophagy in macrophages to clear damaged mitochondria (106). *Sesn2* knockout mice, on the other hand, exhibited defective mitophagy resulting in inflammasome hyperactivity and increased mortality in two separate sepsis models (106).

In diabetic nephropathy, it was found that treatment with Icariin (ICA), an antifibrotic drug, was able to improve physiological index in rats (107). Moreover, the treatment with ICA increased Nrf2, and decreased NRLP3 and Keap1 through Sesn2-dependant mitophagy. Using *Sesn2* siRNA knockdown, treatment with ICA no longer showed suppression of NLRP3, suggesting its

dependence on Sesn2-induced mitophagy to regulate NLRP3 activity. Thus, the protective effect of ICA treatment in diabetic nephropathy may be facilitated by Sesn2's link to NLRP3 (107).

Another study showed the role of *Sesn2* in ameliorating hepatotoxicity and liver fibrosis in cholestatic liver disease. *Sesn2* deficiency promoted pyroptosis through activation of the NLRP3 inflammasome, and knockout mice showed exacerbated liver fibrosis (108). Deficiency of *Sesn2* also increased hepatic ER stress, and overexpression of *Sesn2* reversed this effect. Moreover, inhibition of mTOR using rapamycin, and activation of AMPK using AICAR, was able to reverse the increased ER stress in *Sesn2*-deficient cells, suggesting that Sesn2 acts in an mTORC1/AMPK-dependent manner. This result advocates for the potential role of Sesn2 in regulating NLRP3, and ER stress to attenuate liver injury (108).

1.9.3. ROS

Reactive oxygen and nitrogen species (ROS and RNS), which are by-products of metabolism, are usually counterbalanced by antioxidant systems, but also play an important role in signaling, affecting proliferation and cell death (98). Appropriate levels of ROS are necessary for maintaining physiological homeostasis, however, accumulation of ROS in excessive amounts leads to DNA and protein damage which has been implicated in aging (86,88). These by-products, therefore, need to be tightly regulated, as to ensure signalling and prevent oxidative damage. Peroxiredoxins are a group of enzymes that metabolize peroxides, and Sestrins, modulated by p53 are important facilitators of peroxiredoxin recycling (98). In this way, Sestrins employ the antioxidant firewall providing great potential as therapeutic targets (98).

One example of cellular stress is glucose limitation. In such a scenario, p53 is activated as a method of maintaining cell survival (109). However, p53 is frequently deleted or mutated in cancerous tumors, yet cancer cells can survive metabolically challenging environments (109). Suggesting the presence of other mechanisms of cell survival. This study showed Sesn2 as a downstream target of p53 and the role it plays in protecting cells when challenged by genotoxic, energetic or oxidative stress (ROS). Although *Sesn2* is understood to be regulated by p53, the *Sesn2* transcript was shown

to be post-transcriptionally stabilized regardless of the p53 status, when metabolically challenged (109). Indicating a level of p53-independent function of Sesn2 in cell survival.

Other studies have shown that while *Sesn1* is found to be induced by hydrogen peroxide in a p53-dependant manner, *Sesn2* is not fully dependent on p53 but instead can be directly induced by levels of increased ROS, and even through the activation of Nrf2 and through the JNK/AP-1 pathway (99,110,111).

1.9.4. TLR

A recent study that explored the regulation of TLR-mediated inflammation by Sesn2 showed that Sesn2 inhibited LPS-induced nitric oxide (NO) release and *iNOS* expression in RAW264.7 cells (85). *Sesn2* expression was able to suppress the release of pro-inflammatory cytokines (TNF- α, IL-6, and IL-1 β amongst others) and suppress the production of LPS-induced ROS by inhibiting nicotinamide adenine dinucleotide phosphate (NADPH) oxidase (85). More specifically, overexpression of *Sesn2* was shown to regulate c-Jun, JNK and p38 phosphorylation induced by LPS. This regulation led to decreased AP-1 binding, thus reducing the pro-inflammatory responses (85). By introducing recombinant *Sesn2* into mice via an adenovirus, the effects of severe hepatic injury were attenuated, as seen by the decreased ALT, AST and hepatocyte degeneration (85).

In another study assessing acute lung injury (ALI) and acute respiratory distress syndrome (ARDS), where lung pathology is a hallmark of the disease, authors explored the complex role that Sestrin 2 plays in oxidant defense. Using an LPS-induced model, they found that *Sesn2* knockouts exhibited enhanced ALI, with increased lung NLRP3 inflammasome activation, pyroptosis, and elevated IL-1β and IL-18 in serum and bronchoalveolar lavage fluid. Alveolar macrophages (AMs) from KO mice showed reduced mitophagy whereas ROS, mitochondrial damage, and pyroptosis were elevated. Furthermore, Sesn2 facilitated the expression of the *Sequestosome1* (*SQSTM1*) gene, and induced mitophagy via the Pink1/Parkin pathway. Therefore, Sesn2 may be protective and a potential target for treatment during ALI. These results are of particular interest, given that lung pathology is also a TB disease hallmark (112).

1.9.5. Autophagy

Autophagy is an important bactericidal process in TB disease and plays an important part in cell pathophysiology. Mitophagy is a specialized form of autophagy and is closely linked to the level of ROS in a cell. It is important for maintaining the integrity of mitochondria and can lead to pathological ROS levels if dysregulated (113–115). Another function of Sestrin is to regulate autophagy, thus protecting cells from metabolic and oxidative stress, hypoxia and DNA damage (89). Sestrin could promote autophagy by inhibition of mTOR, which in turn enhances ROS production via inhibiting the autophagy. Multiple studies have shown Sestrin to be a positive regulator of autophagy (116,117). One example involves p62/SQSTM1 and ULK1, which are important players in this process. Sesn2 can bind p62 in turn promotes degradation of its autophagic targets like Keap1 (inhibitor of Nrf2), damaged mitochondria and ubiquitinated proteins, restoring ROS homeostasis and even upregulating the transcription of antioxidant genes (118,119). Sesn2 can target mitochondria to the autophagic machinery and has demonstrated an intrinsic ability to increase ULK1 levels, potentiating its autophagy role. It is suggested that this could also lead to the attenuation of NLRP3 hyperactivation, and immunological homeostasis (106).

1.9.6. mTOR

The role of Sestrin 2 has been implicated in myocardial infarctions (MI), which similarly to TB, is a highly inflammatory process that is detrimental to the host. *Sesn2* was found to be upregulated following MI, and overexpression of *Sesn2* both in mice and *in vitro*, was able to suppress inflammation in classically activated (M1) macrophages. Furthermore, the authors showed that Sestrin 2 acted predominantly by inhibiting mTORC1 signaling and suppressing M1 macrophages and thus had an anti-inflammatory and repair-promoting effect (120).

Lee et al. showed that an accumulation of ROS leads to chronic activation of the target of rapamycin (TOR), activating c-Jun N-terminal kinase (JNK) and FoxO transcription factor resulting in *Drosophila Sestrin* (*dSesn*) levels increasing (88). In contrast, *dSesn* depletion

contributed to age-related pathologies that were reversed when AMPK was pharmacologically activated, or TOR was inhibited (88). The study illustrated Sestrin as a negative feedback TOR regulator, induced by stress, and preventing pathology related to chronic TOR activation possibly caused by reduced autophagy (88). Although these results were demonstrated in a *Drosophila* model, a similar principle may be relevant in the mammalian target of rapamycin (mTOR) system since TOR is a highly conserved regulator of cellular growth.

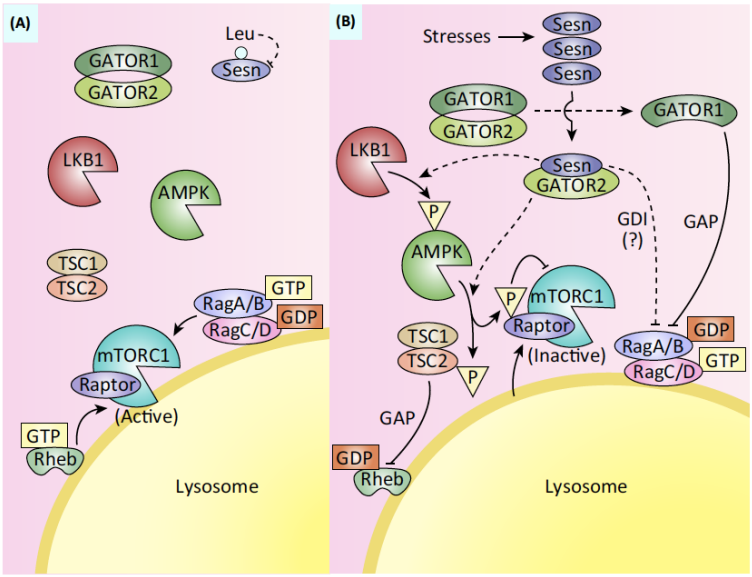

Figure 1.8: **Regulation of mTORC1 by Sestrin.** A) In the absence of stress, Sestrin levels are low, GATOR1 and GATOR2 can form a complex with each other (inhibiting GATOR1) and as a result, mTORC1 is activated with activated RagA/B RagC/D localizing it to the lysosomal membrane and a GTP-loaded Rheb activating its kinase activity. B) Once stress is introduced, Sestrin becomes upregulated and binds to GATOR2, freeing GATOR1 and allowing it to act as a GAP for the RagA/B. As a result, the RagA/B RagC/D becomes unable to localize mTORC1 to the lysosome and instead, it is released into the cytosol. Additionally, the Sestrin GATOR2 complex promotes the activation of AMPK, and although the biochemical mechanism is unclear, the interaction could involve LKB1. The activated AMPK then phosphorylates TSC2 which acts as a GAP for Rheb, leaving it in an inactive GDP-loaded state. In a separate arm of this pathway, a regulatory subunit of mTORC1 called Raptor is also phosphorylated by AMPK, once again inhibiting mTORC1 activity. Lastly, Sestrin may also play a role in the regulation of RagA/B proteins acting as a GDP dissociation inhibitor or GDI. The broken lines in this diagram represent biochemical mechanisms that still require further clarification, whereas the solid lines represent interactions already established (121).

Sestrin 2 inhibits mTORC1 activity by interacting with the GATOR2 protein. This interaction with GATOR2 releases its inhibition of the GATOR1 complex which in turn inhibits mTORC1. However, Sestrin may regulate mitochondrial function, as a recent paper showed that Sestrin 2

was localized in the mitochondria and may directly be involved in controlling mitochondrial function and cell death through mTORC1-independent means (122).

1.9.7. Sestrins; potential role in vaccines

Tailoring the immune system to enhance drug effectiveness is not the only strategy, it may be beneficial to use adjunct therapies to enhance the current BCG vaccine as well. BCG is an important preventative tool against childhood forms of TB, showing effectiveness against TB meningitis, which is fatal to children. However, the same vaccine translates to modest protection in adulthood, and with little understanding of the mechanism (68). A recent study showed that *Sestrin 1* and *Sestrin 2* expression increases during old age, and inhibition of these genes may enhance the amount of influenza-specific CD4T cells after influenza vaccine administration *in vivo* (123,124). Therefore, this may be a strategy to enhance the response of other vaccines. It should be noted that Sestrins provide important roles in reducing inflammatory-associated damage, and long-term blockade of these proteins could result in the proliferation of senescent-like T cells that cause DNA damage. To be a viable treatment option, Sestrin would have to be transiently inhibited, for the duration of the vaccine period to boost its effectivity (123).

1.10. The search for novel Targets for Host Directed Therapies in TB

With the rapid increase in the search for host factors as potential therapeutic targets for TB, scientists have explored many ways to identify them. One particularly powerful method is host transcriptomics coupled with host-pathogen dynamics (125). This method enables the identification of differentially expressed genes that may be exploited or involved in TB disease progression or protection that could be linked to an *Mtb* eradication strategy (126). High-throughput screening, such as microarrays and RNA-sequencing have been tools previously used to distinguish potential targets and are constantly being improved to be more robust. These tools can be used to better identify genes possibly involved in disease (127). Large databases have been generated by consortiums such as the Functional Annotation of Mammalian Genome (FANTOM)

expression profiles, and this helps with the search for interesting trends in gene expression(128–130).

The FANTOM5 study by the international genomics consortium based at RIKEN, Japan used next-generation sequencing to generate comprehensive genome data. In collaboration with Prof. Brombacher (University of Cape Town), we generated a transcriptomic landscape using Cap Analysis of Gene Expression (CAGE), a technique that sequences the 5' capped end of RNA, to demonstrate the gene expression of stimulated and *Mtb*-infected macrophages. Macrophages were stimulated into classically activated M1 state using IFN-γ and alternatively activated M2 macrophages using IL-4 and IL-13. These antagonistic macrophages were infected with the hypervirulent clinical *Mtb* strain HN878, and the expression kinetics were determined over time. In collaboration with bioinformatician, Dr. Sebastian Schmeier at Massey University, this large transcriptomic dataset was analysed, with potential top hits of genes that showed interesting trends in expression, that could potentially be implicated in host responses to *Mtb* infection. Using algorithms like DESeq2 to analyse the differential expression patterns we were successfully able to identify potential protein targets.

The data generated from this study was published (128,129). Graphically represented in Figure 1.9, where we identified *Sestrin* genes, which exhibited interesting patterns post-infection. Of particular interest was *Sestrin 1* which significantly decreased upon *Mtb*-infection, highlighting its potential importance in TB disease whilst *Sestrin 2* and *Sestrin 3* showed inconsistent and subtle changes. These findings may suggest the use and importance of Sesn1 as potential therapeutic targets or as biomarkers for protective immunity.

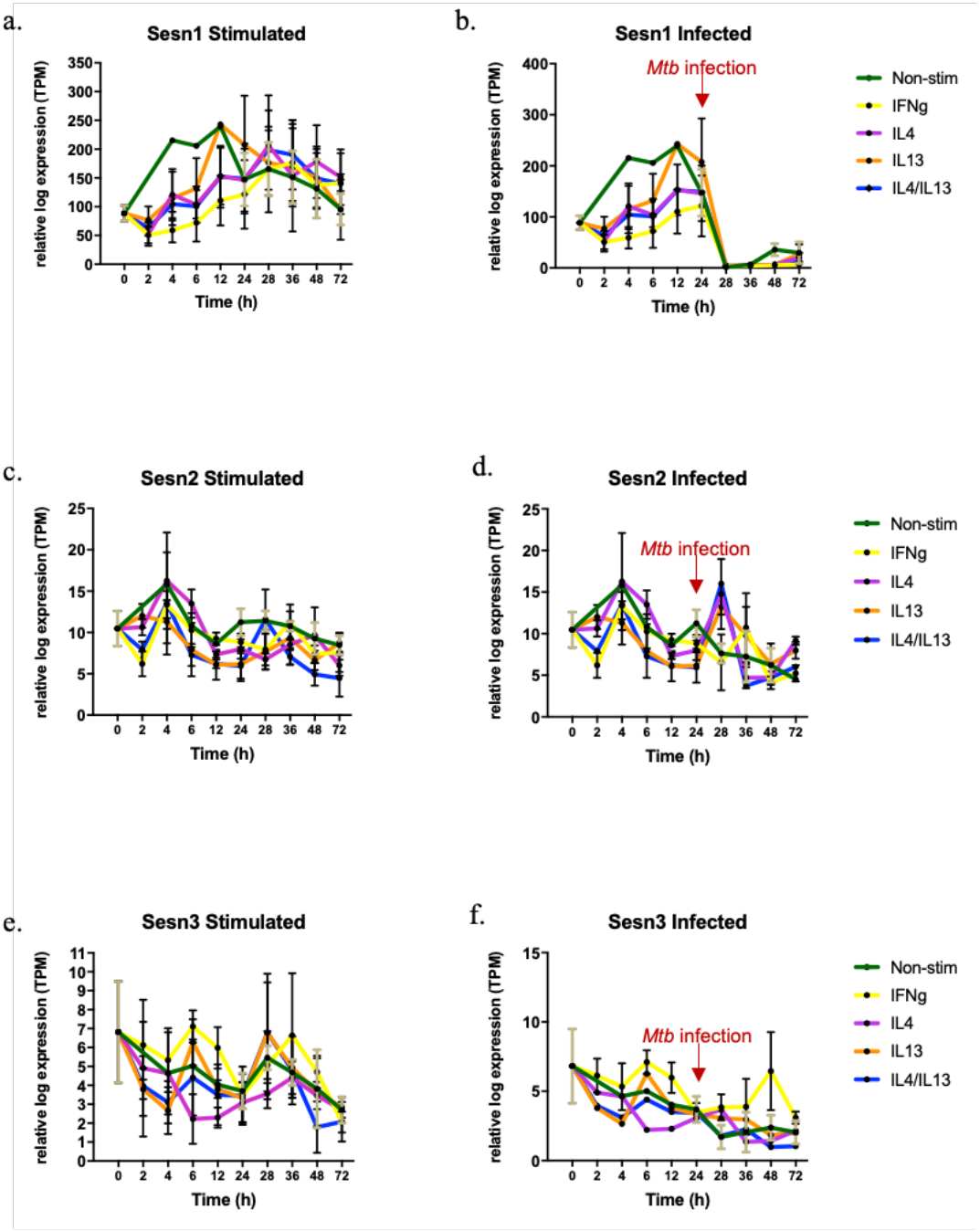

Figure 1.9: **Expression patterns of *Sestrin 1, 2* and *3* over time in stimulated and infected macrophages, plotted using the data retrieved from the FANTOM5 consortium.** a-b) mRNA levels of *Sesn1* are reduced significantly during infection. c-d) *Sesn2* levels have a more subtle upregulation upon *Mtb* infection compared to its counterparts. e-f) *Sesn3* expression levels decrease with infection.

The role of Sestrins has not been studied in infectious diseases, however, their role in other disease models, innate immunity and inflammation gives us a good indication that they may have an important role to play (87).

1.11. Hypothesis

We hypothesize that Sestrins protect against TB disease by counteracting the host detrimental inflammatory immune response.

1.12. Aims

The main aim of this project is to investigate the role of Sestrins in tuberculosis progression and disease outcome and to determine its potential as a candidate for HDT. Given Sesn2's anti-inflammatory and repair-promoting effects in various diseases, we prioritized *Sesn2* for our study. Based on the significant reduction in *Sesn1* expression observed in CAGE data and considering the pivotal role macrophages play in tuberculosis (TB) pathology, we aim to study the macrophage-specific role of *Sesn1* in preclinical models of tuberculosis. The previous literature showed that Sestrins have value as anti-inflammatory proteins, and we intend to elucidate their potentially beneficial role by performing the following objectives:

1.13. Objectives

1. Characterization of the *Sesn2*$^{-/-}$ global knockout mice
2. To determine the role of *Sestrin 2* in host immunity during *Mtb* infection using the *Sesn2*$^{-/-}$ mouse model.
3. Mechanistic studies to determine pathways and the regulation of *Sestrin 2* in macrophages using the *Sesn2*$^{-/-}$ mouse model.
4. Characterization of the *LysM*^{cre}*Sesn1*$^{flox/flox}$ macrophage-specific knockout mice.
5. To determine the role of *Sestrin 1* in macrophage host immunity during *Mtb* infection using the *LysM*^{cre}*Sesn1*$^{flox/flox}$ mouse model.
6. Mechanistic studies to determine pathways and the regulation of *Sestrin 1* in macrophages using the *LysM*^{cre}*Sesn1*$^{flox/flox}$ mouse model

CHAPTER 2: MATERIALS AND METHODS

2.1. Mice

The mice models used for this study were housed in individually ventilated cages under specific pathogen-free (SPF) conditions in the BSL3/BSL2 facilities in the Research Animal Facility (RAF) at the University of Cape Town. Basic requirements for husbandry and housing followed the guidelines stated in the National Centre for the Replacement, Refinement and Reduction of Animals in Research (NC3Rs). All experiments used mice between the ages of 8-12 weeks old and were sex-matched. Mice were monitored regularly and supplied with a normal-chow diet and drinking water. All *in vivo* procedures were performed within the RAF BSL2 and BSL3 facilities. For a baseline reading, mice were weighed before experimentation and thereafter monitored daily and weighed weekly to monitor disease progression. Disease progression was also monitored according to the mouse grimace scale (NC3Rs) which was a determinate of stress and discomfort. Mice were euthanized when the humane endpoint was reached, or at the timepoint of the specified experiment using halothane and cervical dislocation. For anesthesia, mice were given 200µl Phosphate buffered saline (PBS) (137mM sodium chloride, 2.7mM potassium chloride, 8mM disodium phosphate, and 2mM potassium dihydrogen phosphate in ddH_2O) with10mg/kg Rompun® xylazine (Bayer, Leverkusen, Germany) and 100mg/kg Anaket-V ketamine (Centuar Labs, Massachusetts, United States) via intraperitoneal injection.

2.2. Ethics Statement

Experiments performed in this study adhered to the guidelines of the South African National Standard for the Care and Use of Animals for Scientific Purposes (SANS 10386:2008) and were carried out according to the approved protocol by the Animal Research Ethics Committee (AREC) of the Faculty of Health Science, UCT (Protocol number: 019/023, 019/031 and 022/024). The animal ethics and training were conducted to ensure competency and compliance, SAVC authorization number, AR19/17613.

2.3. Sestrin Mouse Models

The *Sestrin 2* global knockout mouse model was obtained from the Ming O. Li lab where *Sesn2*$^{-/-}$ mice were generated using ES *Sesn2*$^{tm1a(KOMP)Wtsi}$ cells from EUCOMM (clone number: EPD0524_3_B11). By generating loxP sites, introns 3-6 were deleted and *Sesn2* knockout was confirmed through PCR analysis using ear clips (Figure 2.1a) (131). The global *Sestrin 2 (Sesn2)* knockout mouse model, was readily available and is characterized by the complete ablation of *Sesn2* expression across all cell types in the organism.

The *Sestrin 1* cell-specific transgenic mouse line was generated using the *Cre-loxP* deletion system by the Ming O. Li lab. The authors generated a murine model by introducing *FloxP* sequences at sites in intron 1 and 6 through homologous recombination with the target vector. A cell-type specific null allele mouse was generated after crossing with a Cre-expressing mouse. This system specifically targets macrophages and neutrophils by driving *Cre* recombinase expression under the control of the *LysM* gene promoter, which is active in monocytes, macrophages, and neutrophils. (Figure 2.1b) (131). We imported *Sesn1*-floxed mice which were crossed with *LysM*^{cre} mice to generate macrophage specific knockout of *Sesn1* (*LysM*^{cre}*Sesn1*$^{flox/flox}$). Due to practical considerations, and availability, the initial experiments were conducted using this macrophage-specific model, which preserved the intact expression of *Sesn1* in other cell types. Conversely, the *Sesn2* null mouse exhibits global ablation of *Sesn2* expression across all cell types. This explains the absence of mRNA for *Sesn2* in the global knockout compared to the reduced mRNA levels for *Sesn1* in the *LysM*^{cre}*Sesn1*$^{flox/flox}$ model, attributable to the incomplete and cell-specific *Cre*-mediated deletion. We did not prioritize *Sesn3* due to its very low expression compared to *Sesn1* and *Sesn2* in *Mtb* infection.

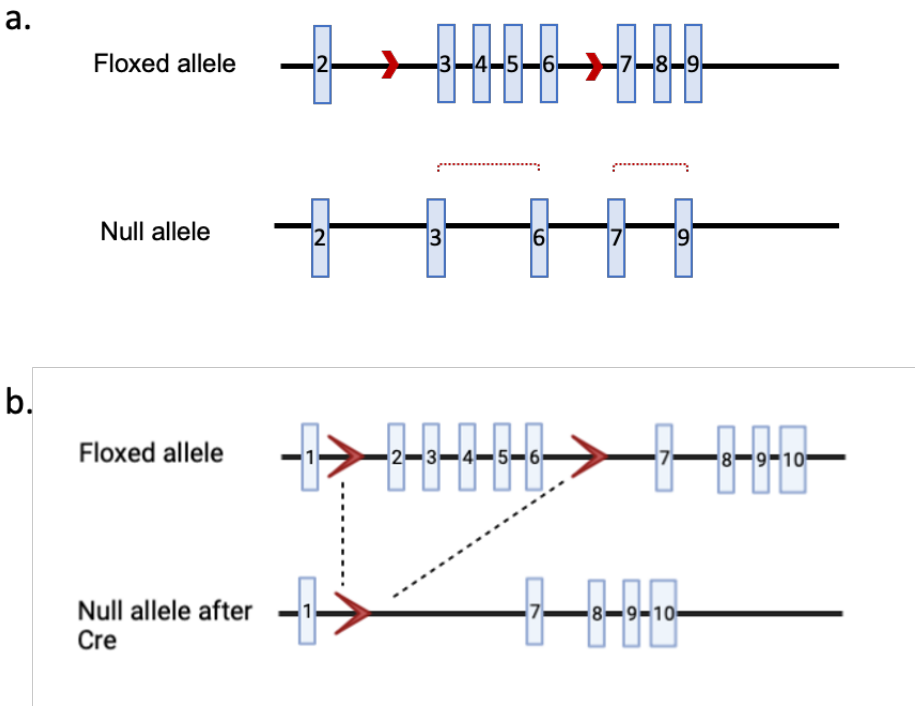

Figure 2.1**: Schematic showing gene deletion of *Sestrin 1* and *Sestrin 2.*** Regions between the floxed/ loxP sites, indicated here by the red arrows, were deleted on expression of the *Cre* enzyme, a) to generate *Sestrin 2* null mice, or b) in a cell-specific manner with *Sestrin 1* (131).

2.4. Characterization experiments

Sestrin (Sesn) wildtype and knockout mice on C57BL/6 background were obtained from Ming Li lab and backcrossed to three generations to in-house C57BL/6 mice. Each group contained 5-6 mice which were euthanized by inhalant halothane. Thereafter, mice were dissected aseptically to collect the lung and spleen, for further processing and analysis of immune cell populations, cytokine responses and pathology.

2.5. Tissue sample processing

2.5.1. Lung

The lung tissue was finely processed with a scalpel and transferred to tubes containing digestion buffer (DMEM containing 0.18 mg/ml Collagenase Type 1 and 0.02 mg/ml DNAse1). After an hour of incubation at 37 °C in a rotator, cells were passed in tandem through 100µm and 70µm sieves and spun down at 400 x g for 5 minutes at 4 °C. Red cell lysis buffer was made up using 155 mM NH_4Cl, 12 mM $NaHCO_3$, 0.1 mM EDTA and was added to samples to lyse erythrocytes. The cells were then spun down and resuspended in complete media and counted by Trypan Blue exclusion method to determine the total number of cells.

2.5.2. Spleen and Lymph Node

The spleen, or tracheobronchial lymph node samples were meshed using a 70µm sieve; after centrifuging for 5 minutes at 400 x g, the samples were then incubated with red cell lysis buffer for 2 minutes. An equal volume of DMEM+10%FBS was then added to deactivate the RCL (red cell lysis) buffer, cells were passed through a 40µm sieve and centrifuged once again under the same conditions. The pellet was then resuspended in 5ml DMEM supplemented with 10% heat-inactivated fetal bovine serum (FBS), in preparation for counting.

2.6. Culturing of *Mycobacterium tuberculosis* (*Mtb*)

All manipulation with *Mtb* was conducted in either the RAF BSL3 or UCT FHS BSL3 facilities in adherence to the Health and Safety Committee. *Mtb* strain HN878 was predominantly used as the clinically hypervirulent strain(132). *Mtb* was cultured in Middlebrook 7H9 liquid medium enriched with 10% oleic acid-albumin-dextrose-catalase (OADC) and 0.5% glycerol. The growth of cultures was measured using optical density (OD) readings at 600nm on the Biowave Cell Density Meter CO8000 (Biochrom Limited, Cambridge, United Kingdom). Cultures were deemed ready when the OD reading reached between 0.6-0.8, after which its concentration was determined by plating for colony forming unit (CFU) assays. After confirmation, stocks were prepared into a 1ml aliquots in 15% glycerol and stored at -80°C until needed.

2.7. *In vitro* and *in vivo* infection with *Mycobacterium tuberculosis*

For *in vitro* experiments, *Mtb* vials were thawed at room temperature. The stock was centrifuged at 10 000x g for 5 minutes, and the pellet was washed and resuspended with 1x PBS. The wash step was repeated to remove any residual glycerol and was resuspended in 1ml cell culture medium lacking penicillin G and streptomycin. The inoculum was then made up to a multiplicity of infection (MOI) of 0.5, was added to wells for infection, and incubated at 37°C and 5% CO2 for the specified time point. An MOI of 1 was lowered to 0.5 to reduce cell death and cell detachment for 3 and 6 days after infection.

For *in vivo* experiments, vials were thawed, and *Mtb* was washed as mentioned above. During the final resuspension step, the pellet was resuspended in sterile 1x PBS. The final inoculum is diluted into sterile saline for intranasal infection of mice to obtain 100-150CFU per animal. The inoculum is also plated for CFU assays before and after the infection, to confirm dosage.

2.8. *Mycobacterium tuberculosis* infection of mice

To ensure accuracy, an inoculum was made up of a maximum of 10 mice. The mice were weighed prior to infection to record baseline levels and were monitored and numbered to ensure they were healthy and recorded individually. Mice were anesthetized via intraperitoneal injection with xylazine and ketamine. The mice were then carefully infected intranasally with 25µl per nostril, for the desired concentration of 100-150CFU. To validate consistent infection, uptake mice were infected first and last in each round of infection. Uptake mice were used as a measure of effective inoculation and were euthanized 24 hours after the infection; lungs were dissected out homogenized and plated for CFUs to be determined. After infection, mice were monitored regularly for signs of stress or discomfort. For mortality experiments, mice were euthanized using halothane at their humane endpoint, determined by loss of 20% weight loss and a grimace scale of 3. For time-course infection studies, mice were euthanized at the indicated time points. An initial infection timepoint was set at 6-weeks and lengthened to 12-weeks of infection to determine the effect of *Sestrin* ablation on immune responses and lung pathology. This was in agreement with

previous literature examining TB at chronic stages in mice, which set an acute timepoint to 2-weeks and murine chronic infection to 12- weeks (133–135)

2.9. Determination of Bacterial Burden in tissue and macrophages

For *in vivo* experiments, 1x PBS was filtered using a 0.2µm filter to prepare dilutions. Lung and spleen samples were homogenized, in 2ml Tween-Saline and diluted using PBS to plate 100µl on 7H11 agar plates supplemented with 10% OADC and 0.5% glycerol. Colonies were counted 2-3 weeks after incubation at 37^{o}C to determine bacterial burdens for time-course infection experiments.

For *in vitro* assays, at the specified time point the supernatant was removed and stored for further ELISA experiments. The cells were washed with 1x PBS and 0.1% Triton X-100 is added to lyse cells and release the intracellular bacteria. Serial dilutions were plated as above to determine the bacterial growth.

2.10. Flow Cytometry Analysis

A single-cell suspension of cells was seeded at a density of $1.5x10^6$ per well in a 96-well V-bottom plate. The plate was centrifuged at 500 x g for 5 minutes, the supernatant was removed, and cells were resuspended in 200µl 1x PBS. The cells used as controls for the Viability stain were resuspended in 200µl ethanol, to induce cell death as a positive signal for the stain. After repeating the centrifugation step, cells were resuspended in 50µl BD 575V viability dye (1:2000 diluted in 1x PBS) and incubated at room temperature for 15 minutes in the dark. After incubation, 150µl FACS buffer (0.1% BSA 0.1% NaN_3 in PBS) was added to the wells, and the plate was centrifuged once again at 500g for 5 minutes to remove unbound antibodies. The cells were resuspended in 50µl of the myeloid or lymphoid antibody cocktails (Table S1). The samples were incubated for 20 minutes in the dark at 4°C. After the incubation 150µl FACS buffer was added to the wells and the plate was centrifuged, the supernatant was discarded and resuspended in 50µl of streptavidin mix if a biotinylated antibody was used in the myeloid or lymphoid mix. The streptavidin was incubated for 20 minutes at 4°C in the dark, after which 150µl FACS buffer was added, the plate

was centrifuged, the supernatant was discarded and resuspended in 100µl PBS. For fixation of cells, 100µl 4% paraformaldehyde was added to the wells and was incubated for 20 minutes in the dark at 4°C. After the incubation, the plate was centrifuged once again, the supernatant was discarded and resuspended in 100µl FACS buffer and samples were acquired on the BD Fortessa, LSR II, or the FACSymphony and analyzed using FlowJo™ Software.

2.11. Enzyme-Linked Immunosorbent Assay (ELISA)

Lung samples either *Mtb*-infected or naïve were homogenized and centrifuged at 2095 x g for 5 minutes to remove tissue debris and collect supernatants. Homogenates were filtered twice with a 0.2 µm filter before conducting the ELISA and were stored at -20°C until further use. We then analyzed levels of a range of chemokines, cytokines, growth factors and antibodies using the standard sandwich ELISA protocol. The primary and secondary antibodies, as well as recombinant mouse protein standards, were obtained from BD Biosciences (New Jersey, United States), BioLegend (California, United States) and R&D Systems (Minnesota, United States). The cytokines, chemokines and growth factors included IL-17, IFNβ, IFNγ, MCP-1/CCL2, Mip1α/CCL3, CCL5, KC/CXCL1, Mip2/CXCL2, CXCL5, CXCL10, IL-2, IL-10, IL-4, IL-6, IL-12p40, IL-12p70, IL-1α, IL-1β, G-CSF, GM-CSF, IL-23, IL-5, IL-13, IGF-1, TNFα, and TGF. To perform the ELISA, 96-well plates were coated with 50µl primary antibody in 1x PBS per well and incubated at 4°C overnight. After washing thrice with wash buffer and 0.05% tween-20) the plates were blocked with 200µl blocking buffer (2% BSA in 1x PBS) and incubated for 3 hours at 37°C. The wash step was repeated and 50µl of sample supernatant was added to the respective wells. To generate a standard curve, we serially diluted a standard using recombinant protein in dilution buffer (1% BSA in 1x PBS). Once diluted, 50µl was added to the standard wells and incubated overnight at 4°C. The plates were washed as before, and 50µl biotinylated secondary antibody in dilution buffer was added to each well and incubated for 3 hours at 37°C. After washing 3 times, 50µl horseradish peroxidase (HRP)-streptavidin or alkaline phosphatase (AP)-streptavidin was added and incubated for an hour at 37°C. Following this incubation, the plates were washed, and 50µl of either substrate was added. For the HRP plates, KPL TMB 2-component Microwell Peroxidase Substrate (SeraCare Life Sciences Incorporated, Massachusetts, United States) was

used. For the AP plates, p-nitrophenyl phosphate disodium salt hexahydrate was used (5 mg/ml 4-nitrophenyl disodium salt hexahydrate) (Sigma-Aldrich®, Merck, Darmstadt, Germany) in AP substrate buffer (1 M diethanolamine, 0.5 mM magnesium chloride, pH 9.8). The plates were incubated at room temperature in the dark to develop for 10-30 minutes. The reaction for HRP plates was stopped using 50µl 1M phosphoric acid to prevent saturation and were read at 450nm with a reference of 540nm. The AP plates was measured at 405nm with a reference of 495nm. The absorbances were taken using the Versamax™ Tunable microplate reader and software analyzer Softmax Pro version 6.3. We consistently collected the same lung lobes for the preparation of lung homogenates, thereby reducing the variance between and within groups. In addition, we performed a head-to-head comparison of cytokines from lung homogenates versus normalized to protein concentrations. This comparison showed that in our experiments, differences in protein concentration didn't affect the overall conclusion on immune response.

2.12. Quantification of Nitric Oxide

A Griess assay was performed to quantify the level of nitric oxide (NO) by measuring nitrite present in cell culture supernatant and lung homogenate samples. Since NO is metabolized to nitrite when oxygen is present, its measure is often used to evaluate the level of NO production (136). To detect levels of NO, a standard curve was generated, using a 1mM sodium nitrite solution serially diluted in DMEM media. The sample supernatants that were previously collected and stored at -20°C were added to a 96-well plate in a 1:1 ratio with 50µl 1% sulfanilamide in 2.5% phosphoric acid. After a 10-minute incubation at room temperature in the dark, 25µl of 0.1% naphthyl-ethylene-diamine in 2.5% phosphoric acid solution was added and incubated again under the same conditions to measure absorbance at 540nm using a reference wavelength of 690nm, with the Versamax™ Tunable microplate reader and Softmax Pro version 6.3 software.

2.13. Histopathological analysis

Lung lobes were fixed in 10% neutral buffered formalin. The tissue was processed using the Leica TP 1020 Processor for 24 hours and subsequently embedded in paraffin wax. The Leica Sliding

Microtome 2000R was used to cut 2 µm-thick sections of the embedded tissues. Three sections with 30µm distance apart per tissue were cut, deparaffinised, and subsequently stained with the hematoxylin/eosin stain. The images were acquired in Nikon Eclipse 90i microscopes and analysed with NIS-Elements AR software (Nikon Corporation, Tokyo, Japan) to determine the granulomatous area and alveolar space as a percentage of the total lung tissue. Alternatively, scanned slides were analyzed using QuPatth Software.

2.14. RNA from Tissue and Cells

Lung lobes were washed once with cold PBS and immersed in 500µL of RNAlater. Alternatively, samples were collected and stored in 350µL RLT buffer supplemented with 1% β-mercaptoethanol. Samples were stored overnight in the fridge at 4^{o}C as per instructions and thereafter at -80^{o}C until homogenization in 500µL of Trizol or the RLT buffer depending on the storage medium. RNA from cells was collected by lysing 5x10^{6} BMDM sample by adding 350µl Trizol or RLT buffer, cells were stored at -80^{o}C until RNA extraction.

2.15. RNA Extraction

Tissue or cell samples that were collected in 500µL Trizol were transferred to gel phase tubes and 100µL chloroform: isoamyl alcohol was added in a ratio of 49:1. Samples were mixed vigorously, incubated on ice for 2 minutes and centrifuged at 4^{o}C for 10 minutes at 18000rpm. A volume of 250µL chloroform: isoamyl alcohol was added again, vigorously mixed, incubated on ice and centrifuged as before. The aqueous phase was transferred to a new Eppendorf, and 1/10 volume of 3M sodium acetate, 0.5µL linear polyacrylamide and 250µL isopropanol (half the original volume of Trizol) was added, mixing after each addition. To precipitate the RNA, the samples were incubated overnight at -20^{o}C. Samples were centrifuged at 4^{o}C for 20 minutes at maximum speed, and the supernatants were removed without disturbing the pellet. The RNA pellet was then washed using 500µL cold 70% ethanol and was vortexed to resuspend the pellet. The samples were washed by centrifuging at 7000 x g for 10 minutes at 4^{o}C, removing the supernatant and repeating the wash step to remove any excess salts. The pellets were then airdried and resuspended in RNAse-free

water, before incubating at 60ºC for 10 minutes. The concentration and purity of the RNA was then measured by the ThermoFisher Nanodrop One UV Spectrophotometer. Alternatively, RNA was extracted using the RNeasy Mini Kit (Qiagen), according to the manufacturer's instructions.

2.16. cDNA Synthesis

We synthesized cDNA using the Transcriptor First Strand cDNA Synthesis Kit from Roche which used Anchored-oligo(dT)18 Primers and Random Hexamer Primers according to the manufacturer's instructions.

2.17. qRT-PCR analysis to quantify mRNA expression.

qRT-PCRs were run using Roche SYBR Green I mix to confirm knockout and determine the expression of the Sestrin family and related genes using the primers specified in Table S2.2.

2.18. BMDM Generation

Mice were euthanized and aseptically dissected to collect the tibia and femur bones. We extracted bone marrow-derived macrophages (BMDMs) by flushing the bone marrow precursor cells from the tibia and femur bones using complete DMEM media. Cells were washed and filtered with a 100µm sieve to remove any remaining tissue. Thereafter cells were centrifuged at 1200rpm for 10 minutes and resuspended in 5ml complete media to prepare for counting. The cell concentration was determined by using 4% trypan blue and counted on a hemocytometer (Neubauer chamber, Paul Marienfield, Lauda-Königshofen, Germany) under a light microscope (Eclipse TS100 inverted microscope, Nikon, Tokyo, Japan). Alternatively, cells were counted using the Biorad TC20 Automated Cell Counter. Cells were seeded and cultured in 150cm^2 tissue culture grade CellStar (Greiner Bio-One International, Kremsmünster, Austria) petri dishes at a concentration of 13x10^{6}cells/culture dish using 25ml PLUTZNIK media. PLUTZNIK media was made using DMEM, 10% heat-inactivated fetal calf serum, 5% heat-inactivated horse serum, 30% M-CSF or

L929 conditioned media, 2 mM L-glutamine, 1 mM sodium pyruvate 100µg/ml penicillin-streptomycin and 50µM β-mercaptoethanol. The isolated cells were incubated at 37°C and 5% CO_2 for 7-10 days until differentiated. An additional 25ml PLUTZNIK media was supplemented on day 5. The L929 conditioned media used in PLUTZNIK contains macrophage colony-stimulating factor (M-CSF) which permits the differentiation of the cells into macrophages. After 7-days of differentiation, the morphological changes of the cells can be confirmed under a light microscope by their elongated appearance. Once this differentiation had been confirmed, the supernatants were discarded, and cells were washed with 1x PBS to remove any non-adherent cells and debris. The remaining adherent cells were lifted using 0.25mg/ml lidocaine-5mM ethylenediaminetetraacetic acid (EDTA) in 1x PBS and incubating for 5 minutes at 37°C. To ensure detachment, cells were gently scraped using a cell scraper. The cells were collected and centrifuged for 10 minutes at 4°C and 1200rpm and resuspended in complete media. The cells were counted as described above and were seeded accordingly. After incubation for 24 hours at 37°C under 5% CO2, various downstream assays were performed.

2.19. Cell Cytotoxicity Assay

To measure levels of cytotoxicity in cells, we used lactate dehydrogenase (LDH) as a marker. The samples used were infected with *Mycobacterium tuberculosis* at an MOI of 0.5. For this assay, the Cytotoxicity Detection Kit, LDH (Roche, Sigma-Aldrich) was used according to the manufacturer's instructions. Cells were seeded in a 96-well plate at a concentration of $1.0x10^5$ in 100µl phenol-free complete media. At the specified time point, the plate was centrifuged at 300 x g and 50µl of the supernatant was removed and added to a separate flat bottom plate. The Cytotoxicity Detection Reagent was made up using the enzyme and dye accordingly, and 50µl was added to each well. The plate was incubated for 30 minutes protected from light at 25°C, after which the results were read at 490nm with a reference wavelength of 600nm, using the Versamax™ Tunable microplate reader and data was analysed using SoftMax Pro 6.3 software (Molecular Devices, California, USA).

2.20. Cell Viability Assay

To measure cell viability, we used the CellTiter-Blue® Cell Viability Assay kit (Promega, Wisconsin, United States) and followed the manufacturer's recommendations. $1.5x10^5$ cells were seeded in a 96-well clear bottom black plate, 20µl CellTiter-Blue® Reagent was added per 100µl complete media and was incubated for 1-4 hours at 37°C and 5% CO_2. After the incubation, the absorbance was measured at 540nm with 600nm as the reference wavelength, using the Versamax™ Tunable microplate reader and data was analyzed using Softmax Pro 6.3 software (Molecular Devices, California, USA).

2.21. CellROX™ ROS Assay

To determine the level of oxidative stress intracellularly, a CellROX® Oxidative Stress Assay (Invitrogen) was used according to the manufacturer's instructions. WT and KO Sesn BMDMs and infected with the HN878 strain of *Mtb*. For this assay, we used the CellROX® Green Reagent Cells were seeded at a concentration of $1.5x10^5$ in a 96-well plate in 150µl of phenol-free complete DMEM media. At the specified time point, the cell supernatant was removed and CellROX® Reagent was made up to a concentration of 5µM in phenol-free complete media, of which, 50µl was added to each well. The plate was incubated for 30 minutes protected from light at 37°C and 5% CO_2. After the incubation, the dye was removed and 100µl PBS was used to wash the excess dye from the cells. The wells were then supplemented with 100µl phenol-free complete media. The plate was read with an excitation wavelength of 485nm and emission wavelength of 520nm using the Versamax™ Tunable microplate reader and data was analysed using Softmax Pro 6.3 software (Molecular Devices, California, USA).

2.22. Metabolic Analysis of Macrophages

To analyze the influence of Sestrins on macrophage metabolic functions during infection and homeostasis, we used the Seahorse Bioanalyzer. The ATP Rate Assay kit was purchased from

Agilent and the protocol was followed as per the manufacturer's instructions. For naïve experiments, we seeded $5x10^4$ cells in the Seahorse cell plate, and for infection experiments $8x10^4$ cells were seeded in PDL-coated Seahorse plates in complete phenol-free DMEM. The cells were allowed to attach for 2-24 hours, and appropriate wells were infected with HN878 *Mtb* at an MOI of 0.5. Prior to starting the assay, the Seahorse cartridge was hydrated using a prewarmed XF Calibrant and was stored for at least 1 hour at 37°C in CO_2-free conditions. Cells were washed with 100µl XF Assay media, comprising of Seahorse XF DMEM pH 7.4, 10mM Seahorse XF Glucose, 1mM Seahorse XF Pyruvate, and 2mM Seahorse XF L-Glutamine. Thereafter, 180µl XF Assay Media was added gently, and incubated at 37°C in a CO_2-free incubator for 45 minutes. Oligomycin and Rotenone/antimycin A were loaded into ports A and B respectively, in the hydrated sensor cartridge and the cartridge was calibrated in the Seahorse analyzer under the Real-Time ATP Rate Assay Protocol. Once calibrated, the cartridge was replaced with the cell plate and the assay protocol was run. Data was analyzed using Seahorse Analytics software and plotted using GraphPad Prism.

2.23. Statistical analysis

The data generated during this study were analyzed using GraphPad Prism version 10. Unless otherwise specified in figure legend, an unpaired student t-test was used with appropriate Welch correction if applicable, when comparing two groups (wildtype and knockout animals), to determine statistical significance.

CHAPTER 3: RESULTS

Objective 1: Characterization of the *Sesn2*$^{-/-}$ global knockout mice.

3.1. Characterization of the *Sesn2*$^{-/-}$ global knockout Mouse

The deletion of *Sesn2* had no morphological and immunological effect in naïve mice.

Mice were generated and gifted by the Ming O. Li lab. Since a full immunological characterization of this mouse had not been done prior, we performed characterization of mice at the naïve state. This is done to establish a baseline and confirm that the gene deficiency does not cause any significant change at the naïve state. We characterized 8-12-week-old *Sesn2* Wildtype (*Sesn2*$^{+/+}$) and Knockout (*Sesn2*$^{-/-}$) mice on a C57BL/6 background and collected the lung and spleen tissues for downstream analysis by flow cytometry, ELISAs, histology and qRT-PCR experiments.

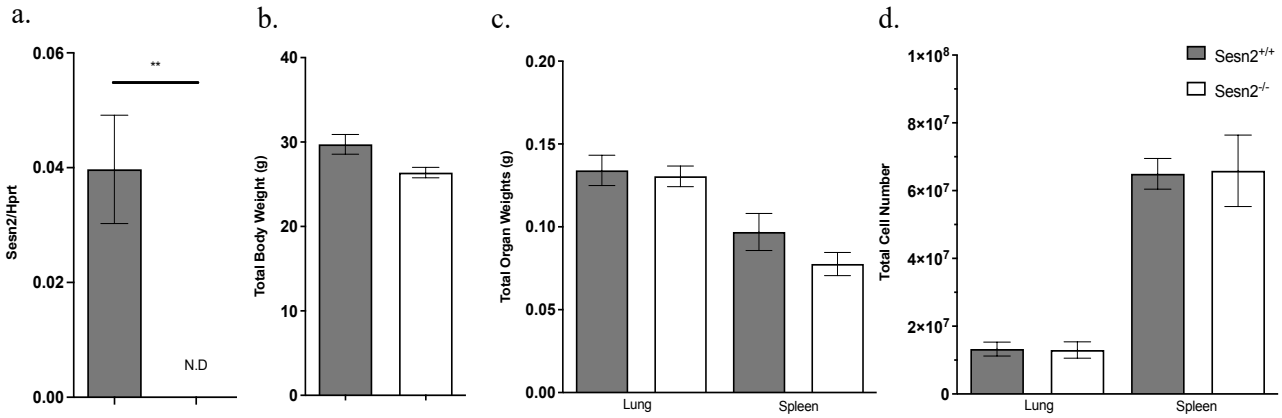

Figure 3.1.1: ***Sesn2* knockout had no effect on baseline measurements in mice.** Lung lobes were collected, and RNA was extracted for qRT-PCR analysis of the expression of *Sesn2* using *Hprt* as the housekeeping gene. Tissues were processed into single-cell suspensions for cell counts. a) qRT-PCR analysis of RNA from naïve lung samples of *Sesn2*$^{+/+}$ and *Sesn2*$^{-/-}$ mice, confirming *Sesn2* knockout. b) Total body weights of mice. c) Total lung and spleen organ weights. d) Total lung and spleen cell numbers. Data show mean ± of n=10-12mice/group of two pooled independent experiments. For statistical analysis, an unpaired student t-test was performed comparing baseline measurements in control versus knockout mice, with the following p-values to denote significance ** $p < 0.01$.

From the lung lobe, we extracted RNA to confirm the *Sesn2* gene knockout. We were not able to detect expression of *Sesn2* in the *Sesn2*$^{-/-}$ mice therefore confirming successful knockout against Hprt as a housekeeping gene (Figure 3.1.1a). We found no significant difference in body weights

or lung and spleen organ weights between mice. There was no difference in lung and spleen cell numbers between mice at a naïve state (Figure 3.1.1b-c). Indicating that deletion of *Sesn2* has no effect on baseline measurements in mice.

To determine the baseline immune responses of this mouse model, we first analyzed a range of pro-inflammatory, anti-inflammatory, and regulatory cytokines and chemokines as well as growth factors. These included IFN-γ, IL-12p40, IL-6, IL-17, IL-1α, IL-1β, TNFα, IL-2, IFNβ, IL-10, TGFβ, IL-4, IL-5, IL-13, GMCSF, CXCL2, CCL2, CCL3, CCL5, and CXCL1. We found no significant difference in the cytokines, chemokines and growth factors in the absence of *Sesn2* in the lungs (Figure 3.1.2a-c). This indicates that at a naïve state, levels of inflammatory mediators are comparable between mice.

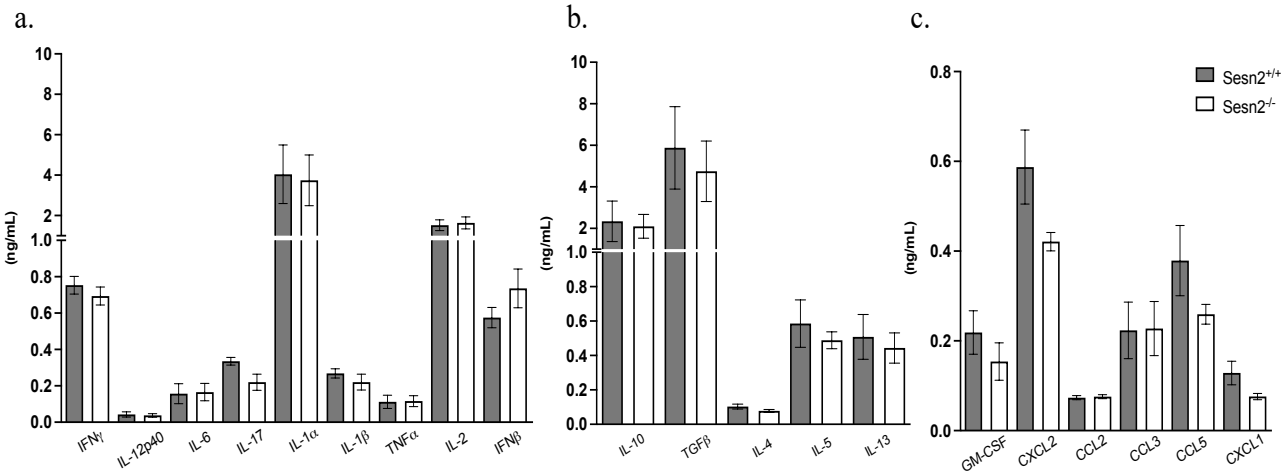

Figure 3.1.2: **The *Sesn2* knockout had no effect on immune responses in the lungs at a naïve state.** Lung homogenates were prepared to collect supernatants for the analysis of cytokines, chemokines and growth factors by ELISA. a) Pro-inflammatory cytokine panel. b) Anti-inflammatory cytokine panel. c) Growth factor and chemokine panel. Data show mean ± SEM of n=10-12mice/group of two pooled independent experiments. For statistical analysis, an unpaired student t-test was performed for comparison of cytokines, chemokines, and growth factor levels in control versus knockout mice.

To further characterize, we analyzed the myeloid and lymphoid immune cell populations using flow cytometry in both the spleen and lungs of these mice. We found no differences in the percentage and absolute cell numbers of the lung lymphoid populations (Figure 3.1.3a and b). The lung CD4 T cell subsets also showed no differences (Figure 3.1.3c). However, we found a higher number of central memory amongst CD8 T cell populations in *Sesn2*$^{-/-}$ animals (Figure 3.1.3d).

We observed more PD1- KLRG1+ CD4 T cell exhaustion markers but no difference was seen in CD8 T in the *Sesn2*$^{-/-}$ mice (Figure 3.1.3d and e). Percentage and absolute lung myeloid cells showed no differences (figure 3.1.3g and h). Although CD8 memory and cDC1 sub-populations showed significant differences, there were no major changes in other immune cell lineage recruitment in the lungs of *Sesn2*-deficient mice at the naïve state.

In the spleen, we observed no differences in lymphoid immune cell recruitment in the absence of *Sesn2* in mice (Figure 3.1.4a and b). Additionally, CD4 and CD8 T cell subsets and exhaustion markers remained unchanged (Figure 3.1.4c-f). Spleen myeloid populations showed only decreased cDC1 cells in both percentage and absolute cell numbers in *Sesn2*$^{-/-}$ mice (Figure 3.1.4g and h). Overall, these differences were too small to exert a biological difference and more of statistical significance due to the small variance, hence we conclude, that overall, there were no major differences in immune populations and the activation/exhaustion of lymphocytes at a naïve state.

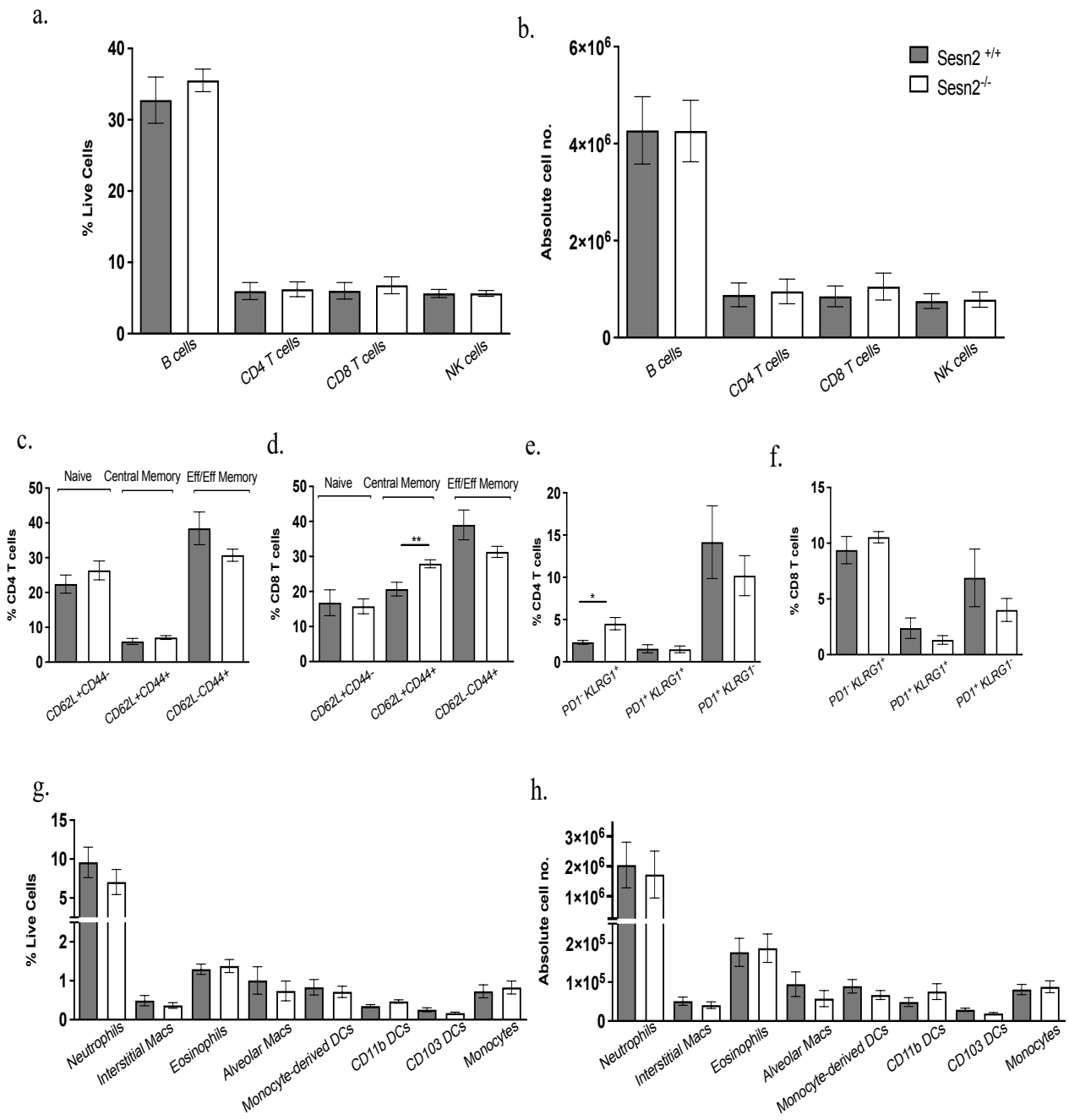

Figure 3.1.3: **The deletion of *Sesn2* showed comparable lung immune cell populations at a naïve state.** Tissues were processed into single-cell suspensions, seeded and stained for either a Myeloid or Lymphoid panel, and acquired on a flow cytometer. a) Percentage of lung lymphoid populations. b) Absolute lung cell number of lymphoid immune cell populations. c) Lung CD4 T cell subsets. d) Lung CD8 T cell subsets. e) Lung CD4 T cell exhaustion profile. f) Lung CD8 T cell exhaustion profile. g) Percentage of lung myeloid cell populations. h) Absolute lung myeloid cell numbers. Data show mean ± SEM of n=10-12mice/group of two pooled independent experiments. For statistical analysis, an unpaired student t-test was used for comparison of immune cell abundance in control versus knockout mice, with the following p-values as significance, *p <0.05, **p <0.01.

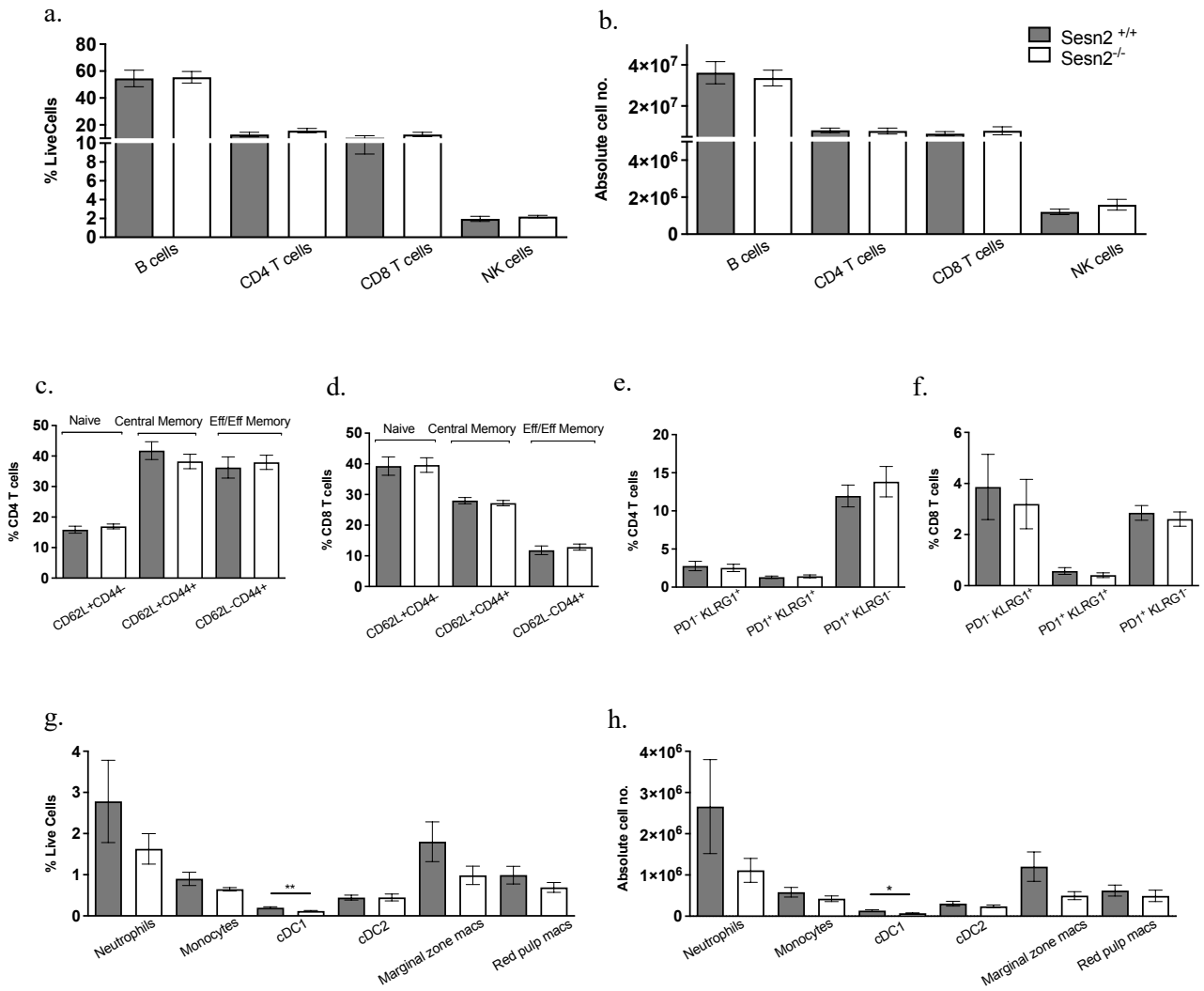

Figure 3.1.4: **The *Sesn2* knockout showed comparable spleen immune cell populations at a naïve state.** Tissues were processed into single-cell suspensions, seeded and stained for either a Myeloid or Lymphoid panel, and acquired on a flow cytometer. a) Percentage of spleen lymphoid immune cell populations. b) Absolute spleen lymphoid cell numbers c) Spleen CD4 T cell subsets. d) Spleen CD8 T cell subsets. e) Spleen CD4 T cell exhaustion profile. f) Spleen CD8 T cell exhaustion profile. g) Percentage of spleen myeloid immune cell populations. h) Absolute spleen myeloid cell numbers. Data show mean ± SEM of n=10-12mice/group of two pooled independent experiments. For statistical analysis, an unpaired student t-test was used for comparison of immune cell abundance in control versus knockout mice, with the following p-values denoting significance, *p <0.05, **p <0.01.

TB is largely characterized by severe lung pathology which is a hallmark of its disease progression. It was therefore essential to compare the lung tissue structure between *Sesn2*$^{+/+}$ and *Sesn2*$^{-/-}$, in the absence of infection, to determine any baseline defect which may influence downstream comparison during infection. We assessed the lung pathology between the mice by using

Hematoxylin & Eosin (H&E) staining and microscope analysis by analyzing the percentage of free alveolar space. The histology analysis revealed that there was no significant difference between the *Sesn2*$^{+/+}$ and *Sesn2*$^{-/-}$ mice (Figure 3.1.5a-c). This suggests that the knockout of *Sesn2* caused no defect in lung structure at the naïve state.

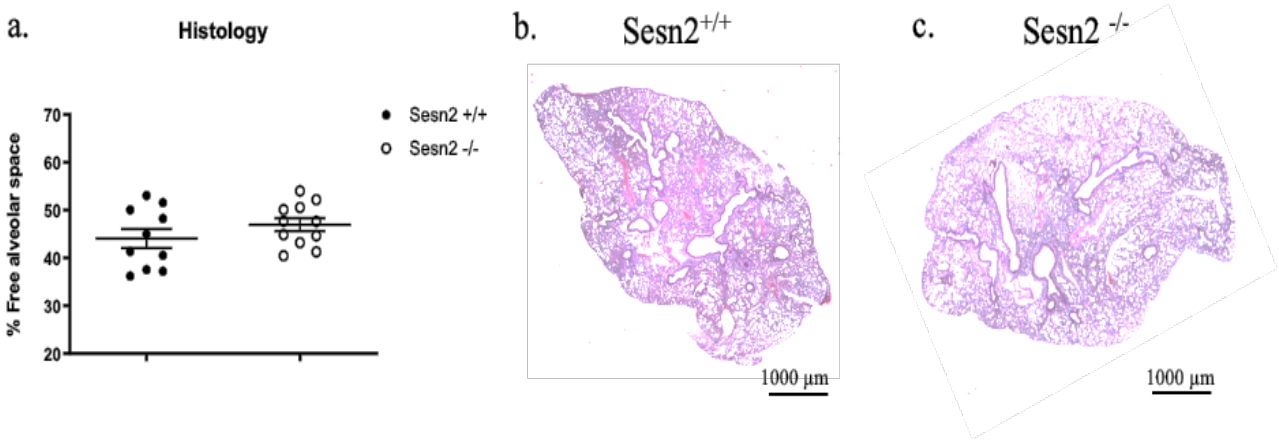

Figure 3.1.5: **The absence of *Sesn2* had no effect on lung histology at a naïve state**. Lung sections were stained with H&E and were scanned at 20x magnification. a) Quantitative analysis of percentage free alveolar space. b) Representative image of *Sesn2*$^{+/+}$ and c) *Sesn2*$^{-/-}$ lung. Data show mean ± SEM of n=10mice/group. For statistical analysis, an unpaired student t-test was performed for comparison of lung tissue pathology in control versus knockout mice.

Collectively, these data showed no significant biological differences in *Sesn2*$^{-/-}$ mice compared to *Sesn2*$^{+/+}$ control animals. There were no major differences in inflammatory phenotype, and this was reflected in the histology analysis, where the percentage of alveolar space between murine lungs was comparable with no apparent tissue pathology. Overall, we showed that the global deletion of *Sesn2* had no impact on the baseline condition in mice.

Objective 2: To determine the role of *Sestrin 2* in host immunity during *Mtb* infection using the *Sesn2*$^{-/-}$ mouse model.

3.2. 6-week time course infection in the *Sesn2* Knockout Mouse

The absence of *Sesn2* increased lung myeloid cell populations and tissue pathology in mice.

TB has a chronic disease progression, and therefore time course studies need to be conducted appropriately. To determine the effect of *Sesn2* deficiency and its role in disease progression, we set the minimum infection duration to 6 weeks after infection. *Sesn2*$^{-/-}$ and *Sesn2*$^{+/+}$ littermate controls were infected with 100CFU HN878 intranasally. The mice were monitored for 6 weeks after which they were euthanized and lungs, lymph nodes, and spleen, were sampled for further analysis.

After 6 weeks of infection, we found no differences in body weight change, lung or spleen weight, as well as lung weight index (figure 3.2.1a-c). There were no differences in lung bacterial burdens, however, the burden was increased in the spleen of *Sesn2*$^{-/-}$ mice (figure 3.2.1d). No differences were observed in LN cell numbers, or lung cell numbers in the *Sesn2*$^{-/-}$ mice when compared to the littermate control animals (Figure 3.2.1e and f). This suggests that after 6-weeks of infection, measurements between mice are still comparable with exception of increased dissemination of *Mtb* in the spleen of *Sesn2*$^{-/-}$ mice.

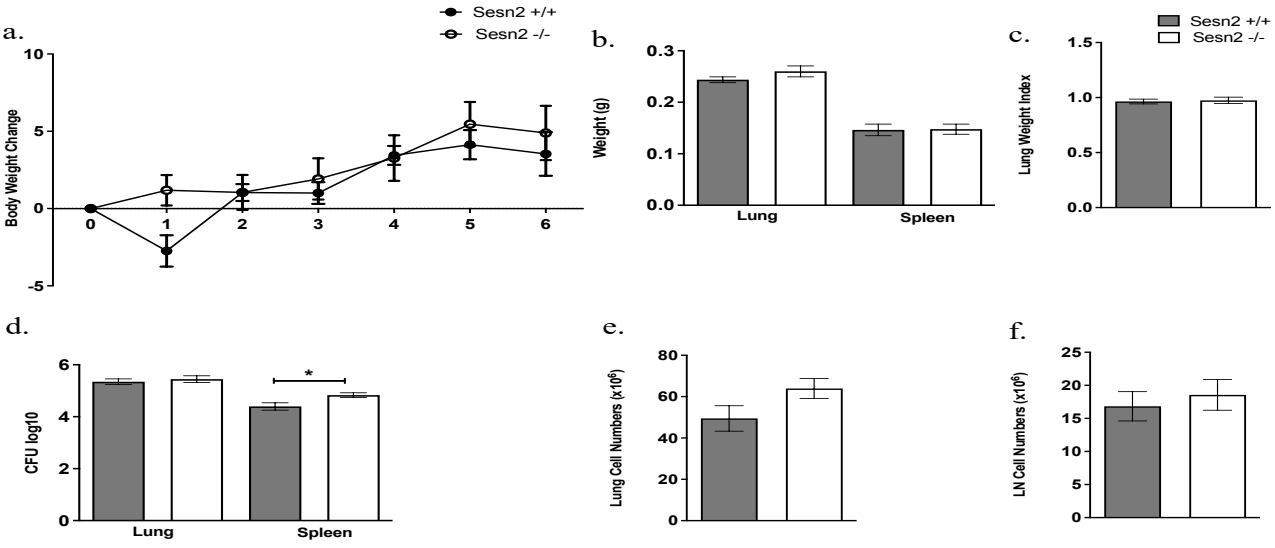

Figure 3.2.1: **The deletion of *Sesn2* increased dissemination of *Mtb* in the spleen of mice at 6-weeks post infection.** Mice were infected with 100 CFUs of HN878 and were sacrificed. The lung and LN were processed into single-cell suspensions to determine cell numbers. The lung and spleen samples were homogenized in tween-saline and plated on 7H11 agar plates to measure bacterial growth. a) Body weight change. b) Total lung and spleen weight. c) Lung weight index. d) Lung and spleen bacterial burdens. e) Total lung cell numbers. f) Total lymph node cell numbers. Data show mean ± SEM of n=12mice/group of two pooled independent experiments. For statistical analysis, an unpaired student t-test was used, for comparison of body weight change, organ weight, CFUs and organ cell numbers in control versus knockout mice, with p-values considered accordingly *p <0.05.

We then analyzed the lung homogenates to determine the immune responses by ELISA. We assessed the following chemokines, pro- and anti-inflammatory cytokines, and growth factors: IFN-γ, IL-12p40, IL-12p70, IL-6, IL-17, IL-1α, IL-1β, TNF, IL-23, IFNβ, TGFβ, IL-4, IL-10, GMCSF, GCSF, CXCL2, CXCL5, CCL2, CCL3, CCL5, CXCL10 and CXCL1. Our analysis revealed no significant differences between the *Sesn2*$^{+/+}$ and *Sesn2*$^{-/-}$ animals at 6-weeks post infection (Figure 3.2.2a-c). Suggesting that at 6-weeks post infection, *Sesn2* deletion does not alter the immune response profile.

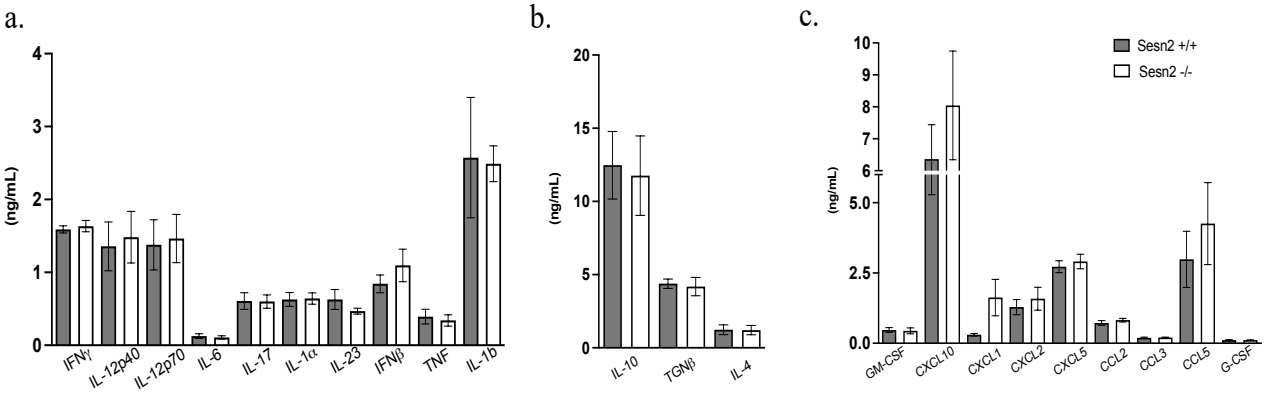

Figure 3.2.2: ***Sesn2* deficiency did not alter immune responses in the lungs at 6-weeks post *Mtb* infection.** Lungs were homogenized to collect supernatants for ELISAs. a) Pro-inflammatory cytokine panel. b) Anti-inflammatory cytokine panel. c) Chemokine and growth factor panel. Data show mean ± SEM of n=12 mice/group of two pooled independent experiments. For statistical analysis, an unpaired student t-test was performed for comparison of cytokines, chemokines, and growth factor levels in control versus knockout mice.

In addition to lung immune responses, we assessed the immune cell recruitment in the lungs of *Sesn2* knockout animals. The analysis of the immune cell populations by flow cytometry showed no significant differences in lung lymphoid populations (Figure 3.2.3a and b) and lymphoid subsets and exhaustion markers (Figure 3.2.3c-f). However, percentage of lung myeloid populations showed increased neutrophils and monocytes and decreased CD103+ DCs in the *Sesn2*$^{-/-}$ mice but absolute cell numbers mirrored the increase in neutrophils and monocytes (Figure 3.2.3g and h). This indicated that after 6 weeks of infection, *Sesn2* deletion had a greater impact on myeloid cell recruitment than on lymphoid populations.

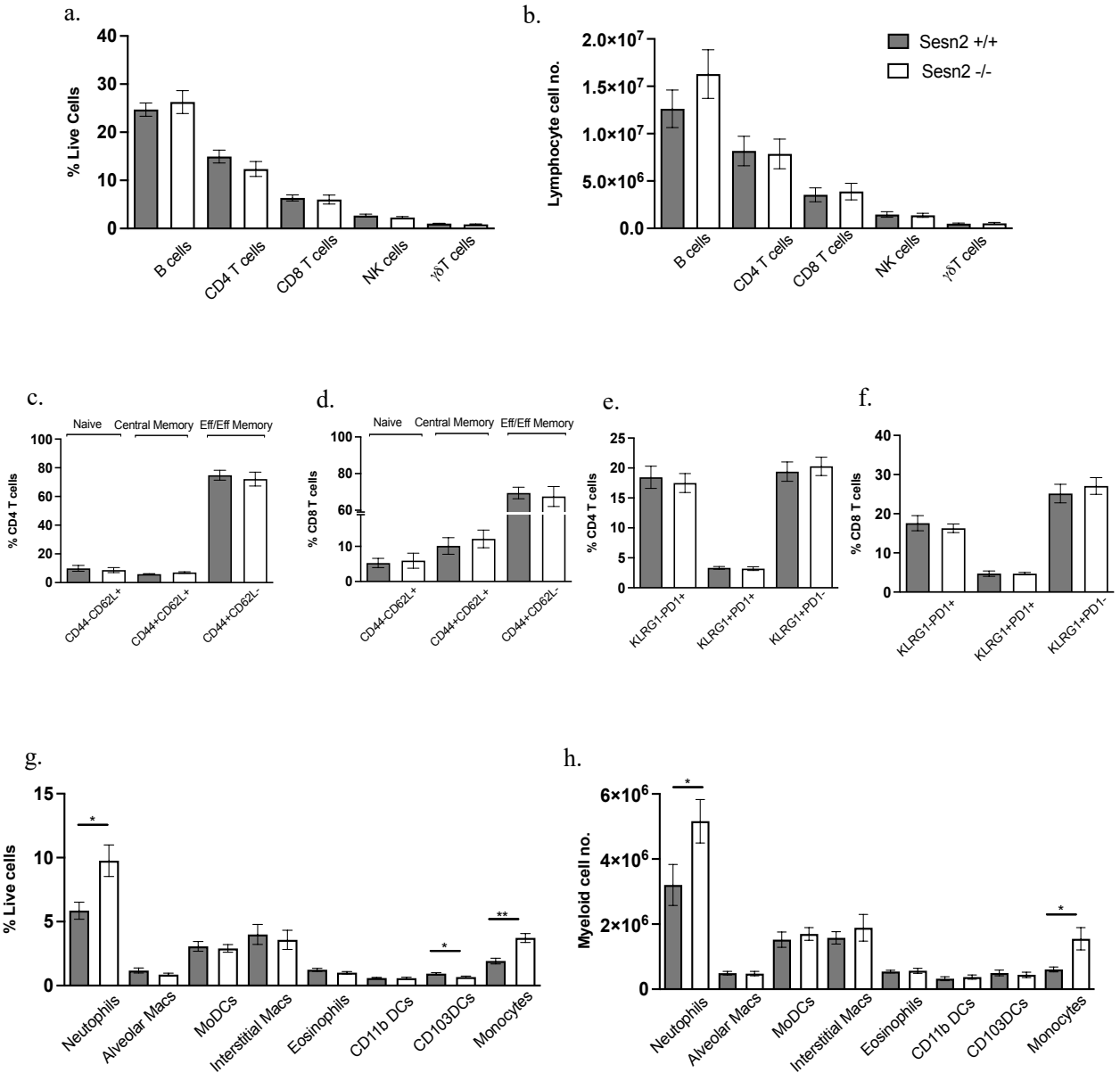

Figure 3.2.3: ***Sesn2*** **knockout mice showed increased myeloid cell populations in the lungs at 6-weeks post** ***Mtb*** **infection.** Lung tissues were harvested to prepare single-cell suspensions, and stained with either a Myeloid or Lymphoid panel, before acquiring cell populations by flow cytometry. a) Lung lymphoid immune cell populations represented as percentages. b) Lung lymphoid populations, represented as absolute cell numbers. c) Lung CD4 T cell subsets. d) Lung CD8 T cell subsets. e) Lung CD4 T cell exhaustion markers. f) Lung CD8 T cell exhaustion markers. g) Lung myeloid immune cell populations represented as percentages. h) Lung myeloid cell populations represented in absolute cell numbers. Data show mean ± SEM of n=12 mice/group of two pooled independent experiments, and statistical analysis was performed using an unpaired student t-test for comparison of immune cell recruitment in control versus knockout mice, with the following p-values as indicators of significance, *p <0.05, **p <0.01.

Besides lungs, lymph nodes were also analyzed for immune cell recruitment by flow cytometry. The results showed an increase in the percentage of NK cells in the *Sesn2*$^{-/-}$ mice, but not absolute cell numbers (figure 3.2.4a and b). Higher CD4 naïve cells and CD8 central memory T cells were observed in the *Sesn2*$^{-/-}$ mice, however, no differences were seen in CD4 and CD8 T cell exhaustion (Figure 3.2.4c-f). Myeloid cell population analysis showed higher percentages of macrophages but lower CD11b migratory DCs and lower MHCII high and low monocytes in the *Sesn2*$^{-/-}$ mice (figure 3.2.4g). In absolute cell number, we found that only the decreased MHCII high and low monocytes were maintained in the *Sesn2*$^{-/-}$ mice (figure 3.2.4h). Overall, we found a decrease in myeloid inflammatory cell recruitment in the lymph nodes of *Sesn2*$^{-/-}$ mice at 6wpi. However, at the same timepoint we observed an increase in lung myeloid populations in the *Sesn2*$^{-/-}$ mice (neutrophils and monocytes) (Figure 3.2.3g and h). Here the difference can perhaps be explained by immune cell compartmentalization between the lungs and LN.

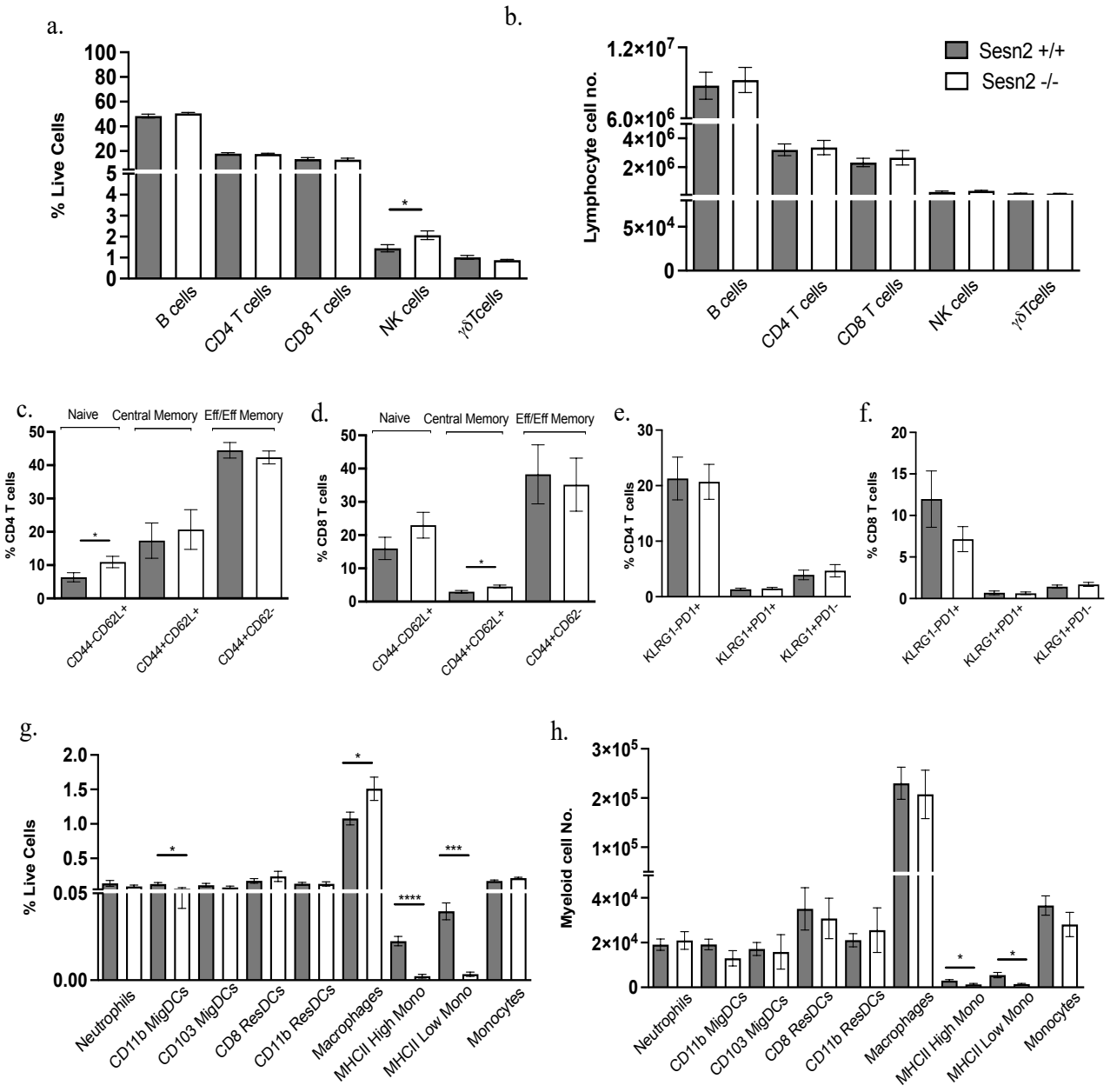

Figure 3.2.4: ***Sesn2*** **knockout mice showed decreased myeloid cell populations in the lymph nodes at 6-weeks post** ***Mtb*** **infection.** Lymph nodes were processed into single-cell suspensions, and stained with either a Myeloid or Lymphoid panel, before acquiring cell populations by flow cytometry a) Lymph node lymphoid immune cell populations represented as percentages. b) Lymph node lymphoid populations, represented as absolute cell number. c) Lymph node CD4 T cell subsets. d) Lymph node CD8 T cell subsets. e) Lymph node CD4 T cell exhaustion markers. f) Lymph node CD8 T cell exhaustion markers g) Lymph node myeloid immune cell populations represented as percentages. h) Lymph node myeloid cell populations represented in absolute cells. Data show mean ± SEM of n=12mice/group of two pooled independent experiments. For statistics, an unpaired t-test was used, for comparison of immune cell recruitment in control versus knockout mice, and the following p values as significant, *p <0.05, ***p <0.001, ****p <0001.

Lastly, we analyzed lung tissue pathology at 6-weeks post-infection, as fibrotic breakdown of lung tissue is a hallmark of TB disease. Histological analysis showed that *Sesn2*$^{-/-}$ mice had significantly decreased free alveolar space compared to their *Sesn2*$^{+/+}$ counterparts (Figure 3.2.5a). As TB progresses, lung tissue becomes fibrotic and breaks down forming caseum and necrotic regions, which decreases lung capacity and function and is represented by a decreased percentage of free alveolar space. This is visible in representative images of *Sesn2*$^{+/+}$ and *Sesn2*$^{-/-}$ lungs (Figure 3.2.5b and c).

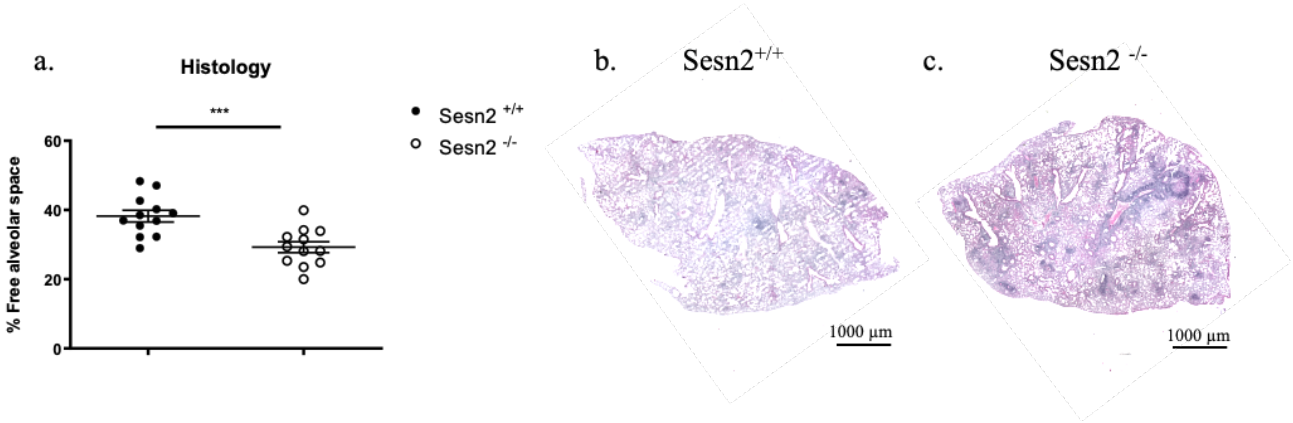

Figure 3.2.5: **The absence of *Sesn2* increased lung pathology after 6-weeks of *Mtb* infection.** Lung lobes were collected and fixed in 10% neutral buffered formalin, stained with H&E and scanned at 20x magnification. a) Quantification of percentage free alveolar space. b) Representative image of *Sesn2*$^{+/+}$ and c) *Sesn2*$^{-/-}$ lung. Data show mean ± SEM of n=12mice/group of two pooled independent experiments. For statistical an unpaired student t-test was used, for comparison of lung tissue pathology in control versus knockout mice, with the following p values denoting significance, ***p <0.001.

Overall, despite comparable bacterial burdens in the lungs, and immune responses, we found increased neutrophilia and monocytes in the lungs of *Sesn2*$^{-/-}$ mice, which may be a contributing factor to the increased lung tissue pathology observed. The most notable result of the 6wpi data, is the increased lung tissue pathology in *Sesn2*$^{-/-}$ mice, as lung pathology is a hallmark of poor disease outcome. These data show that at 6-weeks post-infection, the deletion of *Sesn2*$^{-/-}$ leads to lung pathology in TB infection.

3.3. 12-week time course infection in the *Sesn2* Knockout Mouse

The absence of *Sesn2* increased myeloid and lymphoid cell populations in both lung and lymph nodes and tissue pathology in mice.

Given increased lung tissue pathology in the *Sesn2*$^{-/-}$ mice after 6wpi, we further extended the time point to 12wpi, to assess whether the magnitude of differences increase. To determine the effect *Sesn2* deletion has during a longer infection timepoint, we infected *Sesn2*$^{+/+}$ and *Sesn2*$^{-/-}$ mice with HN878 *Mtb* intranasally with 100 CFU. Mice were monitored for the 12-week duration of the experiment after which they were euthanized, and lungs, spleen and lymph nodes were collected for further analysis.

At 12wpi, we found no significant change in body weight difference, lung and spleen weights, lung weight index, and bacterial burdens, however, there were significantly increased lung and lymph node cell numbers in the *Sesn2*$^{-/-}$ mice compared to the *Sesn2*$^{+/+}$ controls (Figure 3.3.1a-f). This indicated that deletion of *Sesn2* increased total cell numbers in lung and lymph nodes during prolonged infection (12 weeks).

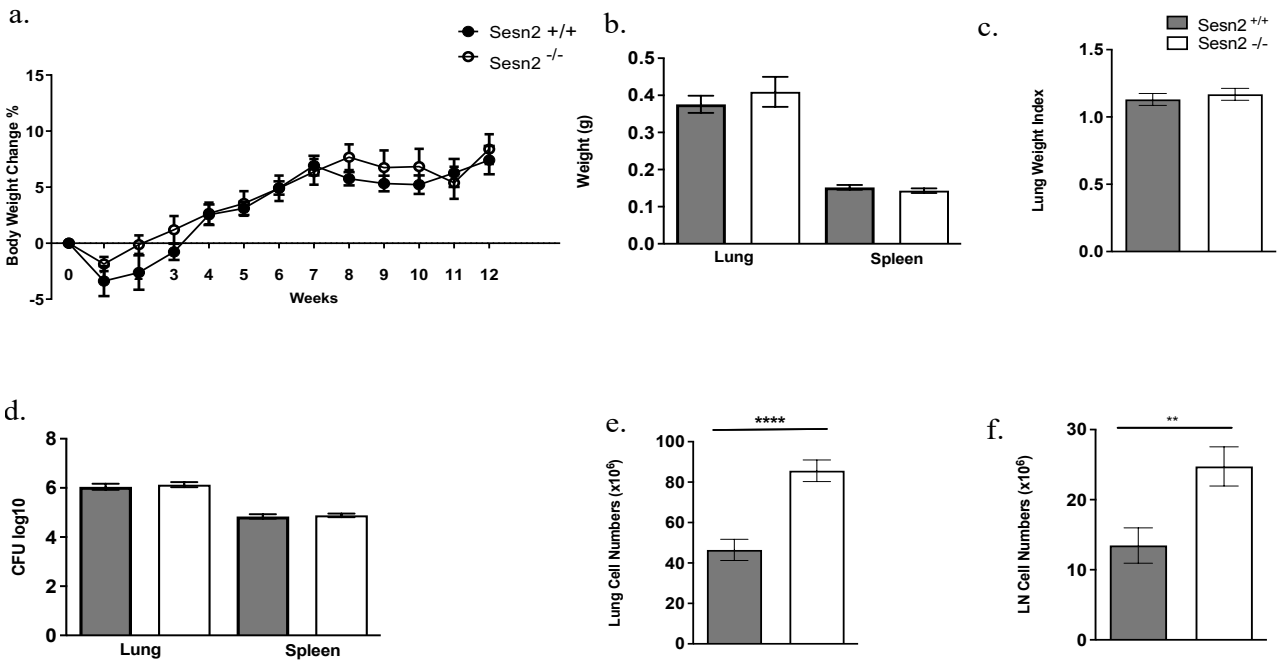

Figure 3.3.1: **The deletion of *Sesn2* increased lung and lymph node cell numbers after 12-weeks of *Mtb* infection.** Mice were infected with 100 CFUs of HN878 and were sacrificed. The lung and LN samples were processed into single-cell suspensions before counting. To measure bacterial growth, the lung and spleen samples were homogenized in tween-saline and grown on 7H11 agar plates. a) Body weight change. b) Total lung and spleen weight. c) Lung weight index. d) Lung and spleen bacterial burden. e) Total lung cell numbers. f) Total lymph node cell numbers. Data show mean ± SEM of n=11mice/group of two pooled independent experiments. For statistical analysis, an unpaired student t-test was used, for comparison of body weight change, organ weight, CFU and organ cell numbers in control versus knockout mice, with p-values considered accordingly, **p <0.01, ****p <0001.

We further analyzed immune responses in the lungs, which showed that there were no significant differences across the pro-inflammatory and anti-inflammatory cytokine panel, nor the chemokines or growth factors that were investigated as indicated (figure 3.3.2a-c). This suggests that even during 12-weeks of infection, *Sesn2* deletion has an insignificant effect on immune response *in vivo*.

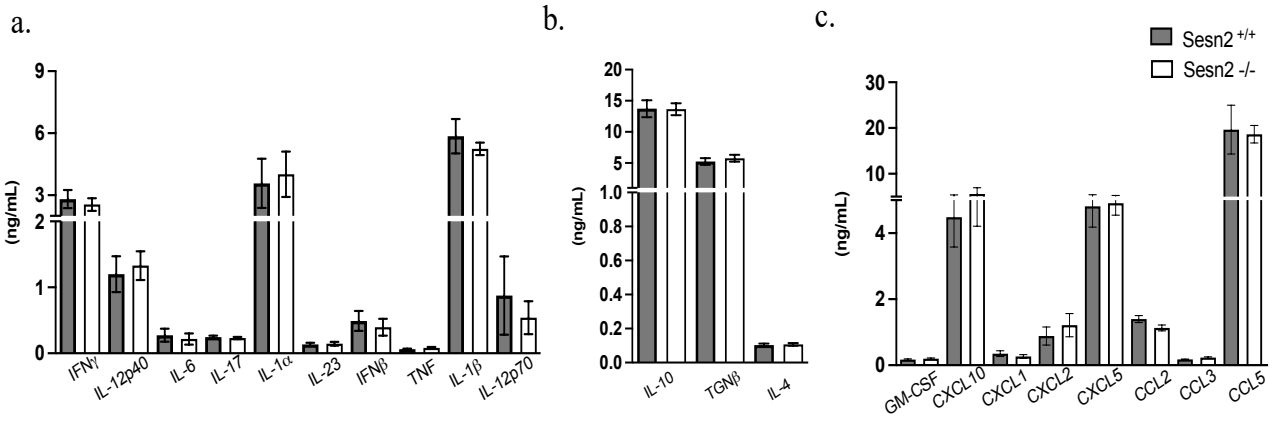

Figure 3.3.2**: *Sesn2* deficiency did not alter immune responses in the lungs after 12-weeks of *Mtb* infection.** Lung lobes were homogenized, and supernatants were collected for ELISA analysis. a) Pro-inflammatory cytokine panel. b) Anti-inflammatory cytokine panel. c) Chemokine and growth factor panel. Data show mean ± SEM of n=11mice/group of two pooled independent experiments. For statistical analysis, an unpaired student t-test was performed for comparison of cytokines, chemokines, and growth factor levels in control versus knockout mice.

Using flow cytometry to distinguish inflammatory immune populations we noticed that overall lung lymphoid populations were increased in the *Sesn2*$^{-/-}$ mice. Significant alterations were observed with B cells and gamma delta T cells exhibiting a robust increase in *Sesn2*$^{-/-}$ mice (Figure 3.3.3a). Absolute cell numbers had a consistent trend with a significant increase in all lymphoid subpopulations in the *Sesn2*$^{-/-}$ mice (Figure 3.3.3b). However, T cell subsets and exhaustion markers showed no significant differences (Figure 3.3.3c-f). The increased numbers of myeloid cells in the lung were not observed when comparing cell percentages (Figure 3.3.3g). However, absolute myeloid cell numbers showed significantly increased neutrophils, interstitial macrophages, eosinophils, alveolar macrophages, and CD11b DCs in the *Sesn2*$^{-/-}$ mice (Figure 3.3.3h). These results strongly suggest that the absence of *Sesn2* drives an increase in lymphoid and myeloid cell populations.

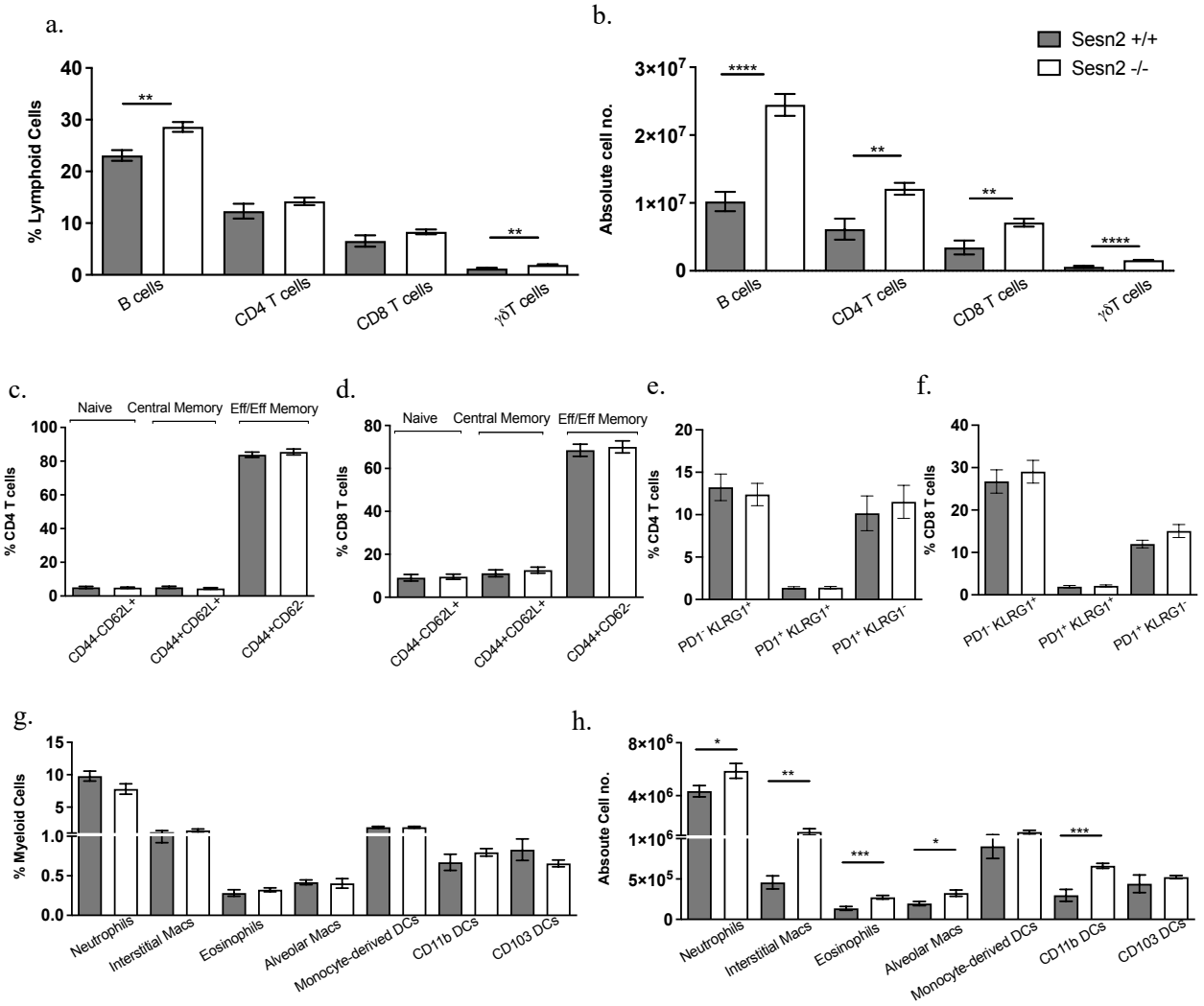

Figure 3.3.3: ***Sesn2* knockout mice showed increased lymphoid and myeloid cell populations in the lungs after 12-weeks of *Mtb* infection.** Lung tissues were processed into single-cell suspensions and stained with either a Myeloid or Lymphoid panel, before acquiring cell populations by flow cytometry. a) Lung lymphoid immune cell populations represented as percentages. b) Lung lymphoid populations, represented as absolute cell numbers. c) Lung CD4 T cell subsets. d) Lung CD8 T cell subsets. e) Lung CD4 T cell exhaustion markers. f) Lung CD8 T cell exhaustion markers. g) Lung myeloid immune cell populations represented as percentages. h) Lung myeloid cell populations represented in absolute cell numbers. Data show mean ± SEM of n=11mice/group of two pooled independent experiments. Statistical analysis was performed using an unpaired student t-test for comparison of immune cell abundance in control versus knockout mice, with the following p-values denoting significance, *p <0.05, **p <0.01, ***p <0.001, **** p <0001.

Similar, analysis was performed in lymph nodes. We found no significant differences in the percentages of lymphoid subpopulations in the draining lymph nodes, however, absolute cell numbers showed significantly higher lymphocyte populations such as B cells, CD4 and CD8 T cells, and gamma delta T cells in the *Sesn2*$^{-/-}$ mice (Figure 3.3.4a and b). Within T-cell populations,

however, memory and exhaustion phenotypes did not differ between mice (Figure 3.3.4c-f). This suggests that deletion of *Sesn2* drives increased lymphoid cell recruitment, but not percentages, in the lymph nodes, consistent with the increased total lymph node cell numbers (Figure 3.3.1f) in the *Sesn2*$^{-/-}$ mice.

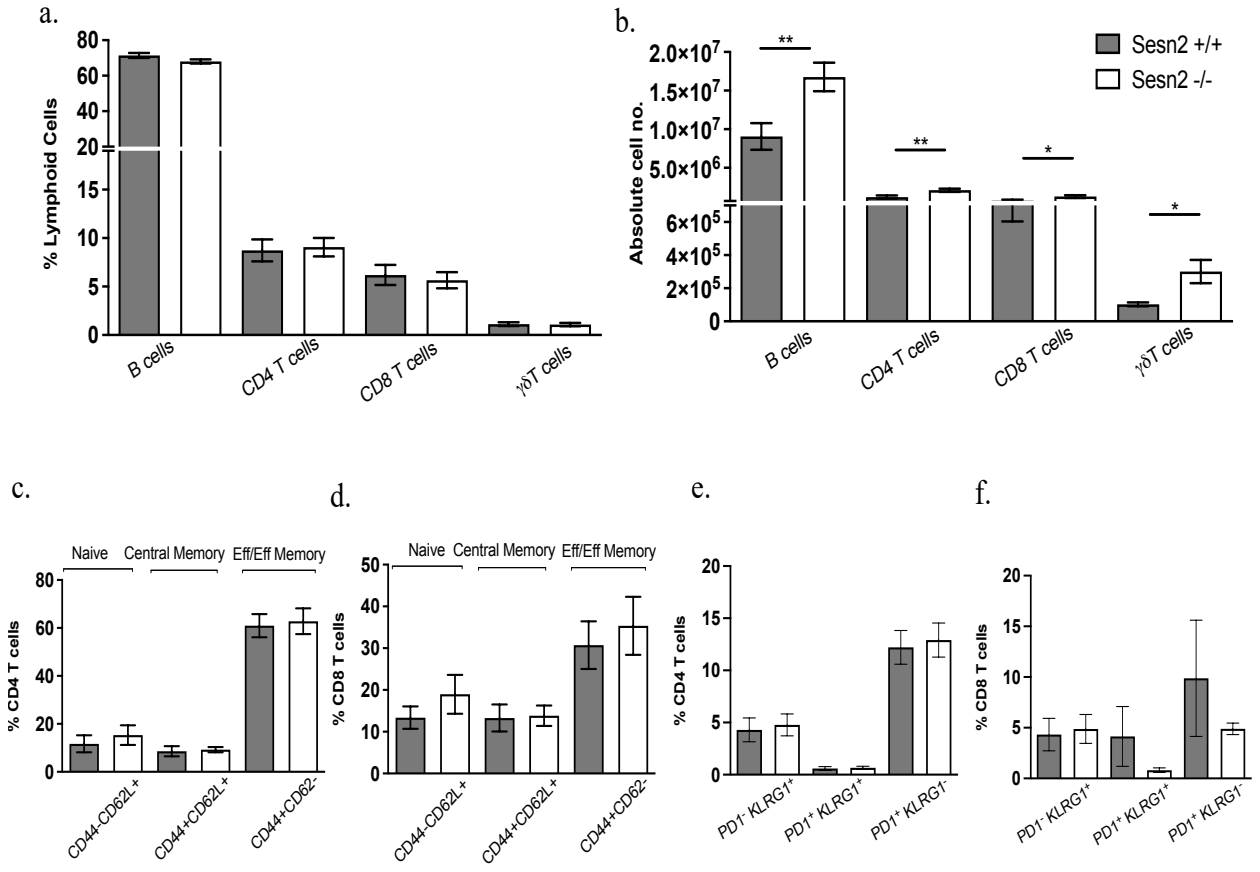

Figure 3.3.4: ***Sesn2* knockout mice showed increased lymphocyte cell numbers in the lymph nodes after 12-weeks of *Mtb* infection.** Lungs were processed into single-cell suspensions and stained with a Lymphoid panel, before acquiring cell populations by flow cytometry. a) Lymph node lymphoid immune cell populations represented as percentages. b) Lymph node lymphoid populations, represented as absolute cell number. c) Lymph node CD4 T cell subsets. d) Lymph node CD8 T cell subsets. e) Lymph node CD4 T cell exhaustion markers. f) Lymph node CD8 T cell exhaustion markers. Data show mean ± SEM of n=11mice/group of two pooled independent experiments. Statistical analysis was performed using an unpaired student t-test for comparison of immune cell abundance in control versus knockout mice, with the following p-values denoting significance, *p <0.05, **p <0.01.

To investigate whether extended infection (12 weeks) influences lung pathology, we determined the lung tissue damage and quantified the percentage of free alveolar space. Lungs with less alveolar space are indicative of more damage and fibrotic tissue. *Sesn2* deficient mice had significantly less free alveolar space, in agreement with the increased lung cell numbers and

pathology (Figure 3.3.5a-c). This indicates that the ablation of *Sesn2* drives lung tissue pathology after 12-weeks of *Mtb* infection.

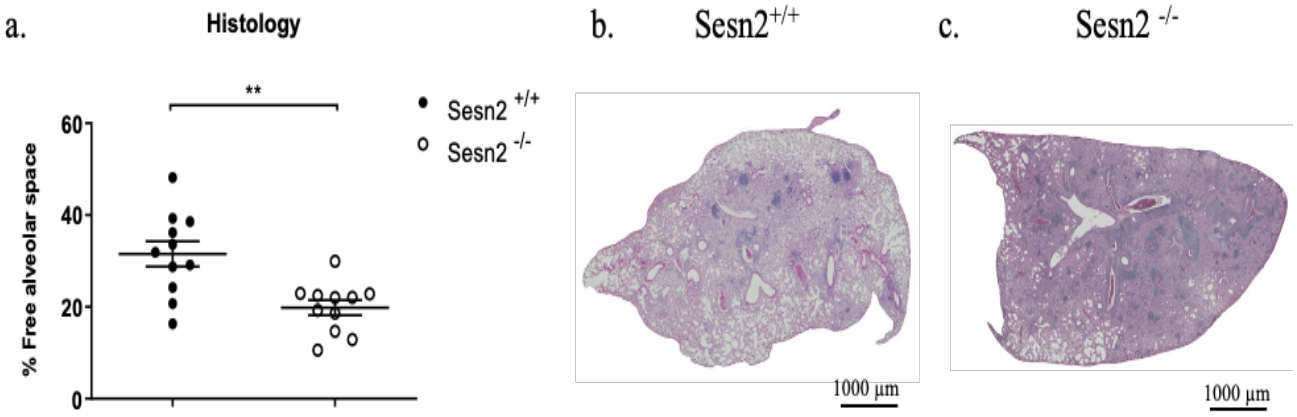

Figure 3.3.5: **The absence of *Sesn2* increased lung pathology after 12 weeks of *Mtb* infection.** Lung lobes were collected and fixed in 10% neutral buffered formalin, stained with H&E and scanned at 20x magnification. a) Quantification of percentage free alveolar space. b) Representative image of *Sesn2*$^{+/+}$ and c) *Sesn2*$^{-/-}$ lung. Data show mean ± SEM of n=11mice/group of two pooled independent experiments. For statistical analysis, an unpaired student t-test was used, for comparison of lung tissue pathology in control versus knockout mice, with the following p values representing significance, **p <0.01.

Overall, these data show a distinct profile in *Sesn2*-deficient mice after 12-weeks of infection. Specifically, increased lung and LN total cell numbers, increased immune cell recruitment and in concordance, increased lung tissue pathology in the *Sesn2*$^{-/-}$ mice. Demonstrating the potential role of *Sesn2* in regulating immune cell recruitment and host lung tissue pathology during 12-weeks of infection with *Mtb*.

3.4. To determine the effect of the absence of *Sestrin 2* on survival of mice during TB disease.

***Sesn2*-deficient mice showed enhanced mortality to *Mtb* infection.**

To understand the *Sesn2* ablation influence the survival of mice in TB disease, we infected *Sesn2*$^{+/+}$ and *Sesn2*$^{-/-}$ mice with 100 CFU of HN878 *Mtb* intranasally, monitored daily and were euthanized

when they reached the humane endpoint. The survival study showed that *Sesn2*$^{-/-}$ mice succumbed to infection earlier than their *Sesn2*$^{+/+}$ counterparts. The mean survival of the *Sesn2*$^{-/-}$ mice, at which 50% of the animals remain, is 26 weeks, compared to the *Sesn2*$^{+/+}$ mice which reach their 50% survival at 33 weeks (Figure 3.4.1). Overall, this finding showed that the absence of *Sesn2* results in increased mortality to TB disease.

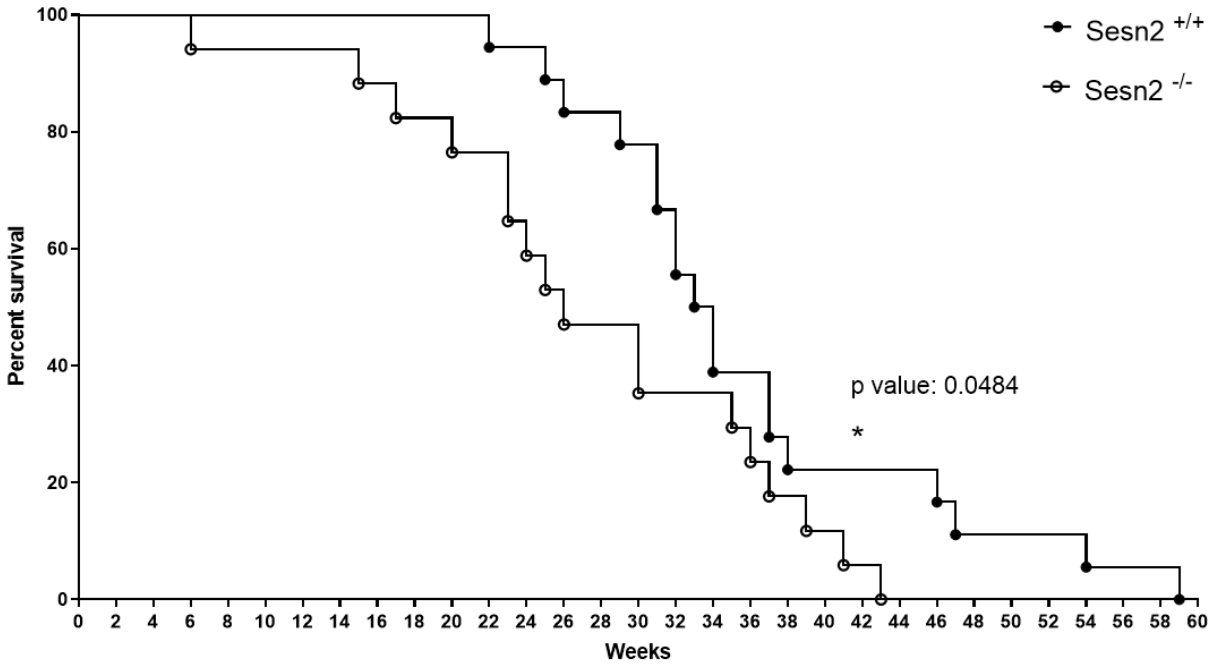

Figure 3.4.1: **Deletion of *Sesn2* increased mortality during TB disease in mice.** Mice were infected with 100 CFU *Mtb* HN878 and monitored closely. At individual humane endpoints, each mouse was euthanized, and the time point was recorded. Data show mean ± SEM of n=18-19mice/group of two pooled independent experiments. For statistical analysis, survival curve comparison was done using the Mantel-Cox test between control versus knockout mice, with the following p values for significance *p <0.05.

Objective 3: Mechanistic studies to determine pathways and the regulation of *Sestrin 2* in macrophages using the *Sesn2*$^{-/-}$ mouse model.

3.5. *In vitro* studies to determine the mechanistic role of *Sestrin 2* in macrophages.

***Sesn2*-deficient macrophages increased bacterial growth, ROS production, cell death, pro-inflammatory cytokine responses and glycolysis.**

We have shown that the *Sesn2*$^{-/-}$ mice have increased lung pathology and reduced survival during TB disease *in vivo* produced by *Mtb* HN878. However, the molecular mechanisms or contributing factors that drive the susceptibility remain elusive. We, therefore, conducted *in vitro* macrophage infection experiments where we harvested BMDMs from *Sesn2*$^{+/+}$ and *Sesn2*$^{-/-}$ mice and infected them with HN878 *Mtb* (MOI of 0.5). Thereafter, we investigated bacterial burden, cytotoxicity, cell viability, pro-inflammatory cytokines and ROS production, as inflammatory markers which may be contributors to pathology at a cellular level.

Interrogating the *Sesn2*$^{-/-}$ mice *in vivo* showed similar bacterial burden except increased at 6wpi in the *Sesn2*$^{-/-}$ spleen. Macrophages are essential innate cells in TB hence we compared bacterial growth at a cellular level. Concurrently, searching for other inflammatory factors that could be driving the increased susceptibility. To measure bacterial burden in macrophages, we set 3dpi and 6dpi time points. At 3dpi, we found that CFUs were significantly increased in the *Sesn2*$^{-/-}$ macrophages compared to the *Sesn2*$^{+/+}$ cells, however, at 6dpi this difference was abolished (Figure 3.5.1a). Indicating that *Sesn2* deficient macrophages are less capable of controlling *Mtb* early after infection.

Our *in vivo* results also established increased lung tissue pathology during infection in the absence of *Sesn2*, we therefore investigated cell death in macrophages *in vitro* using the release of cytosolic LDH as a marker of cytotoxicity. Our data showed that at 1dpi and 2dpi the *Sesn2*$^{-/-}$ macrophages had a higher level of cytotoxicity when compared to control macrophages (Figure 3.5.1b).

To understand drivers contributing to increased cell death and lung tissue pathology, we assessed various inflammatory markers. Since *Sesn2* has known antioxidant properties and regulates ROS through multiple mechanisms, we measured ROS levels in macrophages, knowing its damaging effect on cells. To assess whether ROS could be a driver of cell death, we set corresponding time points at 1- and 2dpi, as ROS has a short half-life, and its effects can be detected earlier than *Mtb* killing. Here, we showed at 1- and 2dpi, ROS was significantly elevated in the *Sesn2* deficient

macrophages compared to their controls, suggesting that ROS may be involved in the increased cell death. Interestingly, to validate our cell death data, we conducted cell viability analysis using CellTiter Blue dye, which showed increased viability in the *Sesn2*$^{-/-}$ mice despite the increased cytotoxicity (Figure 3.5.1b and d). CellTiter Blue dye fluorescently measures the reduction of resazurin dye in metabolically active cells, instead of a direct measure of viability (137). Suggesting a closer look into metabolomics may be necessary to understand the interplay between *Sesn2*, ROS and cell death.

Cytokine environment during TB disease is a crucial factor in immune control and protection. We measured a panel of cytokines. The culture supernatants were collected at 3- and 6dpi to determine immune response. Pro-inflammatory cytokine analysis showed increased IL-1β at 3- and 6-days post infection and increased TNF at 3 days post infection in *Sesn2*$^{-/-}$ macrophages (Figure 3.5.1e and f). In contrast, IL-6 levels showed a decrease in the *Sesn2*$^{-/-}$ macrophages at 3- and 6-days post infection (Figure 3.5.1g and h). No differences were seen in nitrite levels between macrophages (Figure 3.5.1i). Apart from IL-6, there was a general increase in pro-inflammatory markers in the *Sesn2* deficient macrophages.

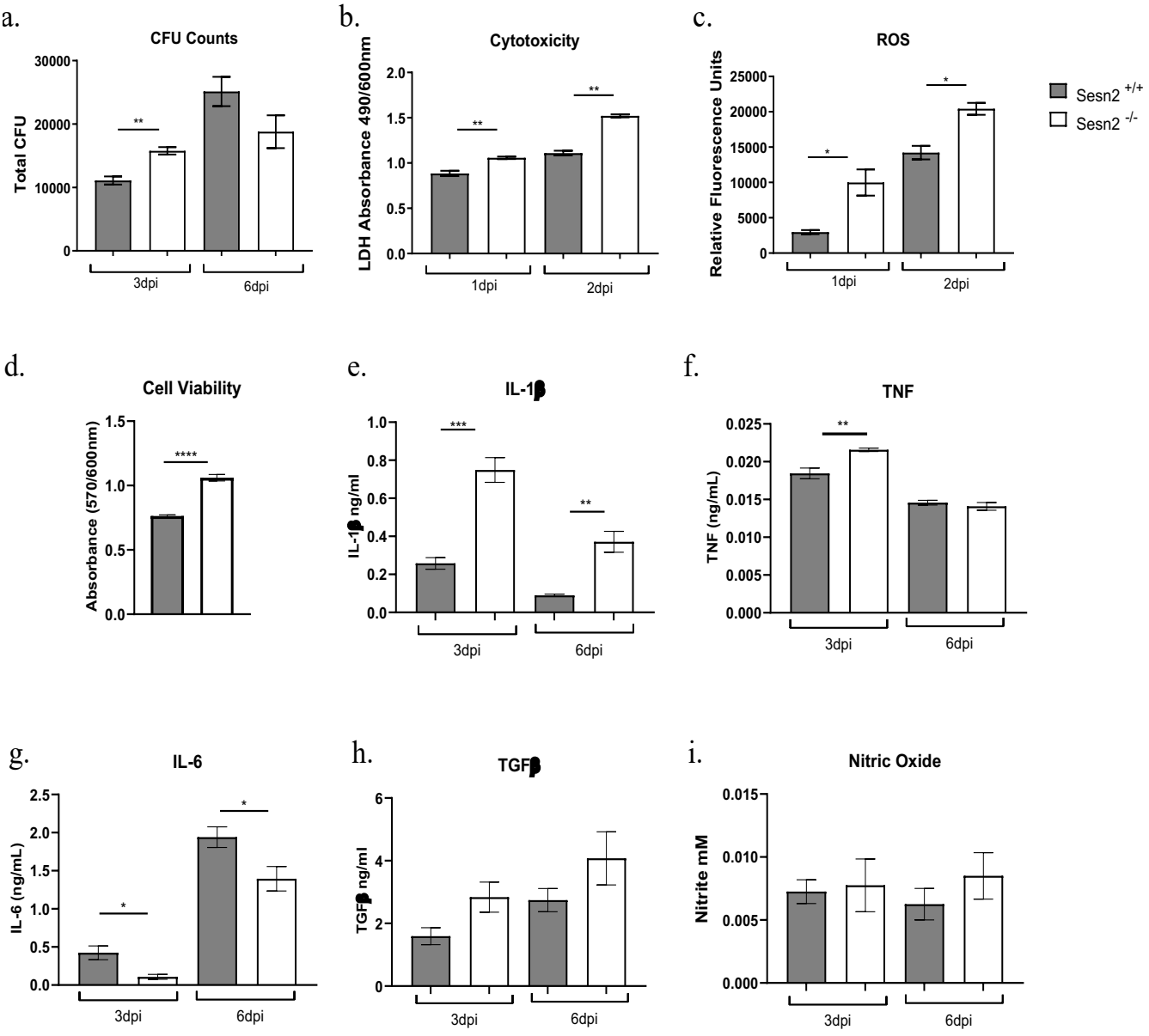

Figure 3.5.1: ***Sesn2*-deficient macrophages showed increased bacterial growth, ROS production and pro-inflammatory cytokine responses *in vitro*.** BMDMs were harvested and generated, after which, $1x10^5$ cells were seeded, and infected with *Mtb* HN878 at an MOI of 0.5. a) Total bacterial burden at 3 days and 6 days post infection. b) Cytotoxicity measured by LDH Assay at 1- and 2-days post infection. c) ROS detection at 1- and 2-days post infection, measured by using the CellROX Assay kit. d) Cell Viability at 2 days post-infection, measured by using Cell Titer Blue dye. e) IL-1β, f) TNF, g) IL-6 and h) TGFβ cytokine secretion measured by ELISA at 3- and 6-days post infection. i) Measurement of nitrite as a proxy of nitric oxide levels using the Promega Griess Reagent. Data shown as mean ± SEM of representative of 2-3 independent experiments. An unpaired student t-test was used for comparison of CFUs, cytotoxic, viability, ROS and cytokine levels in control versus knockout mice, with the p values for significance, *p <0.05, **p <0.01, ***p <0.001, ****p<0.0001.

To elucidate any compensatory or regulatory roles of the Sestrin genes, we extracted RNA at 0-, 4-, 8- and 24-hours post-infection in BMDMs. We conducted qRT-PCR to detect differential expression of the Sestrin family and associated genes. Analysis of *Sesn2* expression confirmed successful knockout, where *Sesn2* expression was not detectable in the *Sesn2*$^{-/-}$ macrophages (Figure 3.5.2a). There were no significant differences in *Sesn1* expression post-infection, however, at a naïve state, *Sesn1* expression was increased in *Sesn2*$^{-/-}$ macrophages (Figure 3.5.2b). Moreover, the expression of *Sesn1* generally decreased during *Mtb* infection (Figure 3.5.2b). *Sesn3* expression was increased in *Sesn2*$^{-/-}$ macrophages prior to infection (0 hours) and at 8 hours post infection. Nevertheless, *Sesn3* expression, in general, was detected at a very low level compared to *Sesn1* and *Sesn2* (Figure 3.5.2c). *Foxo3*, a transcription factor of *Sesn1* and *Sesn3*, showed no significant differential expression in *Sesn2*$^{-/-}$ macrophages (Figure 3.5.2d). Given that ROS levels were elevated in the *Sesn2*$^{-/-}$ macrophages, we assessed the expression of the *Cybb* gene, which encodes the cytochrome b-245 beta chain, that forms a subunit of the enzyme complex NADPH oxidase. In turn, NADPH oxidase catalyzes the transfer of electrons to O_2 thus generating superoxides and H_2O_2 (138). Our analysis showed that *Cybb* was only elevated in the *Sesn2*$^{-/-}$ BMDMs at a naïve state, but not during *Mtb* infection (Figure 3.5.2e). These gene expression kinetic assays showed us that there is minimal genetic compensation from other members of *Sesn* family in the absence of the *Sesn2* in macrophages during *Mtb* infection.

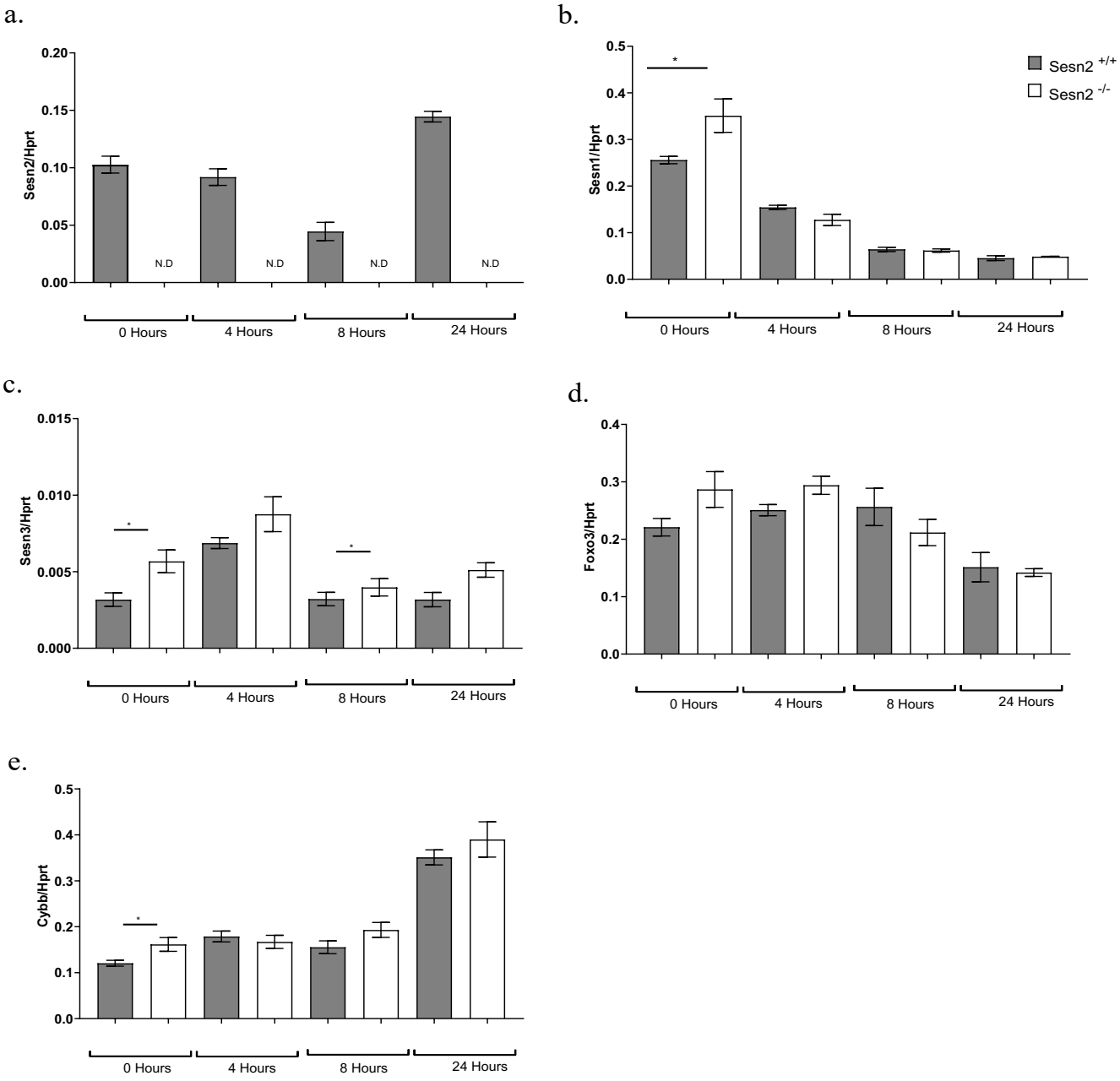

Figure 3.5.2: **The expression of other *Sestrin* family gene members in *Sesn2*$^{-/-}$ BMDMs.** BMDMs were generated and harvested, after which cells were infected with an MOI of 0.5. RNA was collected and extracted from the cells using Trizol, described in Methods. cDNA was synthesized, and qRT-PCRs performed for each gene of interest, using *Hprt* as the housekeeping gene. a) *Sesn2* expression. b) *Sesn1* expression. c) Expression of *Sesn3* in *Sesn2*$^{+/+}$ and *Sesn2*$^{-/-}$ BMDMs. d) Expression of transcription factor *Foxo3* and e) Expression of ROS associated gene *Cybb* in *Sesn2*$^{+/+}$ and *Sesn2*$^{-/-}$ BMDMs. Data show mean ± SEM of n=4/group. For statistical analysis, an unpaired student t-test was used to compare gene expression between control versus knockout mice, and p values were referred to for significance, *p <0.05.

Given the role of *Sesn2* in cellular metabolism, and our increased cell viability and ROS in *Sesn2*$^{-/-}$ macrophages, we performed cell flux experiments using the Seahorse Analyzer to understand

how *Sesn2* affects macrophage energy metabolism during *Mtb* infection (122). Using the Real-Time ATP Rate Assay, we quantified the ATP production rate between *Sesn2*$^{+/+}$ and *Sesn2*$^{-/-}$ BMDMs at a naïve state and 1-day post-infection. Moreover, the Seahorse Assay allowed us to quantify the total ATP production rate, which could be divided between glycolytic and mitochondrial ATP production (oxidative phosphorylation). The Real-Time ATP Rate Assay uses the combination of metabolic inhibitors, oligomycin and rotenone/antimycin A, which are injected at specific points in the assay to inhibit ATP synthase and complex I and III in the electron transport chain. Simultaneously, the Oxygen Consumption Rate (OCR) and Extracellular Acidification Rate (ECAR) are measured dynamically in real-time. Since glycolysis and oxidative phosphorylation are the predominant methods of ATP production, by sequential inhibition, the assay can distinguish between the two methods and provide insight into the cell's metabolic state and ability to transition during stressful conditions (139).

Our primary comparison was the total ATP production rate between the *Sesn2*$^{+/+}$ and *Sesn2*$^{-/-}$ macrophages, to gauge the metabolic activity of the cells. At a naïve state *Sesn2*$^{-/-}$ cells showed a significantly increased total ATP production rate compared to control macrophages (Figure 3.5.3). This trend was consistent during infection, where the total ATP production rate was significantly increased in the *Sesn2*$^{-/-}$ macrophages (Figure 3.5.3). This suggests that *Sesn2*-deficient macrophages consistently show elevated metabolic activity compared to control macrophages.

Interestingly, at 1dpi, the total ATP production rate significantly increased in both *Sesn2*$^{+/+}$ and *Sesn2* $^{-/-}$ macrophages compared to their respective naïve state. *Sesn2*$^{+/+}$ macrophages, at a naïve state elicited an ATP rate of 24.48 pmol/min which increased to 50.3 pmol/min during infection, and *Sesn2*$^{-/-}$ cells increased from 40.92 at a naive state to 66.01 pmol/min post infection (Figure 3.5.3). Moreover, the mode of ATP production showed that both *Sesn2*$^{-/-}$ and *Sesn2*$^{+/+}$ macrophages favored glycolysis over mitochondrial respiration, but *Sesn2*-deficient macrophages displayed glycolytic dependency to a greater extent than control macrophages, at naïve and infected state. (Figure 3.5.3). Notably, *Mtb* infection exaggerated the glycolytic shift in *Sesn2*$^{-/-}$ and *Sesn2*$^{+/+}$ macrophages. This indicates that *Mtb* may influence increasing metabolic activity and reprograming energetics of macrophages, and *Sesn2* deficiency potentiates glycolysis in macrophages.

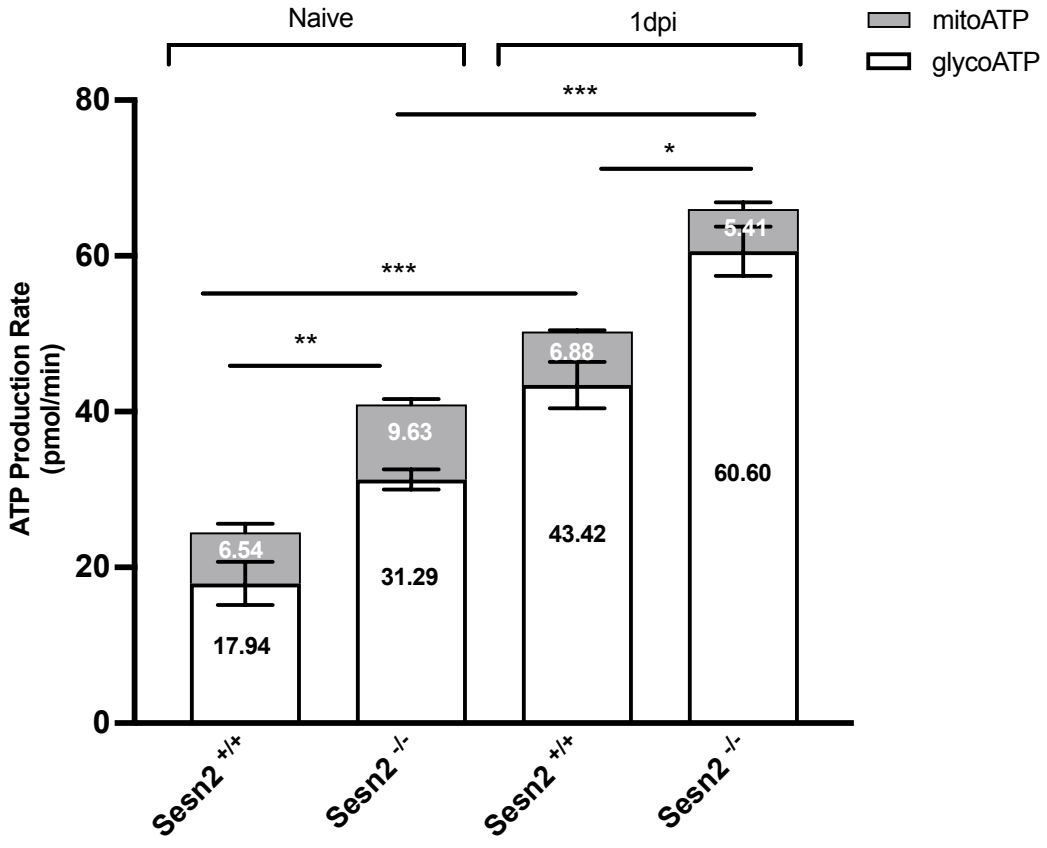

Figure 3.5.3: **Deletion of *Sesn2* increased total ATP production rate and glycolysis in BMDMs.** After BMDMs were generated, harvested, and seeded, they were infected with *HN878* at an MOI of 0.5. Using the Real-Time ATP Rate Assay and Seahorse Analyzer, we quantified the ATP production rate at a naïve state and 1-day post-infection. Data from naïve and 1dpi experiments showed the total ATP production rate and distinguished between mitochondrial versus glycolytic production of ATP. a) Metabolic state of *Sesn2*$^{+/+}$ and *Sesn2*$^{-/-}$ BMDMs at naïve and 1dpi. Data show mean ± SEM of n=2-3 replicates and representative of three independent experiments. For statistical analysis an ANOVA was performed comparing ATP production rate control versus knockout mice, and corrected for multiple comparisons, with the following p values for significance, *p <0.05, **p <0.01, ***p<0.001.

The Seahorse Analyzer also facilitates a measure that reflects the bioenergetics of the cell using the OCR and ECAR values. A further look into bioenergetics using the XF Real-Time ATP Rate Assay showed that at a naïve state, *Sesn2*$^{+/+}$ macrophages leaned towards a more energetic/glycolytic state and were closely associated with the *Sesn2*$^{-/-}$ macrophages (Figure 3.5.4a). However, after *Mtb* infection, *Sesn2*$^{+/+}$ macrophages transitioned to a more quiescent state, and in contrast, *Sesn2*$^{-/-}$ macrophages remained in an energetic state (Figure 3.5.4b). *Sesn2*$^{-/-}$

macrophages have therefore displayed both an increase in total ATP production rate compared to their wildtype counterparts, increased glycolysis, and a distinct energetic profile during infection (Figure 3.5.3 and Figure 3.5.4a and b). Indicating the role of *Sesn2* in regulating metabolism and proposing a link with dysregulated metabolism during *Mtb* infection.

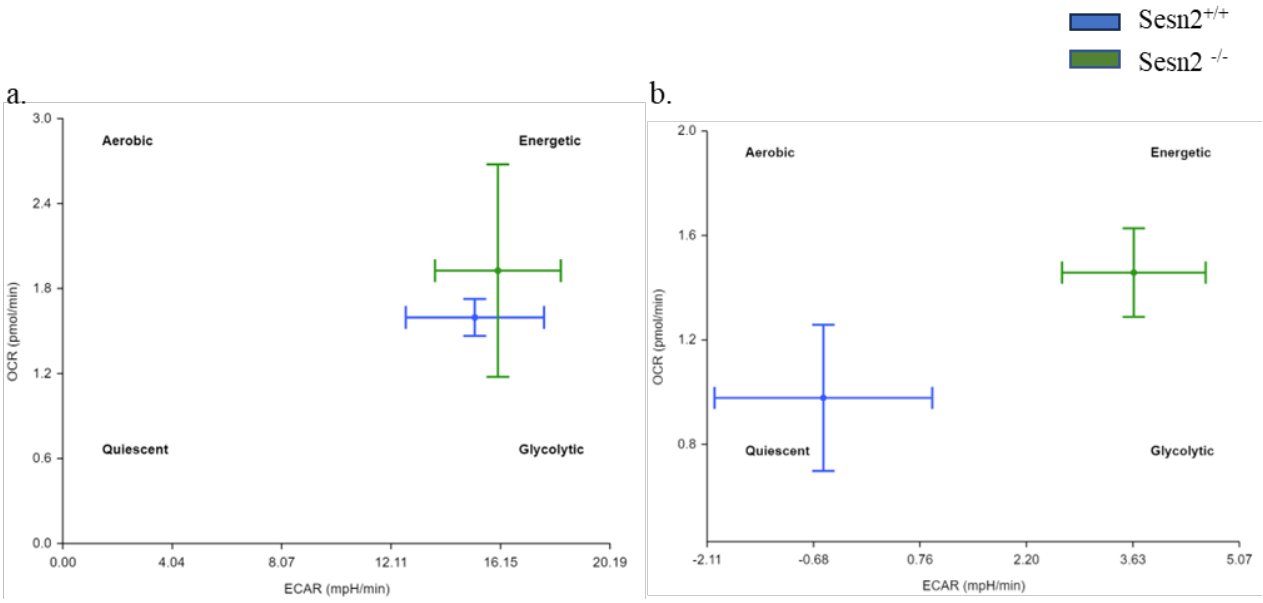

Figure 3.5.4: ***Sesn2*-deficient BMDMs remained in an energetic state after *Mtb* infection.** BMDMs were infected with *HN878* at an MOI of 0.5. Using the Real-Time ATP Rate Assay and Seahorse Analyzer, we analyzed the energetic profile of *Sesn2*$^{+/+}$ and *Sesn2*$^{-/-}$ BMDMs at a naïve state and after 1-day of infection. a) Bioenergetic state of naïve *Sesn2*$^{+/+}$ (blue) and *Sesn2*$^{-/-}$ (green) BMDMs. b) Bioenergetic state of infected *Sesn2*$^{+/+}$ (blue) and *Sesn2*$^{-/-}$ (green) BMDMs. Data representative of 2-3 experiments and analyzed using Seahorse Analytics online software.

Here, we have shown that *Sesn2* deletion in macrophages potentiates a more inflammatory phenotype, with increased pro-inflammatory markers that may be contributing to increased cell death in macrophages, and subsequent increased bacterial burden. Moreover, we have shown that *Sesn2* deletion led to increased metabolic activity. Since ROS is a natural byproduct of metabolism, we propose a possible explanation for the increased ROS in *Sesn2*$^{-/-}$ macrophages. With ROS having known harmful effects on cells, these data are consistent with our hypothesis of ROS-mediated cell death, which is driven by dysregulated increased metabolism in the absence of *Sesn2*. Collectively, these data have shown at a cellular level, the potential role of *Sesn2* as a regulator of inflammatory responses that contribute to TB disease severity.

Objective 4: Characterization of the *LysM*^{cre}*Sesn1*$^{flox/flox}$ macrophage-specific knockout mice.

3.6. Characterization of the *LysM*^{cre}*Sesn1*$^{flox/flox}$ Mouse

The macrophage-specific deletion of *Sesn1* had no major effect on immune response and lung pathology in naïve mice.

Given the important role of macrophages in tuberculosis, we investigated whether a macrophage-specific deletion of *Sestrin* 1 would alter the outcome of TB disease. To this end, the macrophage-specific *Sesn1* knockout (*LysM*^{cre}*Sesn1*$^{flox/flox}$) mouse was generated. Naïve *LysM*^{cre}*Sesn1*$^{flox/flox}$ and *Sesn1*$^{flox/flox}$ littermate control mice, aged 8-12 weeks old were euthanized, and organs collected for characterization, to determine whether the deletion of *Sesn1* in macrophages caused any baseline defect.

From each tissue (lung, spleen, thymus and liver), we extracted RNA to confirm the knockdown of the *Sesn1* gene. Our qRT-PCR analysis showed significantly lower expression of *Sesn1* gene expression in the lung, spleen and liver tissue (Figure 3.6.1a), confirming a successful knockdown of *Sesn1* (Figure 3.6.1a). We also measured the expression of the *Sesn2* gene in these *LysM*^{cre}*Sesn1*$^{flox/flox}$ mice and their littermate controls at a naïve state *in vivo.* This would reveal any compensatory effects *Sesn2* may have when expression of *Sesn1* is reduced. Interestingly, we saw significantly reduced expression of *Sesn2* in the spleen, thymus and liver tissue in the *LysM*^{cre}*Sesn1*$^{flox/flox}$ mice (Figure 3.6.1b). Although there was no significant reduction of *Sesn2* expression in the lung tissue (Figure 3.6.1b), a primary site for *Mtb* infection. Overall, *Sesn1* depletion in macrophages also reduced the expression of *Sesn2 in vivo,* suggesting that *Sesn1* is linked to *Sesn2* via a common regulatory factor.

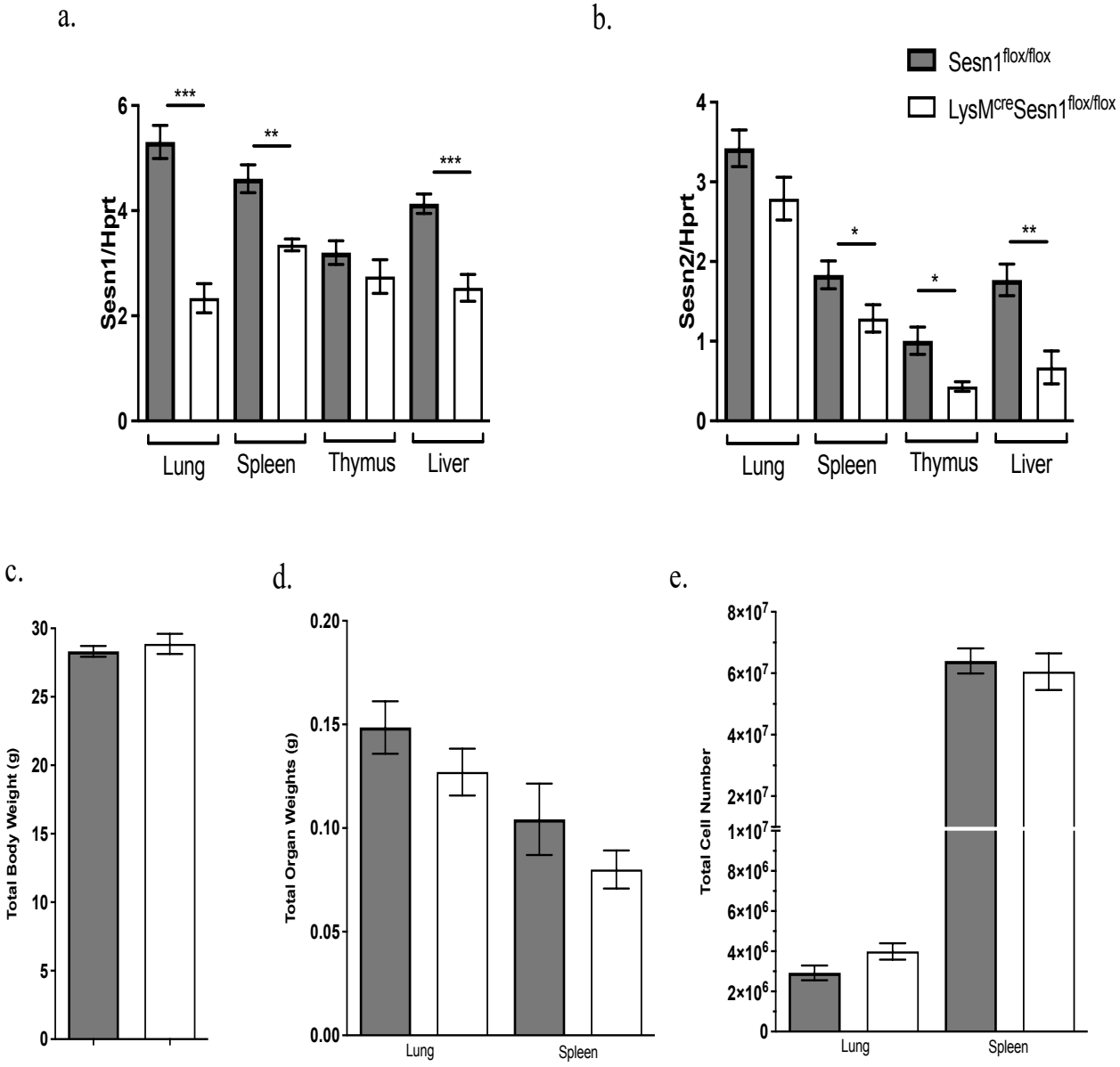

Figure 3.6.1: **The *Sesn1* knockdown in *LysM*^{cre}*Sesn1*$^{flox/flox}$ mice showed comparable baseline measurements.** Naïve mice were euthanized, and organs were collected for analysis (n=6). Tissue samples were dissociated into single-cell suspensions for cell counting, alternatively, tissue was homogenized, and RNA extracted, after which qRT-PCRs were run using Hprt as the housekeeping gene. a) *Sesn1* RNA expression in lung, spleen, thymus and liver tissue in *LysM*^{cre}*Sesn1*$^{flox/flox}$ samples compared to littermate controls. b) *Sesn2* RNA expression in lung, spleen, thymus and liver tissue in *LysM*^{cre}*Sesn1*$^{flox/flox}$ samples compared to littermate controls. c) Body weights. d) Lung and spleen organ weights. e) Total lung and spleen cell numbers. Data show mean ± SEM of n=6mice/group, an unpaired student t-test was used for statistical analysis for comparison of gene knockout, and baseline measurements in control versus knockout mice, with the following p-values denoting significance *p <0.05, **p <0.01, ***p <0.001.

At a naïve state, we found no significant differences in body weight, or lung and spleen weight and cell numbers between the *LysM*^{cre}*Sesn1*$^{flox/flox}$ mice and their littermate controls (*Sesn1*$^{flox/flox}$)

(Figure 3.6.1c-e). The absence of *Sesn1* in macrophages had no major effect compared to the controls at the naïve state.

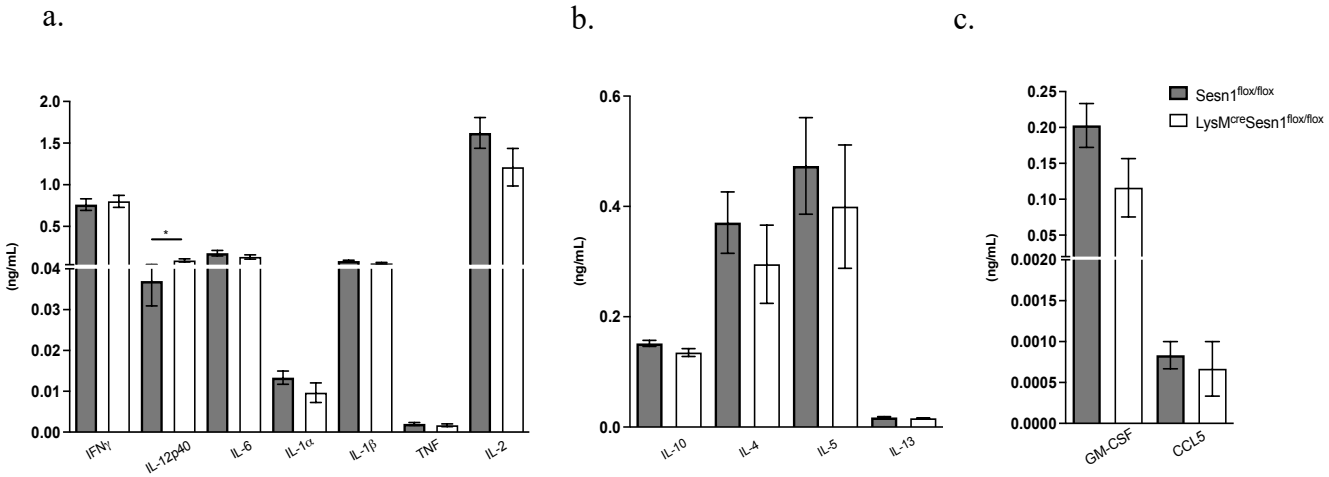

Figure 3.6.2: **Immune responses in the macrophage-specific *Sesn1*-deficient mice are comparable at a naïve state.** Lung homogenates were collected for analysis of cytokines, chemokines and growth factors by ELISA. a) Pro-inflammatory cytokine. b) Anti-inflammatory cytokine. c) Chemokine and growth factor panels. Data show mean ± SEM of n=6 mice/group. For statistical analysis, an unpaired, student t-test was performed for comparison of cytokines, chemokines, and growth factor levels in control versus knockout mice, where *p <0.05 versus control group.

To further characterize the inflammatory profile of the *LysM*^{cre}*Sesn1*$^{flox/flox}$ mouse, we analyzed lung homogenates, at a naïve state by ELISAs. The following pro-inflammatory, anti-inflammatory, and regulatory cytokines, chemokines and growth factors were analyzed; IFN-γ, IL-12p40, IL-6, IL-1α, IL-1β, TNF, IL-2, IL-10, IL-4, IL-5, IL-13, GMCSF, and CCL5. We found that the cytokine milieu between lungs was largely similar, with a minor significance in IL-12p40 production in the *LysM*^{cre}*Sesn1*$^{flox/flox}$ lung homogenates (Figure 3.6.2a-c), however, given the small difference in the magnitude, it may not be biologically relevant. Overall, macrophage-specific deletion of *Sesn1* did not result in gross differences in immune response at a naïve state.

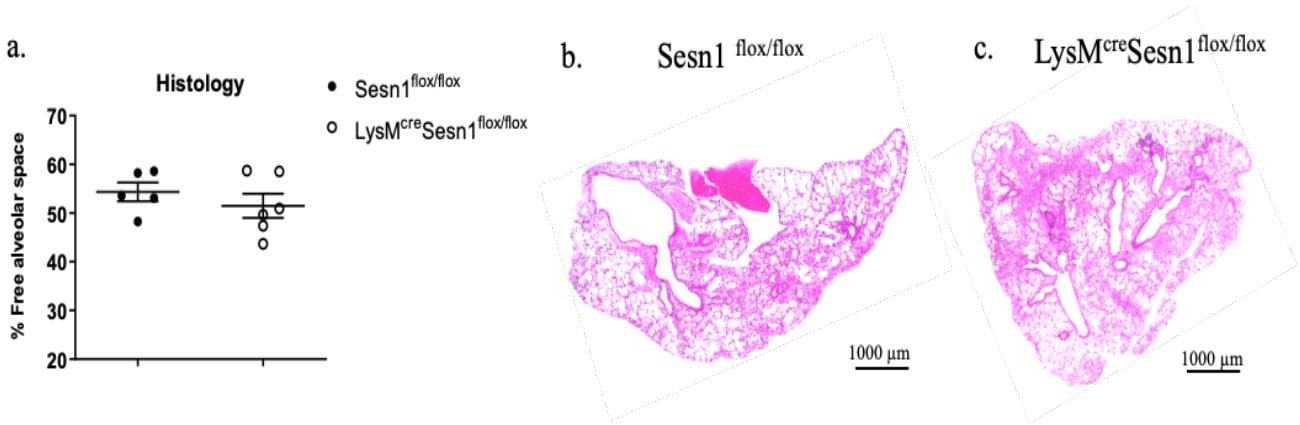

Figure 3.6.3: **The macrophage-specific deficiency of *Sesn1* did not affect lung pathology at a naïve state.** Lung sections were stained with H&E and scanned at 20x magnification. a) Quantification of percentage free alveolar space represented graphically. b) Representative image of *Sesn1*$^{-/-}$ compared with c) representative image of *LysM*^{cre}*Sesn1*$^{flox/flox}$ lung. Data are represented as mean ± SEM of n = 5-6 mice/group. For statistical analysis an unpaired student t-test was used to compare lung tissue pathology between control versus knockout mice.

Since TB is associated with severe pulmonary pathology, it was necessary to compare the lung tissue structure between these mouse models, in the absence of infection, to determine the condition at a naïve state. Using hematoxylin & eosin staining and microscope analysis, we analyzed the percentage of free alveolar space as a measurement of lung tissue pathology. As expected, microscopy analysis demonstrated that there were no significant differences in lung inflammation between the *Sesn1*$^{flox/flox}$ and *LysM*^{cre}*Sesn1*$^{flox/flox}$ mice (Figure 3.6.3a-c). Indicating that the macrophage-specific deletion of *Sesn1* has no effect on lung inflammation at a naïve state.

Overall, there were no significant biological differences, or inflammatory changes and is consistent with no difference in lung tissue pathology at a naïve state in the *LysM*^{cre}*Sesn1*$^{flox/flox}$ mice.

Objective 5: To determine the role of *Sestrin 1* in macrophage host immunity during *Mtb* infection using the *LysM*^{cre}*Sesn1*$^{flox/flox}$ mouse model.

3.7. 6-week time course infection of the *LysM*^{cre}*Sesn1*$^{flox/flox}$ Mouse

The macrophage-specific deletion of *Sesn1* increased lung neutrophilia but had no effect on lung tissue pathology after 6-weeks of *Mtb* infection.

To determine the effect of *Sesn1* deletion in the macrophage-specific knockout mouse model, *LysM*^{cre}*Sesn1*$^{flox/flox}$, we assess these at 6-week infection time point. We used littermate animals as controls, and infected mice intranasally with 100CFU HN878. During the 6-week course of infection, the mice were monitored closely by the grimace scale. After 6-weeks, mice were euthanized, and the lungs, lymph nodes, and spleen were collected for downstream analysis.

No differences were observed in body weight change, lung or spleen weight, or lung weight index after 6-weeks of infection (Figure 3.7.1a-c). Lung and spleen bacterial burden also showed no differences between mice (Figure 3.7.1d). We observed no differences in LN cell counts in the *LysM*^{cre}*Sesn1*$^{flox/flox}$ mice (Figure 3.7.1f). Interestingly, we found significantly higher lung cell numbers in the *LysM*^{cre}*Sesn1*$^{flox/flox}$ mice compared to their littermate controls (figure 3.7.1e). Suggesting that the macrophage-specific deletion of *Sesn1* facilitates increased lung cell numbers after 6-weeks of infection.

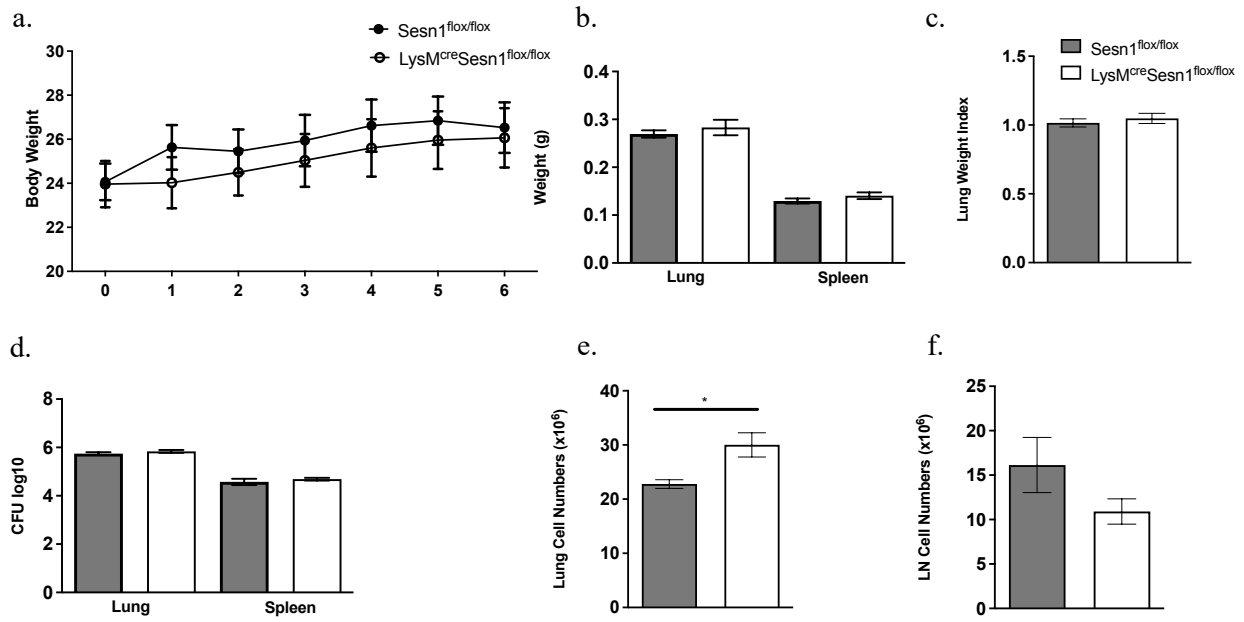

Figure 3.7.1: **The macrophage-specific deletion of *Sesn1* showed increased lung cell numbers at 6-weeks post infection.** Mice were infected with 100 CFUs of HN878 and were sacrificed. The lung and LN were processed into single-cell suspensions to determine cell counts. Lung and spleen samples were homogenized and plated on 7H11 agar plates to determine bacterial growth. a) Absolute body weight over 6-weeks of infection. b) Total lung and spleen organ weight. c) Lung weight index. d) Lung and spleen bacterial burden. e) Total lung cell numbers. f) Total lymph node cell numbers. Data show mean ± SEM of n=11-12mice/group of two pooled independent experiments. For statistical analysis, an unpaired student t-test was used for comparison of body weight, organ weight, CFUs, and organ cel numbers in control versus knockout mice, with p-values considered *p <0.05.

To elucidate the inflammatory profile of the *LysM*cre*Sesn1*flox/flox mice at 6-weeks post infection, we analyzed the following cytokines, chemokines and growth factors by ELISAs: IFN-γ, IL-12p40, IL-12p70, IL-6, IL-17, IL-1α, IL-1β, IL-23, IFNβ, TGFβ, IL-4, IL-10, GMCSF, CXCL2, CXCL5, CCL2, CCL3, CCL5, CXCL10 and CXCL1. We found that the pro-inflammatory cytokines, IL12p70 and IL-23 were reduced in the *LysM*cre*Sesn1*flox/flox mice (Figure 3.7.2a). However, the anti-inflammatory cytokines showed no differences in the lungs (Figure 3.7.2b). Amongst chemokines, CXCL5 (which attracts neutrophils) was increased in the *LysM*cre*Sesn1*$^{flox/flox}$ mice compared to their littermate controls (Figure 3.7.2c). In TB disease progression, increased neutrophilia has been associated with tissue destruction and lung pathology. Suggesting that after 6-week infection, the macrophage-specific deletion of *Sesn1* alters immune mediators that could contribute to increased pathology. Additionally, deletion of *Sesn1* altered pro-

inflammatory, or chemokine mediators but had no effect on anti-inflammatory cytokines. This suggests a role for *Sesn1* in regulating pro-inflammatory responses at 6-weeks post infection.

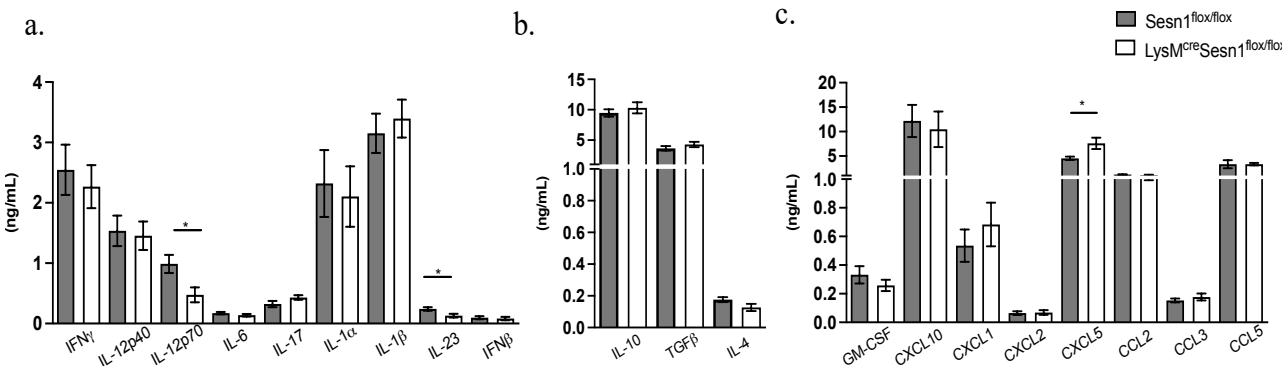

Figure 3.7.2: **The macrophage-specific deletion of *Sesn1* altered immune responses in the lungs after 6-weeks of *Mtb* infection.** Lung samples were homogenized to collect supernatants for ELISA experiments. a) Pro-inflammatory cytokine panel. b) Anti-inflammatory and regulatory cytokine panel. c) Chemokine and growth factor panel. Data show mean ± SEM of n=11-12mice/group of two pooled independent experiments. An unpaired student t-test was used for comparison of cytokines, chemokines, and growth factor levels in control versus knockout mice with the following p-values considered accordingly *p <0.05.

To further understand the immune cell recruitment between the *LysM*^{cre}*Sesn1*$^{flox/flox}$ mice and their littermate controls, we analyzed lung immune cell populations using flow cytometry. Lung lymphoid cell analysis revealed no differences between mice when comparing the frequencies of the populations (Figure 3.7.3a). However, the lung absolute cell numbers showed significantly higher CD4 T cells in the *LysM*^{cre}*Sesn1*$^{flox/flox}$ mice compared to the littermate controls (Figure 3.7.3b). Furthermore, the subsets and T cell exhaustion markers showed a minor decrease in the percentage of CD8 T cell effector/effector memory cells and an increase in the percentage of KLRG1+PD1+ cells in the *LysM*^{cre}*Sesn1*$^{flox/flox}$ mice (Figure 3.7.3d and f). Lung myeloid cell population analysis showed a higher percentage of neutrophils and reduced interstitial macrophages in the *LysM*^{cre}*Sesn1*$^{flox/flox}$ mice (Figure 3.7.3g). This significant increase of neutrophils remained consistent in lung absolute cell numbers; however, the reduced interstitial macrophage observation was abolished in the *LysM*^{cre}*Sesn1*$^{flox/flox}$ mice (Figure 3.7.3h). This suggests that the macrophage-specific deletion of *Sesn1 in vivo* modifies the immune cell milieu in the lungs after 6-weeks of infection, especially increasing neutrophil recruitment that may contribute to tissue pathology.

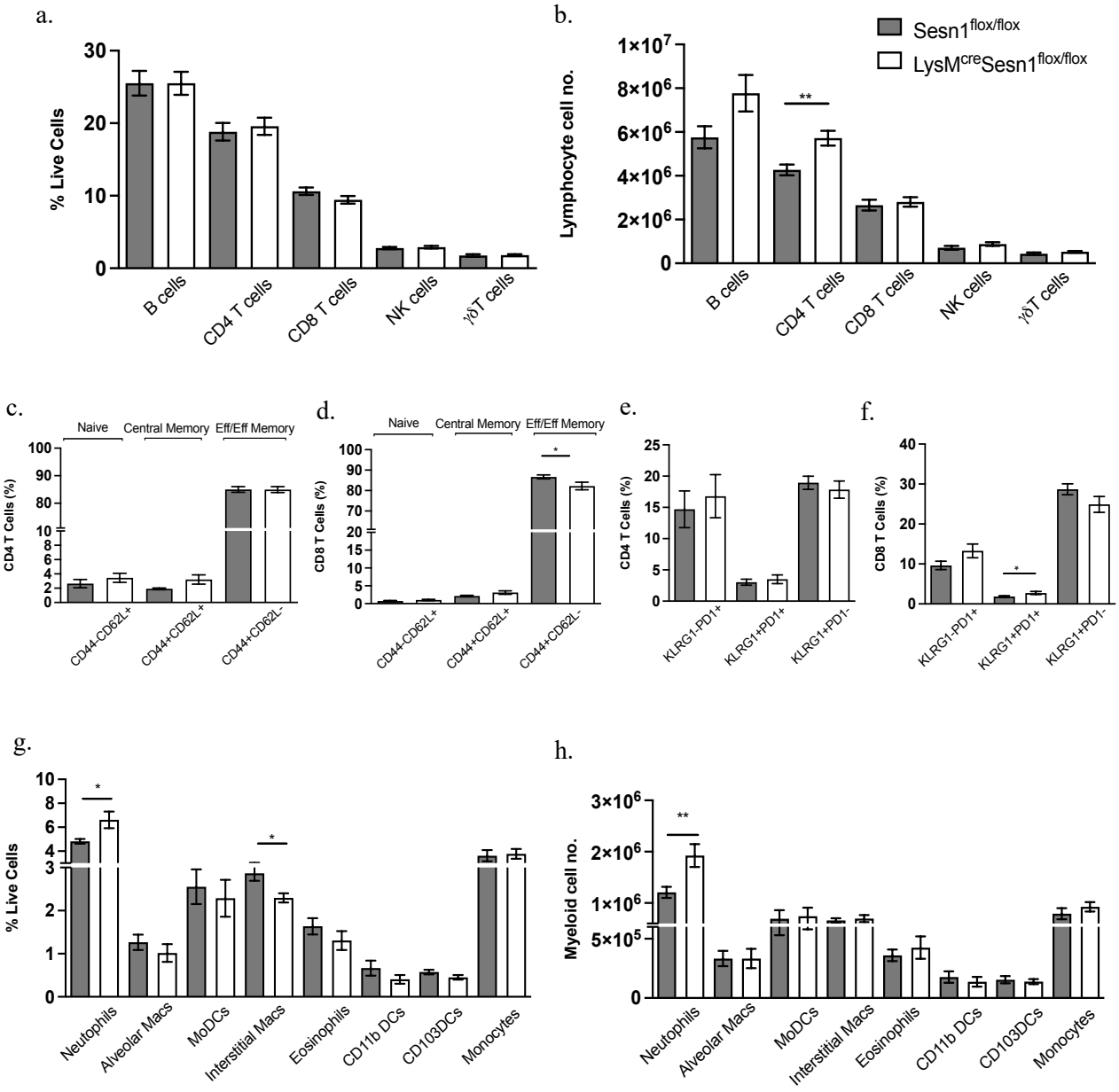

Figure 3.7.3: **The macrophage-specific deletion of *Sesn1* showed altered immune cell recruitment in the lungs after 6-weeks of *Mtb* infection.** Lung lobes were processed into single-cell suspensions. Cells were stained with either a Lymphoid or Myeloid panel and cell populations acquired a) Lung lymphoid immune cell populations represented as percentages. b) Lung lymphoid populations, represented as absolute cell numbers. c) Lung CD4 T cell subsets. d) Lung CD8 T cell subsets. e) Lung CD4 T cell exhaustion markers. f) Lung CD8 T cell exhaustion markers. g) Lung myeloid immune cell populations represented as percentages. h) Lung myeloid cell populations represented in absolute cell numbers. Data show mean ± SEM of n=11-12mice/group of two pooled independent experiments. For statistical analysis, an unpaired student t-test was used for comparison of immune cell abundance in control versus knockout mice, with the following p-values denoting significance, *p <0.05, **p <0.01.

Lymph node lymphoid immune cell population analysis showed no differences when comparing percentages or cell numbers (Figure 3.7.4a and b). The T cell subsets and exhaustion only revealed a minor increase in the percentage of KLRG1+PD1+ CD8 T cells in the *LysM*^{cre}*Sesn1*$^{flox/flox}$ mice (Figure 3.7.4f). Among LN myeloid cell populations, we found an increase in the percentage of CD11b resident DCs and MHCII low monocytes in the *LysM*^{cre}*Sesn1*$^{flox/flox}$ mice, but this significance was abolished when comparing lymph node cell number (Figure 3.7.4g and h). This suggests that the macrophage-specific deletion of *Sesn1* in mice causes minor alterations to LN immune cell populations after 6-weeks of infection.

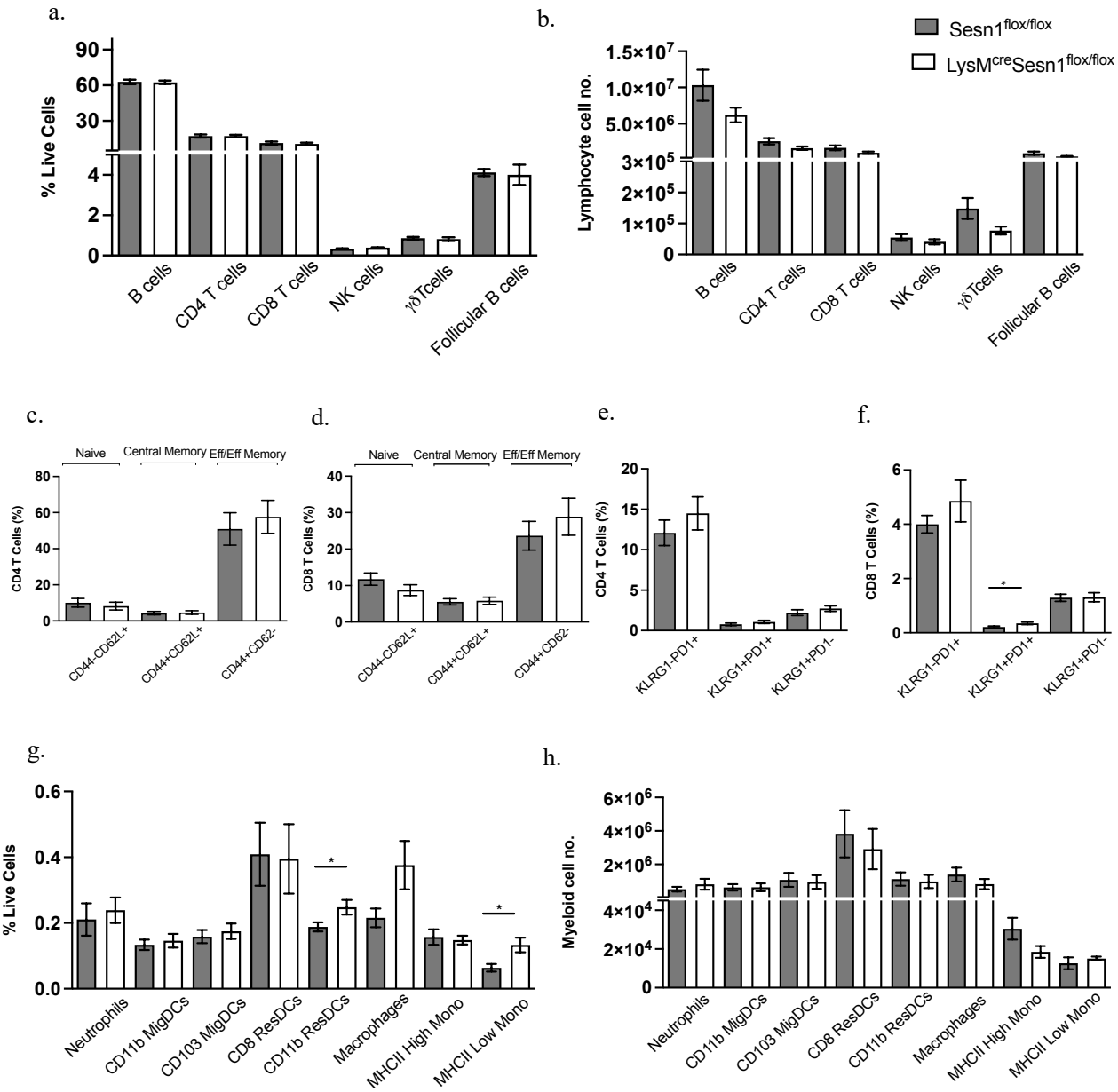

Figure 3.7.4: **The macrophage-specific deletion of *Sesn1* showed minor changes to immune cell populations in lymph nodes at 6-weeks post *Mtb* infection.** Lymph nodes were processed into single-cell suspensions, stained with either a Lymphoid or Myeloid panel and cell populations were acquired. a) Lymph node lymphoid immune cell populations represented as percentages. b) Lymph node lymphoid populations, represented as absolute cell number. c) Lymph node CD4 T cell subsets. d) Lymph node CD8 T cell subsets. e) Lymph node CD4 T cell exhaustion markers. f) Lymph node CD8 T cell exhaustion markers g) Lymph node myeloid immune cell populations represented as percentages. h) Lymph node myeloid cell populations represented in absolute cell numbers. Data show mean ± SEM of n=11-12mice/group of two pooled independent experiments. For statistical analysis, an unpaired student t-test was used for comparison of immune cell abundance in control versus knockout mice, with the following p-values denoting significance, *p <0.05.

Considering increased lung cell numbers and neutrophils in the lung, we determined lung tissue pathology and quantified the percentage free alveolar space in the *LysM*^{cre}*Sesn1*$^{flox/flox}$ and littermate controls. Histology analysis and quantification revealed no difference in the percentage of free alveolar space between mice (Figure 3.7.5a). This was reflected in the representative images (Figure 3.7.5b and c), with large amounts of fibrosis and dark purple granulomatous regions in both the *LysM*^{cre}*Sesn1*$^{flox/flox}$ mice and their littermate controls. This suggests that the deletion of *Sesn1* in macrophages alone has no effect on tissue pathology after 6-weeks of infection *in vivo.*

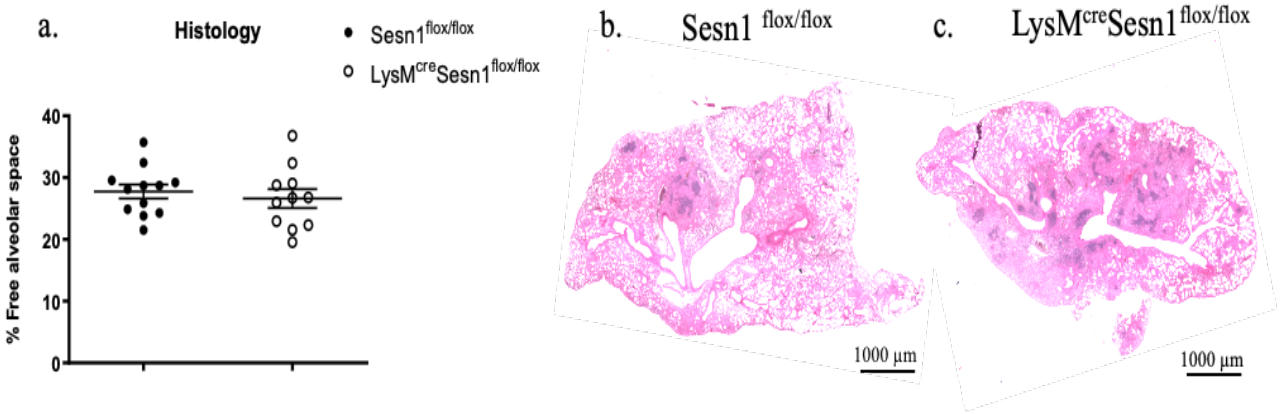

Figure 3.7.5: **The macrophage-specific deletion of *Sesn1* had no effect on lung pathology after 6-weeks of *Mtb* infection.** Lung lobes were fixed in 10% neutral buffered formalin, and stained with H&E. Slides were scanned at 20x magnification. a) Quantification of percentage free alveolar space. Representative image of b) *Sesn1*$^{flox/flox}$ (littermate control) and c) the LysMcreSesn1flox/flox lungs. Data show mean ± SEM of n=11-12mice/group of two pooled independent experiments. For statistical analysis, an unpaired student t-test was performed for comparison of lung tissue pathology in control versus knockout mice.

In summary, the *LysM*^{cre}*Sesn1*$^{flox/flox}$ mice showed a significant increase in CXCL5 secretion, corresponding with increased neutrophils in the lungs after 6-weeks of infection (Figure 3.7.2c and

3.7.3g and h). We also found decreased IL-12p70 and IL-23 production in the lungs (Figure 3.7.2a). Notably, lung CD4 T cell recruitment was increased in the *LysM*^{cre}*Sesn1*$^{flox/flox}$ mice, consistent with the increased lung cell numbers (Figure 3.7.3b and 3.7.1e). *LysM*^{cre}*Sesn1*$^{flox/flox}$ mice displayed reduced percentages of interstitial macrophages in the lungs, and increased percentages of CD11b resident DCs and MCHII low monocytes in the LN (Figure 3.7.3g and 3.7.4g). However, immune cell recruitment was not translated in the tissue pathology in the *LysM*^{cre}*Sesn1*$^{flox/flox}$ lungs (Figure 3.7.5 a-c). Overall, the macrophage-specific depletion of *Sesn1* had no major effect on the outcome of TB disease *in vivo*.

3.8. 12-week time course infection of the *LysM*^{cre}*Sesn1*$^{flox/flox}$ Mouse

The macrophage-specific deletion of *Sesn1* decreased lung neutrophilia but had no effect on lung tissue pathology after 12-weeks of *Mtb* infection.

To further understand the effect of *Sesn1* deletion in macrophages during prolonged infection, we extended the timepoint and investigated the inflammatory and antibacterial responses at 12-weeks post infection. We infected controls and the *LysM*^{cre}*Sesn1*$^{flox/flox}$ mice intranasally with 100CFU HN878. The mice were monitored closely over the 12-week infection period, after which, the mice were euthanized, and the lungs, lymph nodes and spleen were harvested for further processing.

Interestingly, the *LysM*^{cre}*Sesn1*$^{flox/flox}$ mice gained more weight than the littermate controls despite seeing no differences in lung and spleen weight, lung weight index or lung and LN cell numbers (Figure 3.8.1a-c and e-f). Bacterial burden between mice was also comparable with no significant differences (Figure 3.8.1d).

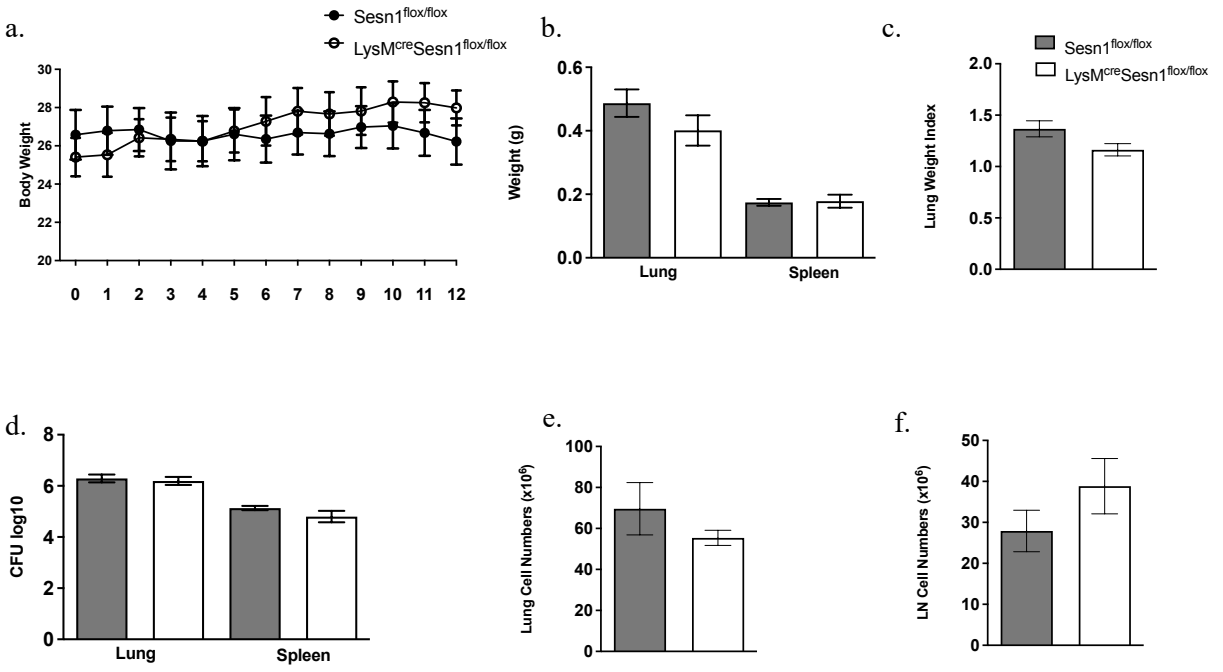

Figure 3.8.1: **The macrophage-specific *Sesn1*-deficiency showed no significant differences at 12-weeks of *Mtb* infection in mice.** Mice were infected with 100 CFUs of HN878 and were sacrificed. Single-cell suspensions were generated from the lung and LN samples for cell numbers. The lung and spleen samples were homogenized and plated on 7H11 agar plates to measure bacterial burden. a) Absolute body weight over the 12-week course of infection. b) Total lung and spleen weight. c) Lung weight index. d) Lung and spleen bacterial burden. e) Total lung cell numbers. f) Total lymph node cell numbers. Data show mean ± SEM of n=11-12mice/group of two pooled independent experiments. For statistical analysis, an unpaired student t-test was used, to compare body weight, organ weight, CFUs, and organ cell numbers between control versus knockout mice, and the following p-values considered accordingly ***p <0.001.

Analysis of immune response in the lungs showed decreased IL-6 and IL-17 in the *LysM*^{cre}*Sesn1*$^{flox/flox}$ mice compared to control mice (Figure 3.8.2a). There were no differences in the anti-inflammatory panel of cytokines (Figure 3.8.2b). Out of the chemokines and growth factors investigated, CXCL10, a potent inflammatory chemokine with leukocyte recruiting function was elevated and CCL3, a chemokine with neutrophil recruiting function was decreased in the *LysM*^{cre}*Sesn1*$^{flox/flox}$ mice compared to the control mice (Figure 3.8.2c). These results suggest that the macrophage-specific deletion of *Sesn1* enabled an immune response shift in the lungs but consistently had no effect on anti-inflammatory cytokines.

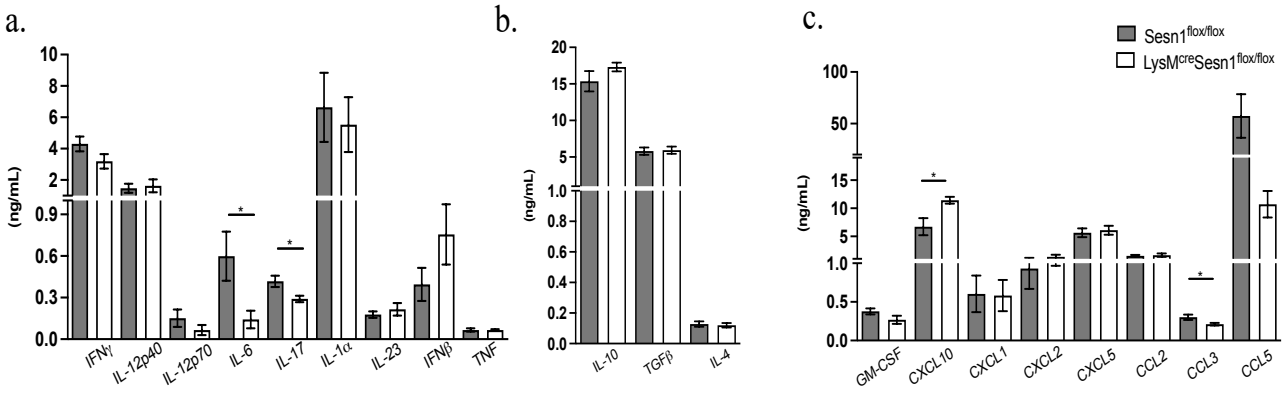

Figure 3.8.2: **The macrophage-specific deletion of *Sesn1* showed altered immune responses in the lungs after 12-weeks of *Mtb* infection.** Lung lobes were homogenized to collect supernatants for ELISA analysis. a) Pro-inflammatory cytokine panel. b) Anti-inflammatory cytokine panel. c) Chemokine and growth factor panel. Data show mean ± SEM of n=11-12mice/group of two pooled independent experiments. For statistical analysis, an unpaired student t-test was used for comparison of cytokines, chemokines, and growth factor levels in control versus knockout mice, with the following p-values used for significance, *p <0.05.

Furthermore, we investigated the immune cell populations in the *LysM*^{cre}*Sesn1*$^{flox/flox}$ mice after 12 weeks of infection using flow cytometry. We investigated lymphoid and myeloid immune cell populations of lung and lymph nodes from the *LysM*^{cre}*Sesn1*$^{flox/flox}$ mice and littermate controls. We found no differences between mice when comparing the percentage and absolute cell numbers of the lung lymphoid immune populations (Figure 3.8.3a and b). Likewise, for CD4 and CD8 T cell subsets, we observed no differences between mice (Figure 3.8.3c and d). Our CD4 T cell exhaustion panel revealed increased KLRG1+PD1+ and more importantly, increased KLRG1+PD1- cells in the *LysM*^{cre}*Sesn1*$^{flox/flox}$ mice indicating higher levels of CD4 T cell exhaustion, but this was not consistent among CD8 T cells (Figure 3.8.3e and f). Lung myeloid analysis showed significantly decreased neutrophils in the *LysM*^{cre}*Sesn1*$^{flox/flox}$ mice compared to the littermate controls, and this was consistent in both cell frequencies as well as the absolute cell numbers (Figure 3.8.3g and h). These results suggest that depletion of *Sesn1* from macrophages, albeit minor, alters the lung immune cell milieu, with a significant decrease in neutrophils seen.

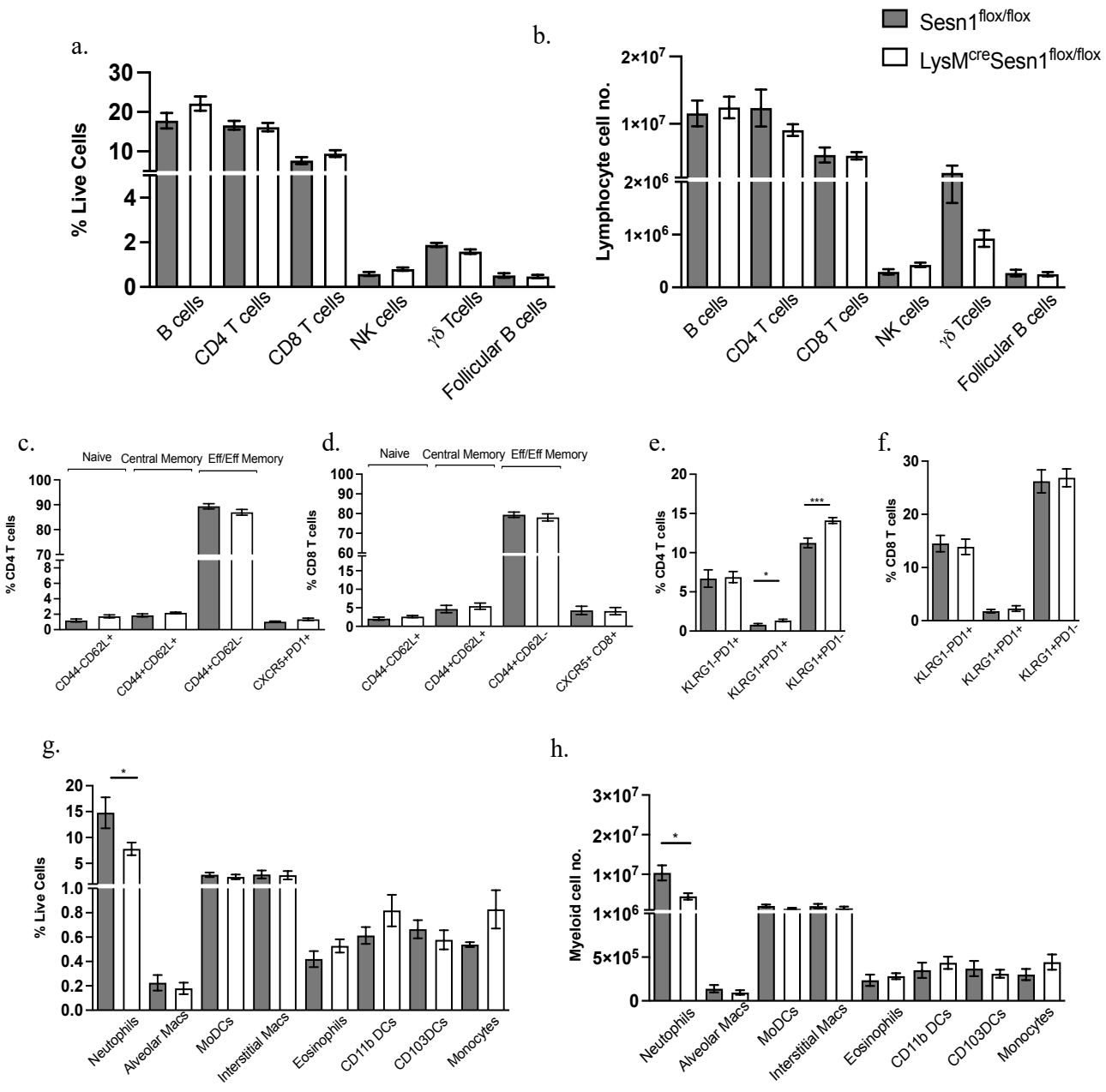

Figure 3.8.3: **The macrophage-specific deletion of *Sesn1* showed altered immune cell recruitment in the lungs after 12-weeks of *Mtb* infection.** Lung lobes were processed into single-cell suspensions. Cells were stained with either a Lymphoid or Myeloid panel and cell populations acquired a) Lung lymphoid immune cell populations as percentages. b) Lung lymphoid populations, represented as absolute cell numbers. c) Lung CD4 T cell subsets including T Follicular Helper cells (CXCL5+ PD1+). d) Lung CD8 T cell subsets T Follicular Helper cells (CXCL5+ PD1+). e) Lung CD4 T cell exhaustion panel. f) Lung CD8 T cell exhaustion panel. g) Lung myeloid immune cell populations as percentages. h) Lung myeloid cell populations represented in absolute cell numbers. Data show mean ± SEM of n=11-12mice/group of two pooled independent experiments. For statistical analysis, an unpaired student t-test was used for comparison of immune cell recruitment in control versus knockout mice, with the following p-values representing significance, *p <0.05, ***p <0.001.

In lymph nodes, we found no differences between lymphoid immune cell percentages or absolute cell numbers between the *LysM*^{cre}*Sesn1*$^{flox/flox}$ mice and controls after 12 weeks of infection (Figure 3.8.4a and b). The T cell subset analysis showed increased naïve CD8 T cells in the *LysM*^{cre}*Sesn1*$^{flox/flox}$ mice, but this trend was not observed in the CD4 T cell panel (Figure 3.8.4c and d). Likewise, the T cell exhaustion panel showed no differences in CD4 T cells but decreased KLRG1+PD1+ CD8 T cells in *LysM*^{cre}*Sesn1*$^{flox/flox}$ mice compared to the littermate controls, indicating reduced T cell exhaustion (Figure 3.8.4e and f). Consistent with our lung myeloid analysis, the lymph node myeloid percentages also showed decreased neutrophil recruitment in the *LysM*^{cre}*Sesn1*$^{flox/flox}$ mice, however, abolished in the absolute numbers (Figure 3.8.4g and h). Suggesting that *Sesn1* depletion showed only minor shifts in LN immune cell populations.

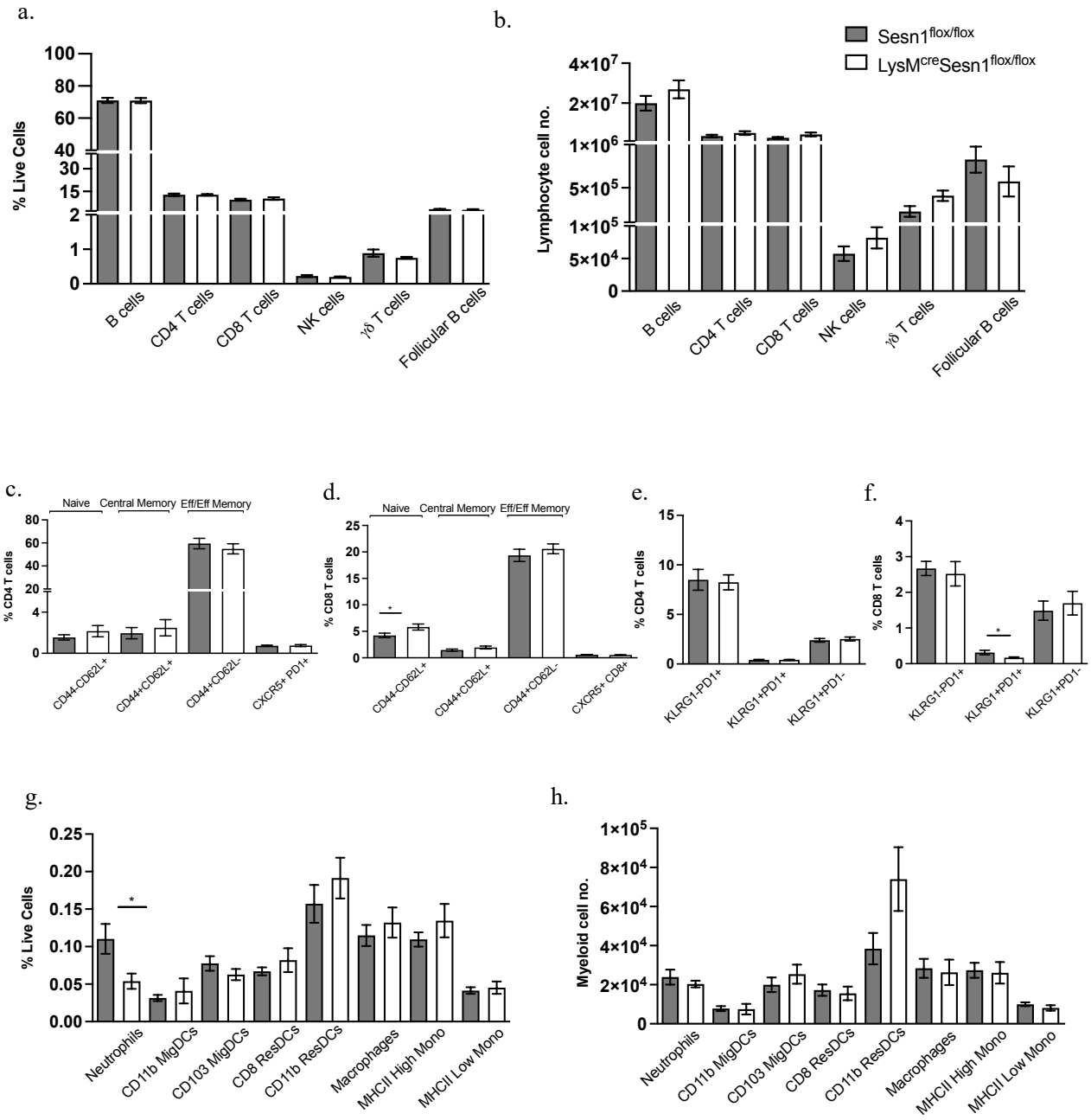

Figure 3.8.4: **The macrophage-specific deletion of *Sesn1* showed minor changes to immune cell populations in lymph nodes after 12-weeks of *Mtb* infection**. Lymph nodes were processed into single-cell suspensions. Cells were stained with either a Lymphoid or Myeloid panel and cell populations acquired a) Lymphoid populations in the LN represented as percentages. b) LN lymphoid populations, represented as absolute cell numbers. c) LN CD4 T cell subsets. d) Lymph node CD8 T cell subsets. e) LN CD4 T cell exhaustion panel. f) LN CD8 T cell exhaustion panel g) Myeloid immune cell populations in the LN represented as percentages. h) LN myeloid cell populations represented in absolute cell numbers. Data show mean ± SEM of n=11-12mice/group of two pooled independent experiments. For statistical analysis, an unpaired student t-test was used for comparison of immune cell recruitment in control versus knockout mice, with the following p-values denoting significance, *p <0.05.

To determine the effect of the *Sesn1* deletion on lung tissue pathology, the percentage free alveolar space was quantified by comparing the lungs of the *LysM*^{cre}*Sesn1*$^{flox/flox}$ and the littermate controls. The macrophage-specific deletion of *Sesn1* in macrophages did not affect the percentage of free alveolar space *in vivo* (Figure 3.8.5a-c). These results show that the macrophage-specific function of *Sesn1* is dispensable during 12 weeks of *Mtb* infection.

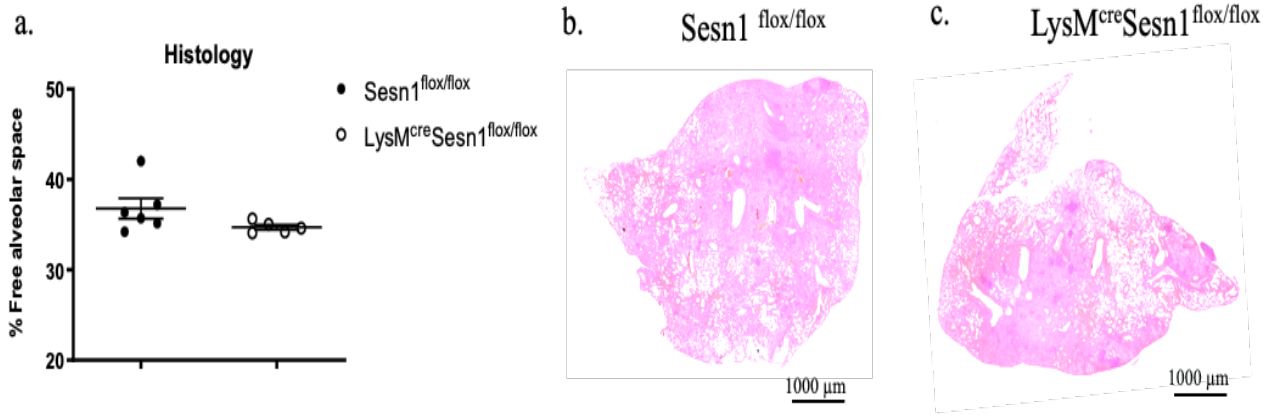

Figure 3.8.5: **The macrophage-specific *Sesn1*-deficiency had no effect on lung pathology after 12-weeks of *Mtb* infection.** Lung lobes were fixed in 10% neutral buffered formalin and stained with H&E. Slides were scanned at 20x magnification. a) Percentage free alveolar space quantified b) Representative section of the *Sesn1*$^{flox/flox}$ and c) *LysM*^{cre}*Sesn1*$^{flox/flox}$ lung from mice. Data are represented as mean ± SEM of n = 5-6 mice/group. For statistical analysis, an unpaired student t-test was performed to compare lung tissue pathology between control versus knockout mice.

Despite minor differences in inflammatory profiles in the *LysM*^{cre}*Sesn1*$^{flox/flox}$ and littermate control mice, overall, it had no major effect on the outcome of TB disease. Together, these data show that the ablation of *Sesn1* specifically in macrophages plays a negligible role in the control of tuberculosis or lung pathology during infection, both at 6- and 12-weeks post infection.

3.9. To determine the effect of the absence of *Sestrin 1* in macrophages on survival of mice during TB disease.

The macrophage-specific deletion of *Sesn1* had no effect on susceptibility to TB disease in mice.

To determine whether the macrophage-specific deletion of *Sesn1* influence the survival of animals during TB disease, we conducted a mortality experiment. Mice were infected with 100 CFU HN878 *Mtb* intranasally and were monitored closely throughout the survival experiment. Mice were euthanized when they reached their humane endpoint, and the date of euthanasia was recorded. The results from the mortality experiments showed no significant difference in susceptibility during TB disease. The mean time at which 50% of the animals succumbed to disease was comparable, with *Sesn1*$^{flox/flox}$ at 34 weeks and the *LysM*^{cre}*Sesn1*$^{flox/flox}$ mice at 39 weeks (Figure 3.9.1). Overall, the absence of *Sesn1* in macrophages does not affect the survival of the host.

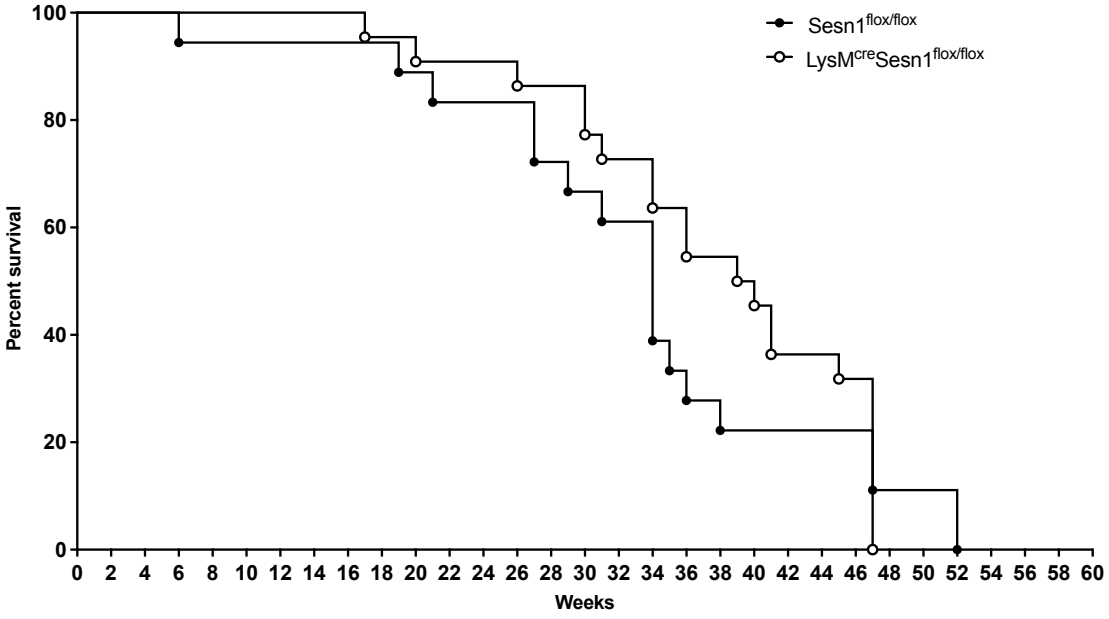

Figure 3.9.1: ***Sesn1* depletion in macrophages had no effect on mortality during TB disease in mice.** Mice were infected intranasally with 100 CFU HN878. Each time point of euthanasia was recorded to generate the survival curve and establish whether the macrophage-specific deletion of *Sesn1* affects susceptibility. Data show mean ± SEM of n=18-22mice/group of two pooled independent experiments. For statistical analysis, a survival curve comparison was done using the Mantel-Cox statistical test for comparison between control versus knockout mice.

Objective 6: Mechanistic studies to determine pathways and the regulation of *Sestrin 1* in macrophages using the *LysM*^{cre}*Sesn1*$^{flox/flox}$ mouse model.

3.10. *In vitro* studies to determine the role of *Sestrin 1* in macrophages.

Sesn1-deficient macrophages increased bacterial growth, ROS production, cell death, pro-inflammatory cytokine responses and showed glycolytic shift.

From our studies of interrogating *LysM*^{cre}*Sesn1*$^{flox/flox}$ mouse, we have seen that the macrophage-specific deletion does not increase susceptibility to TB in an *in vivo* model. Likewise, at longer stages of infection, there are no major changes in inflammation between the *LysM*^{cre}*Sesn1*$^{flox/flox}$ mice and their littermate controls, as well as similar lung tissue pathology. This indicates that the macrophage-specific deletion alone is inadequate to distinguish the role of *Sesn1 in vivo,* whereas other cells express *Sesn1*. We may observe a better effect using a *Sesn1* global knockout mouse model, like *Sesn2*, where we showed increased susceptibility to TB.

Conducting *in vitro* experiments with *Sesn1*-deficient macrophages would therefore give insight into the effect at a pure cellular level since there is no *Sesn1* expression from bystander cells as *in vivo*. We conducted *in vitro* experiments using macrophages differentiated from bone marrow progenitors of *LysM*^{cre}*Sesn1*$^{flox/flox}$ mice and littermate controls. BMDMs were then infected with HN878 *Mtb* at an MOI of 0.5, after which we investigated bacterial burden, cytotoxicity, viability, cytokine profiles and ROS production between these macrophages.

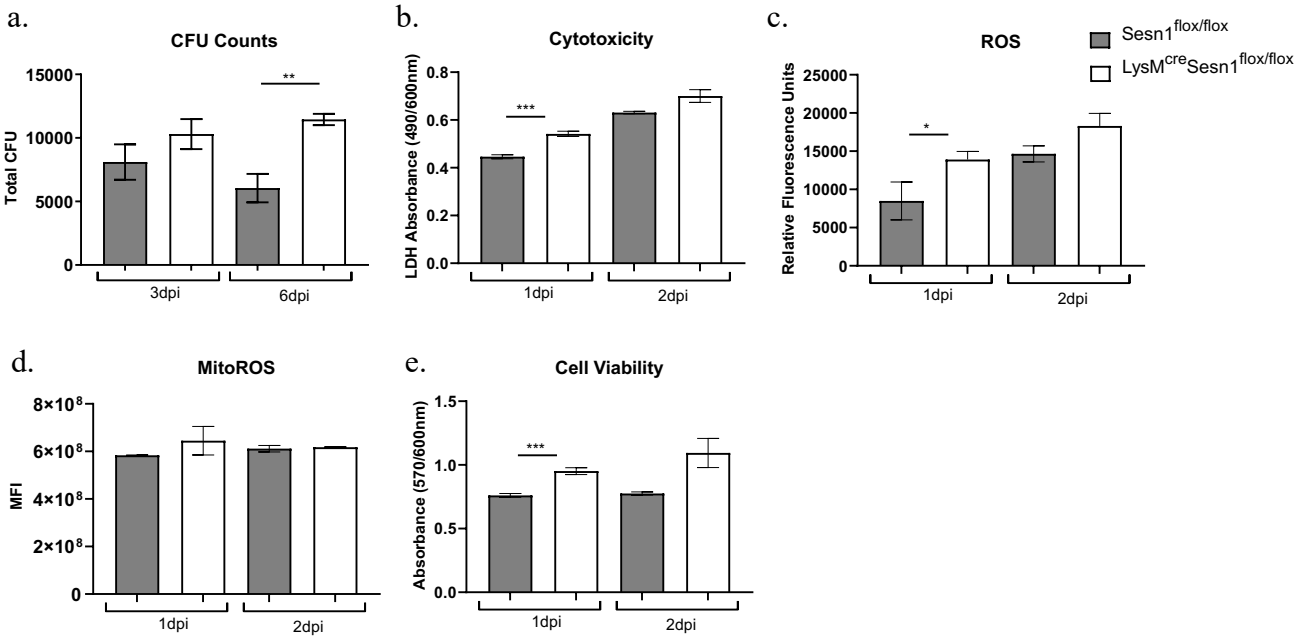

Figure 3.10.1: ***Sesn1*-deficient macrophages showed increased bacterial growth, ROS production and cell death *in vitro*.** BMDMs were seeded at a concentration of $1x10^5$ cells per well and infected with *Mtb* HN878 at an MOI of 0.5. a) Total bacterial burden at 3- days and 6-days post infection in the *Sesn1*$^{flox/flox}$ and *LysM*^{cre}*Sesn1*$^{flox/flox}$ mice. b) Cytotoxicity assay measured by LDH absorbance at 1- and 2-days post infection. c) Levels of ROS at 1- and 2-days post infection, measured by using the CellROX Assay kit. d) Measurement of mitochondrial ROS using MitoTracker Red CMXRos stain. e) Cell viability at 1- and 2-days post infection, measured by using CellTiter blue dye. Data shown as mean ± SEM of representative of 2-3 experiments. For statistics, an unpaired student t-test was used for comparison of CFUs, cytotoxicity, viability, and ROS between control versus knockout mice, with the following p-values referred to for significance, *p <0.05, **p <0.01, ***p <0.001.

From our *in vivo* infection studies, the bacterial burden between mice was largely comparable. We found no differences at 3dpi, however, we observed a significantly higher bacterial growth in macrophages-deficient for *Sesn1* at 6dpi (Figure 3.10.1a). Showing that *Sesn1*-deficient macrophages are less capable of controlling *Mtb* infection. Given that bacterial burden alone doesn't contribute to susceptibility to TB disease, we investigated the link between *Sesn1* and other factors that could be drivers of lung tissue pathology and TB severity(140). We measured cell death in macrophages using the release of cytosolic LDH in the supernatant as a measure, with the intent that it could reflect macrophage cell death within tissues in a full system model. Cytotoxicity data showed a transient significant increase in cell death at 1dpi in *LysM*^{cre}*Sesn1*$^{flox/flox}$ macrophages (Figure 3.10.1b). To understand this increased cell death in the *Sesn1*-deficient macrophages we measured intracellular ROS levels, a driver of cell death which is closely regulated by the Sesn family of genes. Moreover, ROS contributes to increased tissue pathology

and inflammation, we therefore measured LDH, ROS and cell viability at corresponding earlier time points, as the half-life of ROS is short and its effect on cell death can be seen earlier. These assays were conducted at 1- and 2-dpi to detect whether the cellular ROS levels correspond with increased cell death. Levels of intracellular ROS showed a similar trend to the cytotoxicity results, where at 1dpi ROS was significantly higher in the *LysM*^{cre}*Sesn1*$^{flox/flox}$ macrophages but at 2dpi only a trend in increase remained (Figure 3.10.1c). Consistent with our theory that ROS may be potentiating cytotoxicity in cells.

As a means of validating our cytotoxicity results, we measured cell viability using CellTiter blue dye. Quantifying cell viability consistently showed increased viability at 1dpi post infection in the *LysM*^{cre}*Sesn1*$^{flox/flox}$ macrophages, opposing the cell death data. However, the assay itself relies on the reduction of resazurin to resorufin by metabolically active cells, suggesting that *Sesn1*-deficient macrophages may be more metabolically active instead of a direct measure of viability (Figure 3.10.1e) (137). Since ROS is a natural byproduct of metabolism, this urged us to look closer at mitochondrial ROS levels, which showed no significant difference between macrophages, prompting the need to further investigate the link between *Sesn1*, metabolism, ROS and cell death during *Mtb* infection (Figure 3.10.1d).

Given the importance of the cytokine environment during TB disease, a panel of cytokines were chosen based on known pro-inflammatory responses and the role they play during TB pathology, additionally to the role *Sesn1* may play in the regulation of these inflammatory markers. The culture supernatants were collected at 3- and 6dpi to determine immune response. Pro-inflammatory cytokine analysis showed IL-1α secretion was significantly decreased in the *LysM*^{cre}*Sesn1*$^{flox/flox}$ macrophages at 3- and 6dpi (Figure 3.10.2a). In contrast, there was increased IL-1β in *LysM*^{cre}*Sesn1*$^{flox/flox}$ macrophages at 3dpi but not at 6dpi (Figure 3.10.2b). Levels of IL-6 and TGFβ were both significantly increased at 3dpi in *LysM*^{cre}*Sesn1*$^{flox/flox}$ macrophages, but this was not observed at 6dpi (Figure 3.10.2c and f). TNF was also elevated in *LysM*^{cre}*Sesn1*$^{flox/flox}$ macrophages at 3dpi but decreased at 6dpi (Figure 3.10.2d). Nitric oxide levels were measured as another inflammatory marker, however, there was no difference in nitrite measurement between the *LysM*^{cre}*Sesn1*$^{flox/flox}$ and littermate controls (Figure 3.10.2e). These results suggest that in the absence of *Sesn1*, cells are more prone to an inflammatory phenotype.

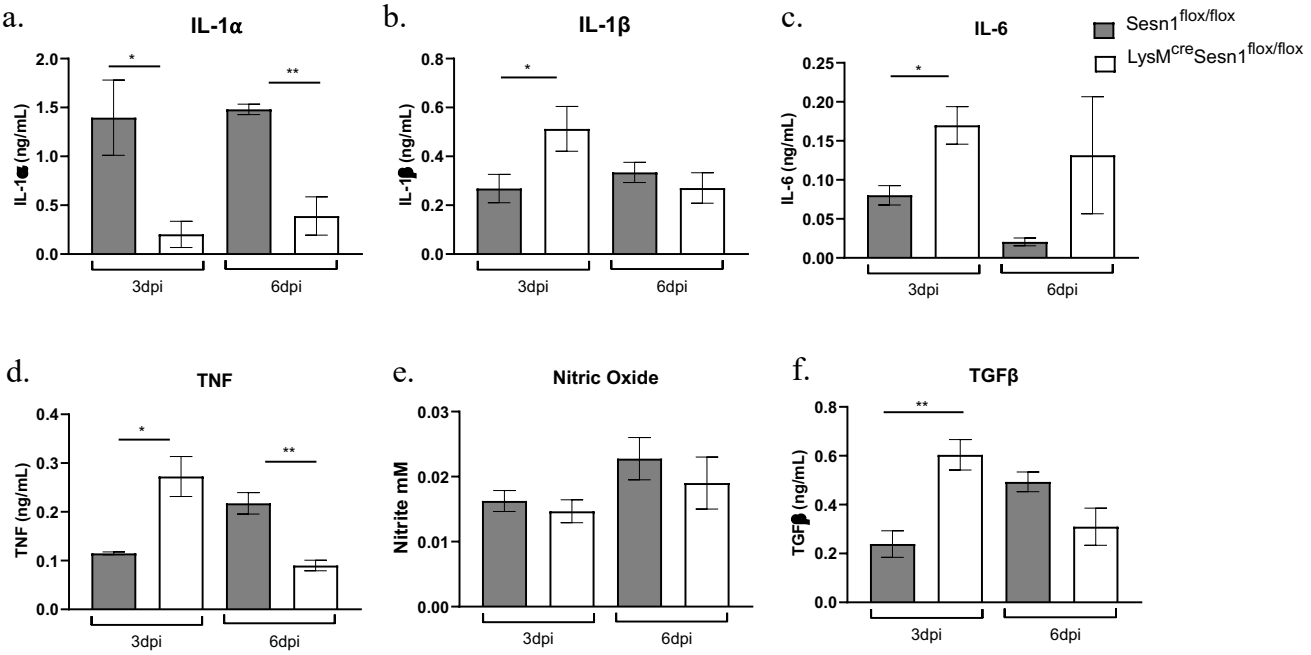

Figure 3.10.2: ***Sesn1*-deficient macrophages showed increased pro-inflammatory responses *in vitro*.** Culture supernatants were collected at 3- and 6-days post infection for ELISA analysis. a) IL-1α, b) IL-1β, c) IL-6, and d) TNF secretion at 3- and 6-days post infection. e) Quantification of nitrite as a proxy of nitric oxide at 3- and 6-days post infection using the Promega Griess Reagent. f) TGF-β levels at 3- and 6dpi measured by ELISA. Data shown as mean ± SEM of representative of 2-3 independent experiments. For statistical analysis, an unpaired student t-test was used to compare cytokine levels and nitric oxide in control versus knockout mice, with the following p-values denoting significance *p <0.05, **p <0.01.

There is more evidence of Sestrin 2 playing a role in mitochondrial regulation, both directly and indirectly. Even though the metabolic pathways of *Sesn2* have not been fully understood yet, the role that Sestrin 1 plays remains more elusive. We have already demonstrated that *Sesn1*-deficient macrophages may be more metabolically active and may not be dependent on mitochondrial production. Therefore, we investigated cell metabolomics to provide a link between the role of *Sesn1*, ROS and cell death during *Mtb* infection. Given that both genes belong to the same family of stress responders, we conducted cell flux experiments with the Seahorse Analyzer to elucidate the role of *Sesn1* in macrophage energy metabolism in naïve and *Mtb* infection. We quantified the ATP production rate between *LysM*^{cre}*Sesn1*$^{flox/flox}$ and *Sesn1*$^{flox/flox}$ macrophages at a naïve state and 24-hours post infection using the Real-Time ATP Rate Assay described previously in section 3.5. Our first comparison focused on the total ATP production rate between the *Sesn1*-deficient and control macrophages, to gauge their metabolic activity. In a naive state, the *LysM*^{cre}*Sesn1*$^{flox/flox}$ macrophages displayed a similar total ATP production rate compared to their littermate controls,

(Figure 3.10.3). Likewise, after 1dpi, there was no significant difference in the total ATP production rate in the *Sesn1*-deficient macrophages compared to control macrophages, although a higher trend was seen (Figure 3.10.3). However, *Sesn1*-deficient and sufficient macrophages showed an increased total ATP production rate after infection, compared to their respective naïve state, especially in the *Sesn1*-deficient cells (Figure 3.10.3). As a secondary analysis, we investigated the method of ATP production, which showed an energetic switch to glycolysis in both macrophages post infection compared to the naïve state (Figure 3.10.3). Statistical analysis of glycolysis in control and *Sesn1*-deficient macrophages showed a significant increase with statistical significance of $p=0.0008$ and $p=0.0021$ respectively, after infection (Figure 3.10.3). Interestingly, *Sesn1*-deficient macrophages displayed significantly more glycolytic ATP production compared to the control cells post infection ($p=0.0272$), whereas at a naïve state, there was no significant difference in glycolysis between macrophages (Figure 3.10.3). This suggests that *Mtb* infection was able to alter the metabolism of these cells. Together with increased total ATP production, this affirms the concept that *Sesn1* plays a regulatory role in cell metabolism, which seems to be more evident after *Mtb* infection.

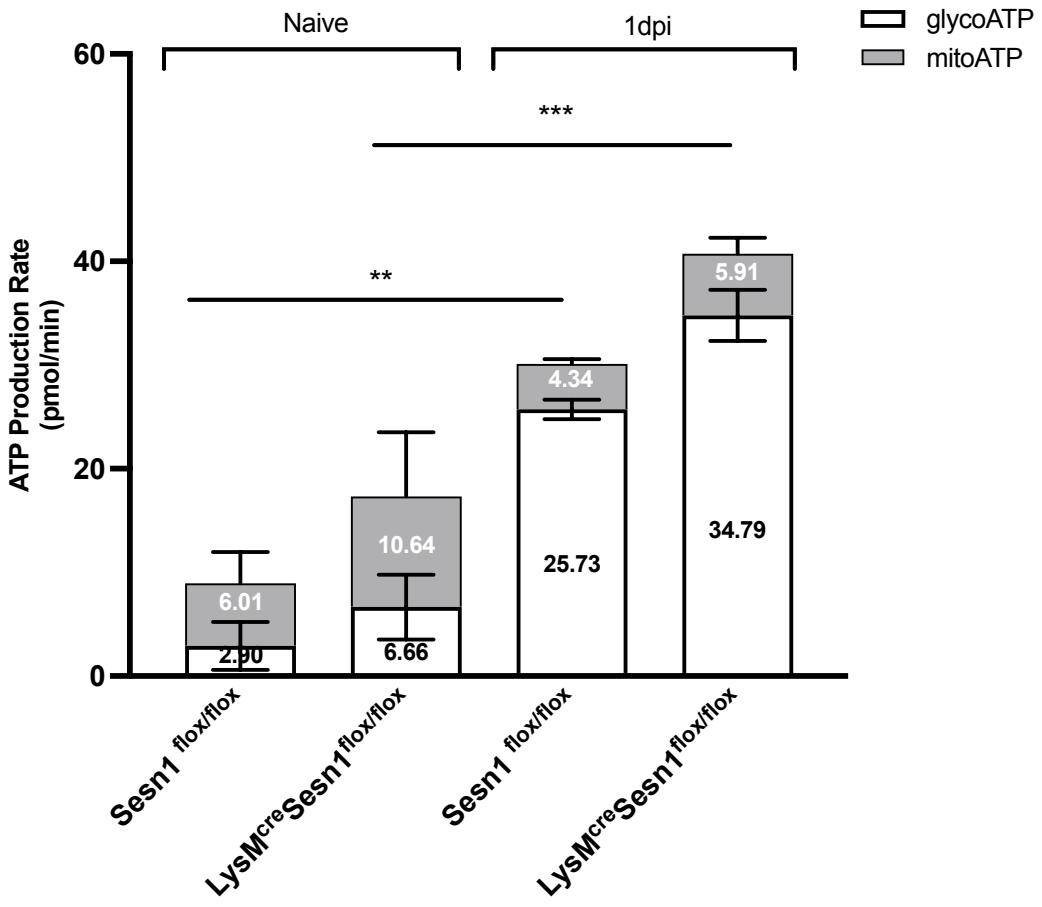

Figure 3.10.3: **Deletion of *Sesn1* in macrophages increased total ATP production rate and glycolysis in BMDMs post infection.** BMDMs were seeded at a concentration of $1x10^5$ cells per well and were analyzed at a naïve state or were infected with HN878 at an MOI of 0.5 for 24 hours. Using the Real-Time ATP Rate Assay and Seahorse Analyzer, the ATP production rate was measured. Results from naïve and 1-day post infection experiments display the total ATP production rate whilst distinguishing between mitochondrial and glycolytic production of ATP. a) Metabolic states of *LysM*cre*Sesn1*$^{flox/flox}$ and *Sesn1*$^{flox/flox}$ naïve BMDMs and BMDMs after 1-day post infection. Data show mean ± SEM of n=2-3 replicates and representative of three independent experiments. For statistical analysis, ANOVA was used, corrected for multiple comparisons to compare ATP production rate in control versus knockout mice, and the following p values were used for significance, **p <0.01, ***p <0.01.

Additionally, the readout showed a snapshot of the bioenergetics of the cell at a basal state, prior to any addition of metabolic inhibitors; and at the time point where inhibitors are injected (under metabolic stress). The *Sesn* family of genes are stress-inducible and their anti-inflammatory roles have been exploited in other disease models but have not been examined in the context of infectious disease. This prompted us to explore the impact of *Sesn1* deletion on the bioenergetic state of macrophages, at a basal state (absence of stress), and under metabolic stress (when

metabolically challenged) after the addition of metabolic inhibitors, oligomycin and rotenone/antimycin A. Analysis of the bioenergetic states of the *LysM*^{cre}*Sesn1*$^{flox/flox}$ and *Sesn1*$^{flox/flox}$ macrophages showed that at a naïve, basal state, *LysM*^{cre}*Sesn1*$^{flox/flox}$ macrophages lean towards a more energetic state and *Sesn1*$^{flox/flox}$ macrophages are more glycolytic, both macrophages closely linked with a metabolically active state (Figure 3.10.4a). During metabolic stress but the absence of *Mtb*, *Sesn1*$^{flox/flox}$ macrophages transition to a more quiescent state (Figure 3.10.4b). In contrast, the *LysM*^{cre}*Sesn1*$^{flox/flox}$ macrophages remain in an energetic state, with a slight increase towards a glycolytic phenotype (Figure 3.10.4b). During infection at a basal state, both macrophages are closely associated with a metabolically active energetic state (Figure 3.10.4c). However, once oligomycin and rotenone/antimycin A are added, the *Sesn1*$^{flox/flox}$ macrophages no longer notably transition to a quiescent state but still shift towards a less energetic state (Figure 3.10.4b and d). The *LysM*^{cre}*Sesn1*$^{flox/flox}$ macrophages, in contrast, have a consistent energetic phenotype, regardless of *Mtb* infection or metabolic stress (Figure 3.10.4a-d). Therefore, *LysM*^{cre}*Sesn1*$^{flox/flox}$ macrophages have demonstrated a consistent energetic state even under metabolic inhibition, suggesting a dysfunctional regulation of metabolism in the absence of *Sesn1*.

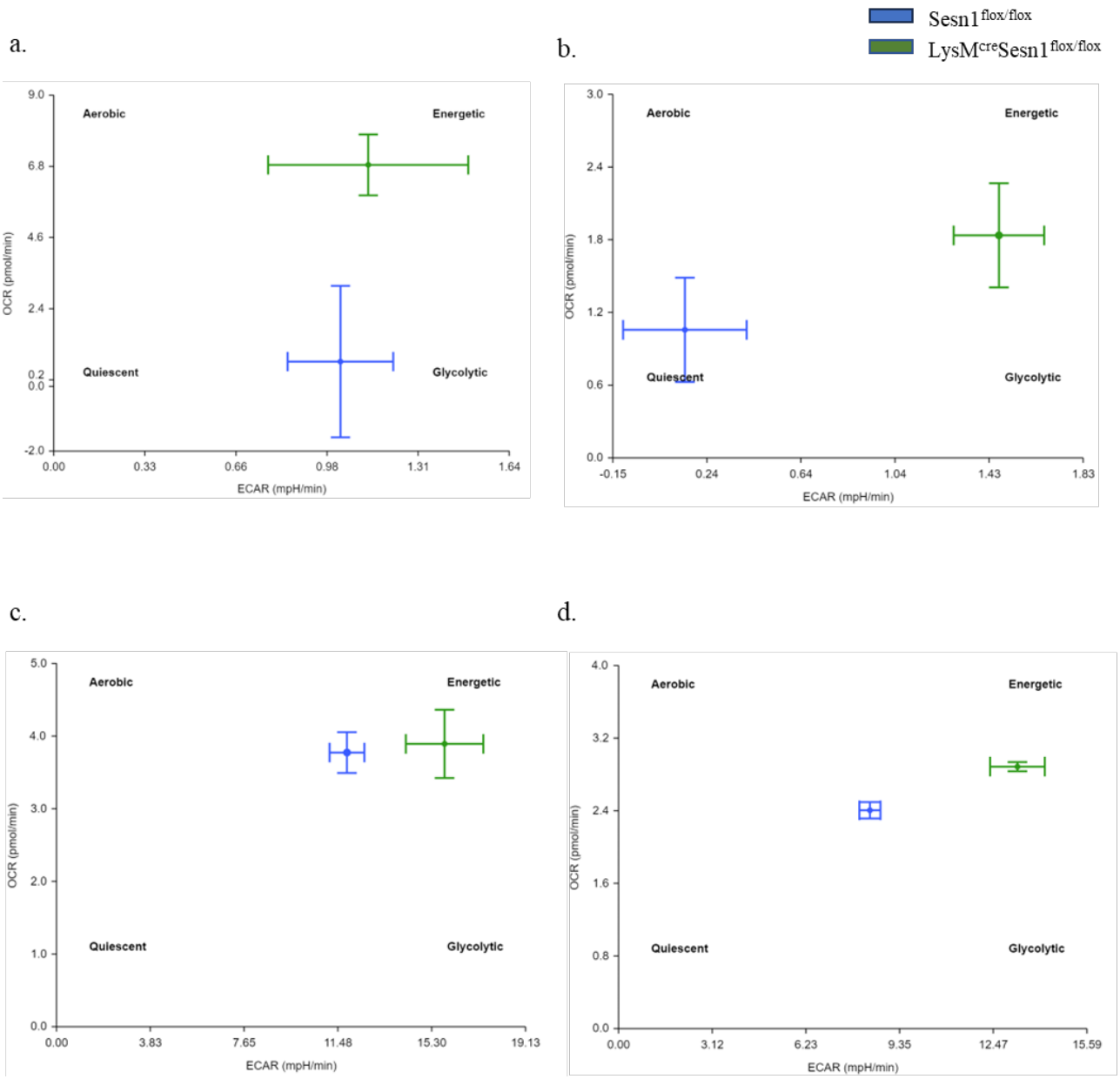

Figure 3.10.4: ***Sesn1*-deficient macrophages showed a consistent energetic state.** BMDMs were seeded at a concentration of $1x10^5$ cells per well and using the Real-Time ATP Rate Assay and Seahorse Analyzer, we analyzed the bioenergetic profile of *LysM*^{cre}*Sesn1*$^{flox/flox}$ and *Sesn1*$^{flox/flox}$ BMDMs at a naïve state and after 24-hours of infection. Measurements were taken at a basal state of the cells, and at the point of metabolic stress using metabolic inhibitors a) Naïve, the basal metabolic state of *LysM*^{cre}*Sesn1*$^{flox/flox}$ (blue) and *Sesn1*$^{flox/flox}$ (green) BMDMs. b) Naïve metabolic state of *LysM*^{cre}*Sesn1*$^{flox/flox}$ (blue) and *Sesn1*$^{flox/flox}$ (green) BMDMs after the addition of metabolic inhibitors, oligomycin and antimycin A/Rotenone (metabolic stress). c) Basal metabolic state of *LysM*^{cre}*Sesn1*$^{flox/flox}$ (blue) and *Sesn1*$^{flox/flox}$ (green) BMDMs after 1-day post infection. d) Metabolic state of infected *LysM*^{cre}*Sesn1*$^{flox/flox}$ (blue) and *Sesn1*$^{flox/flox}$ (green) BMDMs after addition of metabolic inhibitors, oligomycin and antimycin A/Rotenone (metabolic stress). Data shown is representative of 2-3 independent experiments, analyzed and generated using Seahorse Analytics online software.

Collectively, our data suggest that *Sesn1*-deficient macrophages display a more inflammatory phenotype that may potentiate cell death *in vitro*. Shown here with increased pro-inflammatory cytokines (apart from IL-1α), increased ROS, and increased cell death which may be facilitating the increased bacterial burden in macrophages. Furthermore, these macrophages may be less efficient at regulating metabolism, resulting in increased metabolic rate and energetic state despite stressful conditions. ROS being a natural byproduct of cell metabolism, it is likely that the absence of *Sesn1* increased metabolic rate in these cells is responsible for the high levels of ROS. Here, we showed that the *Sesn1* may dampen inflammatory responses in macrophages, and its regulation of ROS, which is a driver of cell death at a cellular level.

CHAPTER 4: DISCUSSION AND CONCLUSION

Tuberculosis remains a burden faced by millions of people around the world, predominately in low- to middle-income countries (2). Despite efforts to eradicate this disease, it is still able to persist and adapt to its environment within the host, under immune defense (17). Despite evolving treatment strategies, we are failing to effectively diagnose, treat and prevent tuberculosis disease with traditional antibiotic therapy and vaccines (68).

It was previously thought that an inadequate immune response to *Mtb* was the driving force behind susceptibility but is now understood to be a far more complex problem (66,67). Tuberculosis disease indeed requires a pro-inflammatory response to control infection, however, hyper-inflammatory responses at a chronic stage may contribute to increased lung tissue pathology and worsen disease outcomes in individuals (67,84). It remains uncertain why selected individuals progress to active TB while others can remain latently infected or recover from tuberculosis, highlighting the need for a deeper understanding of the intricate host immune dynamics during infection. Thus, our approach to eradicate tuberculosis needs to be multifaceted, and using host-directed therapies to limit damage by balancing the immune response, while killing *Mtb* with antibiotics, may provide the next breakthrough (68).

The focus of our study was to understand the role of Sestrins, a family of stress-inducible, anti-inflammatory proteins, that have been overlooked in infectious diseases (85,88,89,141). The role of Sestrins in non-communicable diseases has been extensively studied, providing valuable insights into their potential benefits in infectious diseases such as tuberculosis, where balancing the immune system and promoting tissue repair are critical. Sesn1 is regarded as a potential tumor suppressor in cancer, with the genetic locus 6q21, which contains *Sesn1*, frequently lost in several malignant cancers, including leukemia, lymphoma, and cancers of the pancreas, stomach, and kidney (142). Additionally, a study showed that expression of all three *Sestrins* was elevated in patients with permanent atrial fibrillation compared to those in sinus rhythm, suggesting that Sestrins may serve as protective factors in atrial fibrillation (143). However, the dynamics of all three Sestrins remain incompletely understood and may involve independent regulatory

mechanisms. For example, research by Wang et al. demonstrated increased expression of *Sesn2*, rather than *Sesn1* or *Sesn3*, in patients with ischemic and dilated cardiomyopathy (141,144).

Research on Sesn3 has exhibited roles in insulin resistance and cancer, and detrimental effects during epilepsy (145–147). In a study focusing on hepatic insulin sensitivity, *Sesn3* KO mice showed insulin resistance and glucose intolerance, whilst *Sesn3* transgenic mice were protected. The Sestrin 3 protein was shown to directly activate mTORC-Akt signaling, enhancing and regulating hepatic insulin sensitivity and glucose metabolism (147). Another study investigating the effects of cucurbitacin B on lung cancer cells found that Sesn3 is crucial for the anti-cancer activity of cucurbitacin B. Noting that epidermal growth factor receptor (EGFR) regulates cell proliferation, differentiation, and apoptosis in normal cells, the treatment specifically increased *Sesn3* expression in EGFR-mutant lung cancer cells, but not in EGFR-wild type cells. Furthermore, Sesn3 was found to play a role in apoptosis induced by cucurbitacin B in both EGFR-mutant and EGFR-wild type lung cancer cells (146). A third study investigated the role of Sesn3 in the central nervous system, highlighting its potential involvement in epilepsy. It was found that *Sesn3* was the transcriptional module, encoding proconvulsive cytokines and Toll-like receptor signaling genes in macrophages, microglia, and neurons. Notably, *Sesn3* ablation in zebrafish significantly reduced chemically induced behavioral seizures. These findings suggest the possible pro-epileptic effect of Sesn3 and demonstrates the varied functions of Sestrins in different central nervous system disorders (145).

While Sesn2 is relatively well-characterized, with a substantial body of research and literature available, the roles of Sesn1 and Sesn3 in various diseases are less well understood, leaving their full functional capacities unclear. Furthermore, the dynamic expression patterns and potential compensatory functions of different *Sesn* isoforms within the context of the same disease remain to be elucidated (141).

Given the extensive literature on Sesn2 and its anti-inflammatory and repair-promoting effects in various diseases, we prioritized *Sesn2* for our study. However, CAGE data from the FANTOM5 study revealed a marked decrease in *Sesn1* expression following *Mtb* infection, prompting us to investigate *Sesn1*, despite limited evidence in the literature (128,129). We did not prioritize *Sesn3*

due to its very low expression levels compared to *Sesn1* and *Sesn2*, indicating *Sesn3* may play a minor or no role during *Mtb* infection, hence *Sesn3* knockout mice weren't generated.

Using a *Sesn2* null and *Sesn1* macrophage-specific knockout mouse model, we showed that *Sesn2*-deficiency resulted in increased lung pathology and enhanced mortality in TB disease. However, macrophage-specific deletion of *Sesn1* had no major effect on the TB disease outcome. The depletion of *Sesn1* in macrophages/neutrophils alone proved insufficient to elicit a phenotype, this may be due to the compensatory expression of *Sesn1* in other cell types obscuring its full biological impact. This limitation could result in a lack of observable effects in the cell-specific knockout model. Subsequently, a global *Sesn1* knockout mouse model was generated to address limitations of the cell-specific approach. The experiment is ongoing, beyond the scope of this thesis and part of future investigations. Moreover, using macrophages derived from these models, we found increased bacterial growth, pro-inflammatory responses, ROS production accompanied with cell death *in vitro*. Our *in vitro* data provides a more direct evaluation of *Sesn1* function, as macrophages are the primary cells analyzed, ensuring complete *Sesn1* depletion in these cells *ex vivo*.

For the purpose of our study, we used the *Mtb* HN878 strain but is difficult to assume how a different strain or lineage of *Mtb* would influence the outcome of host-pathogen interaction. However, from previous literature, it is plausible that we may observe an overlap and differences in results. Studies use various strains, from H37Rv to Erdman, and this question would remain. Among infections, there is a growing prevalence of clinical isolates from the W-Beijing family, including HN878, estimated to be responsible for approximately 50% of TB cases in East Asia and approximately 13% of isolates worldwide (148). Furthermore, studies have identified HN878 as being a large contributor of drug resistance and highly associated with individuals living with HIV (12,13). Lastly, it is suggested that the BCG vaccine may be less protective against W-Beijing *Mtb* strains, including HN878, possibly contributing to its successful emergence and spread (148). This served as motivation to use HN878 *Mtb* strain for infection in our studies. A further motivation for using HN878 is the following study that supported the use of HN878 for infection of mice to study immune parameters during TB disease. The study found that HN878-infected mice developed granuloma structures closer to granulomatous structures in humans, with bacilli-

loaded macrophages surrounded by lymphocytes. In contrast, H37Rv triggered unorganised clusters of macrophages in between lymphocytes, presenting HN878 as a more appropriate strain to use in mouse models (14). Another study found that the IL-17 pathway was dispensable for protective immunity against H37Rv and CDC1551 but was necessary for early protection against HN878 (15). Thus, confirming differing results based on the strain used. Based on this evidence, I would suggest that optimizing HDTs using hypervirulent *Mtb,* which has high prevalence, is preferable. If an effective HDT is revealed using HN878, it will have a widespread benefit, help target drug resistance and reducing burden in the population. It is my speculation that using highly virulent HN878 could replicate a 'worst case scenario' in tackling the TB burden, with the assumption that TB caused by *Mtb* strains of lower virulence could also be alleviated. However, one need to perform experiments which each strain to reveal the underlying differences in immune response mounted by different *Mtb* strain to support or reject the potential as HDT candidates.

Sestrin 2 has demonstrated its ability to alleviate tissue damage in various inflammatory disease models (105,108). Additionally, elevated levels of *Sesn2* have been associated with tissue healing, for instance, after myocardial infarction (120). This role of *Sesn2* has not been investigated during TB disease, where lung tissue pathology is a crucial determinant of disease outcome, we have demonstrated, that the absence of *Sesn2* in mice led to an increased inflammatory response during infection (Figure 3.3.3). This was associated with increased lung tissue pathology in *Sesn2* knockout mice (Figures 3.2.5 and 3.3.5), and subsequent mortality to *Mtb* infection *in vivo* (Figure 3.4.1). Thus, supporting the concept that *Sesn2* is an important player in regulating processes involved in pathology. In contrast to *Sesn2*, macrophage-specific deletion of *Sesn1* had no effect on lung pathology during disease and proved to be dispensable in mortality studies (Figure 3.7.5, 3.8.5 and 3.9.1). Given this, it is speculative, that the simultaneous deletion of other family members (*Sesn1* and *Sesn3*), to ablate all antioxidant responses from all 3 paralogues of Sestrin may be more dramatic (97,98). However, our RNA analysis showed no major changes in the expression of other *Sestrins* in *Sesn2*$^{-/-}$ macrophages. Moreover, *LysM*^{cre}*Sesn1*$^{flox/flox}$ mice showed decreased *Sesn2* expression in lung tissue *in vivo.* This suggests that in our study there was no major compensatory effect from the *Sesn* family of genes, but we cannot ignore that *Sesns* were still expressed and shared similar regulatory roles displaying a level of redundancy (88).

The mechanism behind decreased *Sesn1* expression during *Mtb* infection remains unclear and was identified using our previously reported transcriptomics study (128,129). Furthermore, our expression data from WT and *Sesn2*$^{-/-}$ macrophages, showed decreasing *Sesn1* levels over the course of *Mtb* infection *in vitro* (Fig 3.5.2b). Thus far it is known that *Sesn1* expression is dependent on transcription factors p53 and Foxo in response to DNA damage and oxidative stress (142). We saw a similar trend increase between *Foxo3* and *Sesn1* expression in *Sesn2*$^{-/-}$ macrophages prior to infection (Fig 3.5.2b and d). This suggests that the transcription factor, *Foxo3* may be involved in positive regulation of *Sesn1*.

In other diseases, *Sesn1* is regarded as a possible tumour suppressor in cancer. The genetic locus 6q21 (which contains *Sesn1* is often lost during malignant cancers including, leukemia and lymphoma, and cervical, pancreatic, stomach and kidney cancers (142). Furthermore, follicular lymphomas are often associated with 6q21 translocation and genetic mutations in the *EZH2* gene (encoding histone lysine methyltransferase), where the EZH2 protein is a down-regulator of Sesn1 (153). In cardiac failure, *Sesn1* expression decreased during pressure overload- and phelylephrine (PE)-induced cardiac hypertrophy. Knockdown of *Sesn1* exacerbated PE-induced cardiac hypertrophy, while overexpression of *Sesn1* prevented hypertrophy by regulating autophagy through the AMPK/mTORC pathway (154,155). Although it is unclear what mechanisms drive the decrease in *Sesn1* during TB disease, differential *Sesn1* expression has been observed in other disease models, and the impact on disease severity and outcome depends on the disease in question.

The roles of Sestrins have not been clearly elucidated in communicable diseases, however studies have used LPS to demonstrate the anti-inflammatory role of Sestrins. Knockdown of *Sesn2* in HUVECs, THP-1 cells and aortic tissue from C57BL/6 mice resulted in increased NFκB phosphorylation and pro-inflammatory cytokine secretion. *Sesn2* knockdown in HUVEC cells displayed elevated levels of LPS-induced ROS, cell toxicity and endoplasmic reticulum (ER) stress. The study showed that the pro-inflammatory effects were nullified upon treatment with an AMPK activator, suggesting that *Sesn2* knockdown aggravates pro-inflammatory responses via an AMPK-dependent pathway and Sesn2 could provide therapeutic relief in balancing inflammation (104) Furthermore, antioxidant genes such as *catalase* and *superoxide dismutase (SOD2)* were downregulated, and the production of ROS was increased when cells were stimulated with LPS. Furthermore, the expression of matrix metalloproteinase *(MMP) 2* and *MMP9*, which are activated

by ROS, were increased in the *Sesn2*-depleted H9c2 cells, and LPS-induced cell death increased (105).

A recent study that explored the regulation of TLR-mediated inflammation by Sesn2 showed that Sesn2 inhibited LPS-induced nitric oxide (NO) release and *iNOS* expression in RAW264.7 cells. *Sesn2* expression was able to suppress the release of pro-inflammatory cytokines (TNF- α, IL-6, and IL-1 β amongst others) and suppress the production of LPS-induced ROS by inhibiting nicotinamide adenine dinucleotide phosphate (NADPH) oxidase (85). More specifically, overexpression of *Sesn2* was shown to regulate c-Jun, JNK and p38 phosphorylation induced by LPS. This regulation led to decreased AP-1 binding, thus reducing the pro-inflammatory responses (85). By introducing recombinant *Sesn2* into mice via an adenovirus, the effects of severe hepatic injury were attenuated, as seen by the decreased ALT, AST and hepatocyte degeneration.

Given the antioxidant role of Sestrins, a study investigated whether *Sestrin* 2 expression was altered in the brains of individuals with HIV-associated neurocognitive disorders (HAND) due to neuronal oxidative stress (156). Comparing HAND with Alzheimers Disease (AD), the results suggested a distinct role for *Sestrin* 2 in HAND pathophysiology compared to AD, with Sestrin 2 immunoreactivity localising in different regions of the brain. In summary, differences in immunohistology patterns between HAND and AD suggested distinct mechanistic pathways, despite a shared involvement of oxidative stress. Alternatively, this difference may have reflected varying severity or stages of oxidative stress between HAND and AD (156). In this sense, Sestrins may play a similar role in communicable and non-communicable diseases as an antioxidant protein that regulates ROS. However, multiple transcription factors and signalling pathways underpin the role of Sestrins, namely, p53, Foxo3, ROS, TLRs, among others, and depending on the disease in question the specific role of Sestrin may vary.

Of importance, the depletion of *Sesn2* resulted in significant lung tissue pathology at both time points (Figure 3.2.5 and 3.3.5). However, at 12wpi we found a greater effect on immune cell recruitment in *Sesn2*-deficient mice compared to at 6wpi (Figure 3.3.3 and 3.2.3). *Sesn2* has been closely associated with age-related pathologies, with expression increasing during maturation, reducing immunity in older populations (123). In addition, our preliminary finding showed no difference in lung tissue pathology at 3-weeks of infection (Figure S1a-c), supporting our theory

that *Sesn2* plays a more impactful role during prolonged disease and is consistent with the literature on the importance of *Sesn2* in age-related pathologies (123).

Sestrin 1 and Sestrin 2 have been studied in various organs, including the heart, brain, liver and lungs, and have shown disease ameliorating effects specific to these organs. For example, knockdown of *Sesn2* led to the expression of cardiac fibrotic factors, such as collagen type I and II in the heart tissue of C57BL/6 mice (105). *Sesn2* deficiency promoted pyroptosis through activation of the NLRP3 inflammasome, and knockout mice showed exacerbated liver fibrosis (108). Research is more limited for the role of Sesn1 in organs, but studies have shown that knockdown of *Sesn1* exacerbated PE-induced hypertrophy, while overexpression of *Sesn1* prevented cardiac hypertrophy by regulating autophagy through the AMPK/mTORC pathway (154,155). Studies have therefore shown different biological outcomes for these genes, even in the same organ, suggesting that these genes have different roles despite possessing similar anti-inflammatory functions. This is supported by the difference in transcription and regulatory factors, between these two genes.

For our study, the primary organs examined during *Mtb* infection were lungs and lymph nodes. These two organs can be described as two separate compartments in the context of *Mtb* infection and TB disease. The lungs are the site of infection and will possess organ-specific factors that shape the outcome of TB disease, distinct from the environment within lymph nodes. The reported tissue-repairing, anti-fibrotic role of Sesn2 may have a greater effect in the lung tissue than the lymph nodes in this scenario, where fibrotic lesions in the lung may lead to worsened outcome.

Secondly, expression of all three *Sestrins* vary in different organs, and may be a contributing factor to the difference and impact that *Sesn1* and *Sesn2* play in the lung and lymph nodes. While no expression data is available for *Sesn1* and *Sesn2* in the lymph nodes, the Mouse ENCODE transcriptome database demonstrates the differential expression of these genes in other organs. For example, *Sesn1* is expressed at 6.12 FPKM in the lungs, and 16.15 FPKM in the heart (157).

Lastly, given that TB is a spectrum of disease, the duration of infection may also influence the organ environment, for instance, the immune cell milieu, and immune cell infiltration early on in infection in the lungs and lymph nodes versus later in disease. Since Sestrins are stress inducible proteins, the environment in which they are responding to will impact their role. Therefore organ-

specific factors/environment, such as inherent gene expression levels and immune cell landscape may explain the observed differences between the lungs and the lymph nodes.

Our interrogation of factors contributing to lung pathology *in vivo* revealed increased neutrophils in both the macrophage-specific *Sesn1*- and *Sesn2*-deficient mice (Figure 3.2.3, 3.3.3 and 3.7.3). Neutrophilia has been linked to exacerbated TB and lung tissue damage in animal models (158–160). However, the macrophage-specific *Sesn1*-deficiency revealed opposing neutrophil recruitment between the two 6- and 12-weeks further confirmed with no major effect on lung pathology (3.7.3, 3.8.3, 3.7.5 and 3.8.5). *Sesn1*, has been shown to promote autophagy, ameliorate hypertrophy, and able to reduce ROS by potentiating Nrf2 and regulating Keap1 resulting in a cytoprotective effect (87,161,162). As expected, the absence of *Sesn1* resulted in increased ROS production in macrophages. Even though macrophages play a crucial role in TB disease, they are not the only determinant of TB manifestation. It is known that various leukocytes, their functionality and complex interactions contribute to disease outcomes (17–19). Therefore, it is likely that other cells compensated for intact *Sesn1*, and macrophage-specific deletion proved negligible *in vivo*. However, *Sesn1*$^{-}$deficient macrophages isolated from the *LysM*^{cre}*Sesn1*$^{flox/flox}$ mice would recapitulate an environment null of *Sesn1* at a cellular level. To elucidate the role of *Sesn1 in vivo*, it would be interesting to generate a global ablation of the gene for future studies.

Pertaining to neutrophilia, IL-1β cleavage and activation, dependent on the NLRP3 inflammasome, has been shown to enhance neutrophil recruitment and lung pathology (158–160). *Sesn2* has been linked to the NLRP3 inflammasome, suppressing its activity by promoting mitophagy (106) and by extension, linking *Sesn2* to IL-1β secretion. However, we demonstrated that despite increased neutrophils, the levels of IL-1β remain unchanged *in vivo* (Figure 3.3.2 and 3.3.3). In contrast, both *Sesn2*$^{-/-}$ and *Sesn1*$^{-/-}$ macrophages showed elevated IL-1β levels *in vitro* (Figure 3.5.1e and 3.10.2b). This disparity can be explained by noncanonical mechanisms of IL-1β processing, *in vivo* (163). A previous study showed that ablation of NLRP3 in macrophages decreased IL-1β, demonstrating canonical inflammasome involvement (dependent on NLRP3). However, *in vivo* depletion of NLRP3 in mice caused no change to IL-1β levels, alluding to noncanonical processing of IL-1β independent of NLRP3, and consistent with our results (164–166). Since *Sesn2* was previously shown to reduce NLRP3 activation, and elevate levels of IL-1β

in macrophages, but not *in vivo* (164–166). Additionally, our metabolic analysis of *Sesn1*- and *Sesn2*-deficient macrophages displayed a glycolytic shift after infection (Figure 3.5.3 and 3.10.3) and recent studies have linked increased IL-1β secretion to glycolytic reprogramming by *Mtb*, positively correlating to ATP levels within cells (Figure 3.5.3), further explaining our increased IL-1β in the absence of *Sesn2* (167–169).

In contrast to IL-1β, IL-1α secretion was significantly decreased in *LysM*^{cre}*Sesn1*$^{flox/flox}$ macrophages. It's been previously shown that blocking IL-1α in innate response, increased susceptibility to chronic TB disease in mice (170). Consistent with this, low levels of IL-1α could be a contributor to increased cell death and bacterial growth in *LysM*^{cre}*Sesn1*$^{flox/flox}$ macrophages *in vitro*. Interestingly, IL-1α and IL-1β have opposing trends in *Sesn1*-deficient macrophages. The exact regulation, roles and secretion of these IL-1 cytokines during bacterial infections remains elusive and continues to be studied (171). While IL-1β is important in initial mycobacterial control, chronically elevated levels cause the expression of tissue-damaging inflammatory mediators, prostaglandin E2 and metalloproteinases (MMPs) (172–174), whereas IL-1α is indispensable to protection (170,171). The non-redundancy of IL-1α and IL-1β supports our data of differential secretion in response to *Mtb* infection, with the former serving as protective and the latter contributing to tissue pathology (171,172).

In macrophages, we detected increased TGFβ production in the absence of *Sesn1* (but not in *Sesn2*$^{-/-}$ mice) (Figure 3.5.1h and 3.10.2f). TGFβ has been linked to characteristic tissue destruction during TB disease (175,176). Another study that analyzed the localization of cytokines and histopathological changes during pulmonary TB found TGFβ to be at its highest during severity, associated with necrosis, and interstitial fibrosis (177), indicating that TGFβ may have a primary role in TB immunopathogenesis. TNF secretion also increased in *Sesn1*- and *Sesn2*-deficient macrophages; a cytokine linked to increased susceptibility during hyper-inflammatory responses during TB disease (84). Secretion of IL-6 had opposing results in *Sesn1*- and *Sesn2*-deficient macrophages, with increased and decreased levels respectively (Figure 3.5.1f and 3.10.2d). This result in *Sesn2*$^{-/-}$ macrophages was surprising, considering that overexpressing *Sesn2* in macrophages showed decreased IL-6 levels in a previous study (85). Collectively, we detected

greater pro-inflammatory cytokine responses in the absence of *Sesn1* and *Sesn2* in macrophages, (Figure 3.5.1 and 3.10.2) demonstrating the role of Sestrins in regulating immune responses (120).

Our *in vivo* studies, for example the *Sesn2* 6wpi experiment, showed no differences in cytokines, chemokines or growth factors between groups. However, we observed an increase in immune cell recruitment in the absence of *Sesn2*, including the myeloid population which is largely due to the back calculation of absolute cell number to the lung, which was significantly increased in the knockout group. Notably, the ELISA panel we focussed on may not have encompassed the defect, however, we included all major cytokine/chemokines reported in the TB field. Therefore, it is unclear what led to the significant increase in immune cell recruitment. Moreover, cytokines have a dichotomous role dependant on their microenvironment, concentrations and the interplay between present cytokines and immunometabolism (13).
Additionally, while CFU load is a key factor in TB disease research, it is not the sole determinant of disease progression/outcome. The heightened pathology of *Sesn2* KO mice, despite similar CFU levels, suggests that their susceptibility is independent of antigenic load. Another study focusing on B cells, found a similar phenomenon, where B cell deficient mice were more protected despite having similar CFU counts to the wildtype mice (134). The authors concluded that this protection was not based on a lower bacterial load, but rather the role of B cells in augmenting inflammation within the lung microenvironment (134). Here we propose that the increased infiltration of immune cells, including myeloid cells, did not control CFU, but did contribute to increased lung tissue pathology. Additionally, we hypothesize, that increased ROS levels in the absence of *Sesn2*, as demonstrated in macrophage *in vitro* studies, may also contribute to tissue damage.

Sestrins are important regulators of mTOR, controlling cell growth and mitochondrial integrity of cells and eliminating dysfunctional mitochondria that produce excess ROS (88,92,94). Subsequently, *Sesn2* tightly regulates the accumulation of ROS (98,120). Consistent with the literature, we found elevated ROS accumulation in *Sesn1*- and *Sesn2*- deficient macrophages (Figure 3.5.1c and 3.10.1c), which may be associated with pathophysiological tissue damage, and at a cellular level may manifest as increased cell death observed in the *Sesn1* and *Sesn2*-deficient macrophages (Figure 3.2.1b) (85,105,120). This is accompanied by *Sesn1*- and *Sesn2*- deficient macrophages which displayed higher bacterial burden but displayed no differences in the lung *Mtb*

burdens *in vivo*. It is uncertain whether macrophages were less capable of controlling *Mtb* growth, or whether increased cell death and immune aberration facilitated a more permissible environment for *Mtb* (Figure 3.5.1a). In this context, having reported accumulation of ROS and increased cell death, our contradictory cell viability result was unexpected (Figure 3.5.1d and 3.10.1e). We speculate that this measurement reflects the metabolic activity of cells rather than a robust measurement of viability, considering that CellTiter Blue dye relies on cellular reduction of resazurin to resorufin in metabolically active cells (137). To corroborate these results, our metabolomic data showed significantly increased total ATP production rate in macrophages deficient in *Sesn2* (only a trend increase in *Sesn1* deficient macrophages) (Figure 3.5.3 and 3.10.3), suggesting that Sestrin deficiency indeed increased metabolic activity.

Considering the role of Sestrins in mTOR regulation, mitophagy and ROS are known, we investigated macrophage metabolomics to elucidate the role of Sestrins during *Mtb* infection. Here, we show an increased total ATP production rate post infection compared to the naïve state in *Sesn1*- and *Sesn2*-deficient macrophages (Figures 3.5.3 and 3.10.3). Furthermore, we demonstrate that post infection, macrophages transition to a glycolytic dependence of ATP production in *Sesn1*- and *Sesn2*-deficient cells. *Mtb* infection has shown a role in reprogramming cell metabolomics, but this phenomenon is not fully understood and lacks consensus (168,178). A recent study described a similar glycolytic metabolic shift induced by *Mtb* infection (168). However, cell energetics during *Mtb* infection is dependent on the strain and concentration of inoculum, additionally to the cell type being infected (178). Infection with virulent *Mtb* did not cause a drastic glycolytic shift that was observed with avirulent or killed *Mtb* (178). Moreover, hMDMs and THP-1 cells showed distinct energetic profiles post infection (178). Hereby, substantiating the variable results, our data represent increased ATP production rate and glycolytic shift in BMDMs, with an MOI of 0.5, in contrast to hMDMs or THP-1 cells inoculated at an MOI of 5. It is feasible that low MOI used in our study may explain glycolytic phenotype closer to avirulent *Mtb* (178). Moreover, analysis of bioenergetic states demonstrated that ablation of *Sesn1* or *Sesn2* induced a consistent energetic phenotype in macrophages, despite *Mtb* infection, suggesting dysfunctional metabolic activity and atypical cell response to stress (Figure 3.5.4 and 3.10.4). *Sesn1*-depleted macrophages remained in an energetic state even under metabolic stress (Figure 3.10.4b), using oligomycin and antimycin A to recapitulate metabolically challenging environments. A previous study, found

Sesn2 to be protective in a p53-independent manner, assisting cancer cells to survive even under metabolic stress (109). In the presence of stress, either mediated through p53 or directly through increased ROS, *Sesn2* is expressed and suppresses mTORC activity, thereby regulating cellular growth and metabolism (94,109). The consistent energetic state of *Sesn1*- and *Sesn2*-deficient macrophages strongly suggests an aberrant cell response to stress in the absence of these regulatory proteins.

To substantiate the relevance of *Sesn1* and *Sesn2* in mice versus humans, we can compare the relative expression of these genes between the species. Using the ENCODE mouse transcriptome database, *Sesn1* and *Sesn2* are expressed at a similar level in murine lungs, approximately 6 FPKM, where FPKM represents Fragments Per Kilobase of transcript per Million mapped reads (157). In human lungs, *Sesn1* expression is measured at 14 FPKM, considerably higher than *Sesn2*, at 3 FPKM (179). Considering that the lungs are the site of *Mtb* infection, the differential expression between these two models motivates *Sesn1* relevance in humans, as it is expressed the highest in human lungs. While mouse models have value in understanding mechanisms and provide the tool for experimenting *in vivo*, translating findings to human studies may have alternate results.

We suggest, that in the absence of *Sesn1* or *Sesn2*, mTORC remains active despite cellular stress, and contributes to the accumulation of ROS. While ROS is crucial for signaling, elevated levels are known to have damaging, inflammatory effects. To support this, we've demonstrated that macrophages deficient in *Sesn1* or *Sesn2* remain in an energetic state despite metabolic stress, or *Mtb* infection and Sestrin deficiency consistently showed increased total ATP production rate, indicative of increased metabolic activity. Since ROS is a natural bioproduct of metabolism, in the absence of either Sestrin, ROS levels accumulate, possibly contributing to increased cell death, and *in vivo*, contributing to lung pathology during TB disease. ROS-associated tissue damage and inflammation have been studied in other inflammatory disease models, where Sesns are shown to alleviate the damage caused (112). Substantiating our hypothesis of ROS-mediated cell death (Figure 4.1). Our proposed mechanism does not discount the contribution of other drivers of lung pathology, *per se,* but rather suggests the role of aberrant ROS accumulation in the pathophysiology of TB disease. Further studies to reaffirm this hypothesis could include overexpression and concurrent knockdown experiments. Additionally, proof of concept can be

tested by treating Sestrin-deficient cells with N-acetyl cysteine (NAC). NAC, a precursor of the master antioxidant Glutathione, is known to reduce ROS accumulation in cells and would confirm whether cell death is mediated by ROS accumulation (180).

Given the reported roles of Sestrins, as HDT targets, upregulating *Sestrins* could help mitigate TB-associated tissue pathology, which worsens disease outcome. However, due to Sestrins' anti-inflammatory effects, individuals with inherently weak immune responses might experience adverse outcomes, similar to findings from the Vietnamese trial where glucocorticoid treatment in participants with *LTA4H* variants impaired TB outcomes by disrupting TNF's dual role in resistance and susceptibility to *Mtb* (84). While excessive immune responses exacerbate TB pathology, a sufficient immune response remains essential for infection clearance.

Our study demonstrated that *Sesn2* ablation led to increased immune cell infiltration, lung tissue pathology, and greater mortality in mice. Therefore, therapies enhancing *Sesn2* levels may reduce immune infiltration, pathology, and associated mortality. However, given genetic variability in the population and Sestrins' role in ROS regulation, over-reduction of ROS in some individuals could impair critical microbicidal and signalling functions.

Further studies are required to confirm whether increased *Sestrin* levels reduce immune cell responses. However, existing evidence associates elevated *Sestrin* levels in aged populations with immune decline, contributing to heightened susceptibility to infections and malignancies (84). Additionally, studies have shown increased *Sestrin 1* and *Sestrin 2* expression in aging, with inhibition of these genes enhancing influenza-specific CD4 T-cell responses post-vaccination (84). The authors advocated for temporary inhibition of Sestrins to boost vaccine responses while cautioning against long-term blockade due to potential side effects, such as DNA damage (84).

Sestrins play crucial roles in limiting inflammation-induced damage, but dysregulation could lead to oxidative and immune response imbalances. As such, therapeutic strategies targeting Sestrins must balance their transient inhibition or potentiation to minimize side effects. Any intervention altering immune responses must be carefully tested prior to confirming its effect in TB patients.

In summary, the concern is that efforts to mitigate excessive inflammation, which is damaging, may inadvertently suppress immune responses in certain individuals. Immune responses to TB are highly variable and the potential side effect of targeting Sestrins, could be worsening TB outcomes in certain individuals either due to excessively low ROS levels (reducing its microbicidal activity), insufficient immune cell recruitment, or diminished pro-inflammatory responses. This is particularly relevant given that *Sestrin* overexpression has been shown in other studies to reduce pro-inflammatory cytokine production (85).

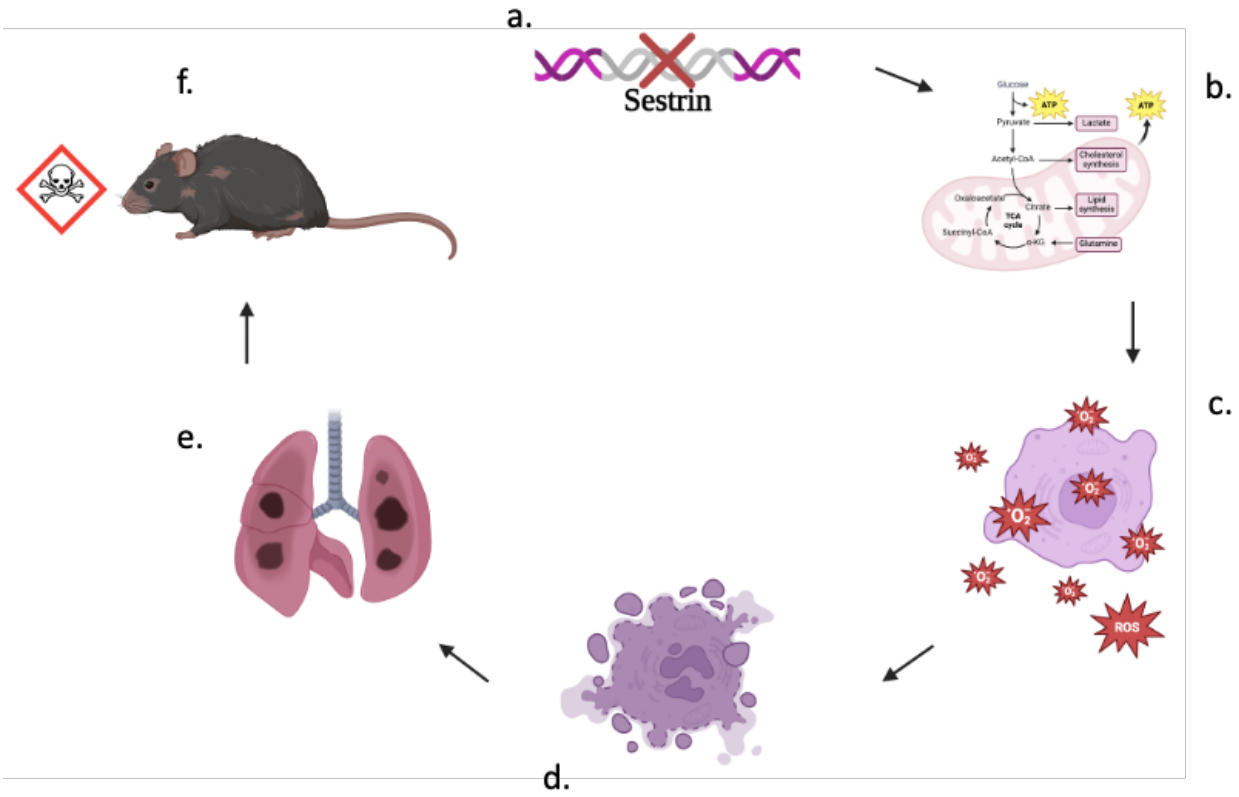

Figure 4.1: **Sestrins modulation of inflammation during *Mtb* infection.** Upon a) *Sestrin* gene ablation, b) metabolism is dysregulated and increased even in the presence of stress. This drives the c) accumulation of ROS, causing cytotoxic effects and d) cell death. In an *in vivo* model, increased cell death may manifest as e) increased lung tissue pathology, contributing to increased f) susceptibility to TB disease in mice. Generated using Biorender.

Our results showed that ablation of *Sesn1* or *Sesn2* in macrophages led to increased ROS levels, cell death, and elevated ATP production. *In vivo*, *Sesn2* knockout mice exhibited increased lung tissue pathology and mortality. These findings suggest Sestrins as key regulators of ROS in

response to stress during TB disease. Since ROS is a natural byproduct of metabolism, the increased metabolic rate in *Sestrin*-deficient macrophages likely drives ROS accumulation. We therefore propose that Sestrins regulate ROS, potentially via modulation of mTORC activity. Collectively, our data support a ROS-mediated pathology hypothesis, with increased macrophage death observed *in vitro,* and exacerbated lung pathology *in vivo*. This reaffirms the benefit of balancing the immune response during TB to mitigate tissue damage. Furthermore, these results enhance our understanding of host immunity to TB by illustrating the pathological consequences of excess ROS, which is canonically viewed as microbicidal.

Currently, no drug directly targets Sestrins to include in an experimental approach to further explore the role of Sestrins in TB immunity and as tractable drug targets for HDT. However, *Sestrin 2 (or Sestrin 1)* overexpression *in vitro* or in mouse models could validate our knockdown results. We would hypothesize that *Sestrin 2* overexpression would reduce ROS, lung pathology, and mortality. If a Sesn2-specific drug were available, that increased Sesn2 protein levels, its effects during infection could be tested in WT and *Sesn2*$^{-/-}$ mice, assessing whether increased Sesn2 rescues the knockout phenotype and enhances WT protection (decreased lung tissue pathology and mortality). Testing Sestrins as HDTs would require adjunct treatment with first-line TB drugs to evaluate therapeutic efficacy and lung pathology reduction, in tandem with overexpression experiments. Indirect approaches, such as targeting Foxo3 to upregulate *Sestrins* or using NAC to mitigate ROS, could also provide insights into the role of Sestrins as HDTs. Given our hypothesis on ROS mediated pathology, NAC would reduce ROS accumulation in cells and may rescue the *Sesn2* knockout phenotype.

Balancing the hyper-inflammatory response to TB has triggered research into reducing ROS levels as an HDT. While ROS levels are important in signaling, prolonged accumulation causes damage to the host during chronic TB disease (89,98,112). NAC has demonstrated ROS-reducing effects while facilitating *Mtb* microbicidal functions. Subsequently, various clinical trials have been investigating the potential of NAC as an adjunctive therapy, with the hope of our next breakthrough in TB treatment and eradication of this disease that has plagued us for centuries (180–184).

REFERENCES:

1. World Health Organization. Global tuberculosis report 2024 [Internet]. 2024. Available from: https://www.who.int/teams/global-tuberculosis-programme/tb-reports/global-tuberculosis-report-2024.
2. Cohen A, Mathiasen VD, Schön T, Wejse C. The global prevalence of latent tuberculosis: A systematic review and meta-analysis. European Respiratory Journal. 2019;54(3).
3. World Health Organization. Global tuberculosis report 2020. World Health Organization; 2020.
4. Global tuberculosis report 2023 [Internet]. 2023. Available from: https://iris.who.int/.
5. WHO. WHO TB burden report 2018 [Internet]. Vol. 63, Workplace Health and Safety. 2018. 476 p. Available from: https://apps.who.int/iris/handle/10665/274453
6. Hayman J. Mycobacterium ulcerans: an infection from Jurassic time? Lancet. 1984 Nov;2(8410):1015–6.
7. Rothschild BM, Martin LD, Lev G, Bercovier H, Bar-Gal GK, Greenblatt C, et al. Mycobacterium tuberculosis complex DNA from an extinct bison dated 17,000 years before the present. Clin Infect Dis. 2001 Aug;33(3):305–11.
8. Hershkovitz I, Donoghue HD, Minnikin DE, Besra GS, Lee OYC, Gernaey AM, et al. Detection and molecular characterization of 9,000-year-old Mycobacterium tuberculosis from a Neolithic settlement in the Eastern Mediterranean. PLoS One. 2008;3(10):e3426.
9. Kapur V, Whittam TS, Musser JM. Is Mycobacterium tuberculosis 15,000 years old? Vol. 170, The Journal of infectious diseases. United States; 1994. p. 1348–9.
10. Bos KI, Harkins KM, Herbig A, Coscolla M, Weber N, Comas I, et al. Pre-Columbian mycobacterial genomes reveal seals as a source of New World human tuberculosis. Nature. 2014 Oct 23;514(7253):494–7.
11. Cambau E, Drancourt M. Steps towards the discovery of Mycobacterium tuberculosis by Robert Koch, 1882. Vol. 20, Clinical Microbiology and Infection. Blackwell Publishing Ltd; 2014. p. 196–201.
12. Ducati RG, Ruffino-Netto A, Basso LA, Santos DS. The resumption of consumption -- a review on tuberculosis. Mem Inst Oswaldo Cruz. 2006 Nov;101(7):697–714.
13. Natarajan A, Beena PM, Devnikar A V, Mali S. A systemic review on tuberculosis. Indian J Tuberc. 2020 Jul;67(3):295–311.
14. Daniel TM. The history of tuberculosis. Respir Med. 2006;100(11):1862–70.
15. Cambau E, Drancourt M. Steps towards the discovery of Mycobacterium tuberculosis by Robert Koch, 1882. Clin Microbiol Infect. 2014 Mar;20(3):196–201.
16. Schatz A, Bugle E, Waksman SA. Streptomycin, a Substance Exhibiting Antibiotic Activity Against Gram-Positive and Gram-Negative Bacteria. ∗†. Proceedings of the Society for Experimental Biology and Medicine [Internet]. 1944 Jan 1;55(1):66–9. Available from: https://journals.sagepub.com/doi/abs/10.3181/00379727-55-14461
17. Pai M, Behr MA, Dowdy D, Dheda K, Divangahi M, Boehme CC, et al. Tuberculosis. Nat Rev Dis Primers [Internet]. 2016;2(1):16076. Available from: https://doi.org/10.1038/nrdp.2016.76
18. Lin, P.L., Ford, C.B., Coleman, M.T., Myers, A.J., Gawande, R., Ioerger, T., Sacchettini, J., Fortune, S.M. and Flynn JL. Sterilization of granulomas is common in active and latent tuberculosis despite within-host variability in bacterial killing. Nat Med. 2014;20(1):75.
19. Cosma CL, Sherman DR, Ramakrishnan L. The secret lives of the pathogenic mycobacteria. Annu Rev Microbiol. 2003;57:641–76.

20. Ndlovu H, Marakalala MJ. Granulomas and inflammation: host-directed therapies for tuberculosis. Front Immunol. 2016;7:434.
21. Guirado E, Schlesinger LS, Kaplan G. Macrophages in tuberculosis: Friend or foe. Vol. 35, Seminars in Immunopathology. 2013. 563–583 p.
22. Frieden TR, Sterling TR, Munsiff SS, Watt CJ, Dye C. Tuberculosis. Lancet. 2003 Sep;362(9387):887–99.
23. Nuermberger E, Bishai WR, Grosset JH. Latent tuberculosis infection. Semin Respir Crit Care Med. 2004 Jun;25(3):317–36.
24. Stamm CE, Collins AC, Shiloh MU. Sensing of Mycobacterium tuberculosis and consequences to both host and bacillus. Immunol Rev. 2015 Mar;264(1):204–19.
25. Upadhyay S, Mittal E, Philips JA. Tuberculosis and the art of macrophage manipulation. Pathog Dis. 2018 Jun;76(4).
26. Erwig LP, Kluth DC, Walsh GM, Rees AJ. Initial cytokine exposure determines function of macrophages and renders them unresponsive to other cytokines. J Immunol. 1998 Aug;161(4):1983–8.
27. Stout RD, Suttles J. Functional plasticity of macrophages: reversible adaptation to changing microenvironments. J Leukoc Biol. 2004 Sep;76(3):509–13.
28. Porcheray F, Viaud S, Rimaniol AC, Léone C, Samah B, Dereuddre-Bosquet N, et al. Macrophage activation switching: an asset for the resolution of inflammation. Clin Exp Immunol. 2005 Dec;142(3):481–9.
29. Biswas SK, Sica A, Lewis CE. Plasticity of macrophage function during tumor progression: regulation by distinct molecular mechanisms. J Immunol. 2008 Feb;180(4):2011–7.
30. Stout RD, Watkins SK, Suttles J. Functional plasticity of macrophages: in situ reprogramming of tumor-associated macrophages. J Leukoc Biol. 2009 Nov;86(5):1105–9.
31. Murray PJ, Wynn TA. Protective and pathogenic functions of macrophage subsets. Nat Rev Immunol. 2011 Oct;11(11):723–37.
32. Famelis N, Geibel S, Van Tol D. Mycobacterial type VII secretion systems. Vol. 404, Biological Chemistry. De Gruyter Open Ltd; 2023. p. 691–702.
33. Martinez-Pomares L, Linehan SA, Taylor PR, Gordon S. Binding properties of the mannose receptor. Immunobiology. 2001 Dec;204(5):527–35.
34. Lee SJ, Evers S, Roeder D, Parlow AF, Risteli J, Risteli L, et al. Mannose receptor-mediated regulation of serum glycoprotein homeostasis. Science. 2002 Mar;295(5561):1898–901.
35. Medzhitov R, Janeway CJ. Innate immunity. N Engl J Med. 2000 Aug;343(5):338–44.
36. Chieppa M, Bianchi G, Doni A, Del Prete A, Sironi M, Laskarin G, et al. Cross-linking of the mannose receptor on monocyte-derived dendritic cells activates an anti-inflammatory immunosuppressive program. J Immunol. 2003 Nov;171(9):4552–60.
37. Singh CR, Moulton RA, Armitige LY, Bidani A, Snuggs M, Dhandayuthapani S, et al. Processing and presentation of a mycobacterial antigen 85B epitope by murine macrophages is dependent on the phagosomal acquisition of vacuolar proton ATPase and in situ activation of cathepsin D. J Immunol. 2006 Sep;177(5):3250–9.
38. McNally AK, Anderson JM. Interleukin-4 induces foreign body giant cells from human mono- cytes/macrophages. Differential lymphokine regulation of macrophage fusion leads to morphological variants of multinucleated giant cells. Am J Pathol. 1995;147:1487–99.

39. Ishikawa E, Ishikawa T, Morita YS, Toyonaga K, Yamada H, Takeuchi O, et al. Direct recognition of the mycobacterial glycolipid, trehalose dimycolate, by C-type lectin Mincle. J Exp Med. 2009 Dec;206(13):2879–88.
40. Heitmann L, Schoenen H, Ehlers S, Lang R, Hölscher C. Mincle is not essential for controlling Mycobacterium tuberculosis infection. Immunobiology. 2013 Apr;218(4):506–16.
41. Armstrong L, Medford ARL, Uppington KM, Robertson J, Witherden IR, Tetley TD, et al. Expression of functional toll-like receptor-2 and -4 on alveolar epithelial cells. Am J Respir Cell Mol Biol. 2004 Aug;31(2):241–5.
42. Hayashi F, Means TK, Luster AD. Toll-like receptors stimulate human neutrophil function. Blood. 2003 Oct;102(7):2660–9.
43. Dasari P, Nicholson IC, Hodge G, Dandie GW, Zola H. Expression of toll-like receptors on B lymphocytes. Cell Immunol. 2005;236(1–2):140–5.
44. Kadowaki N, Ho S, Antonenko S, De Waal Malefyt R, Kastelein RA, Bazan F, et al. Subsets of human dendritic cell precursors express different toll-like receptors and respond to different microbial antigens. Journal of Experimental Medicine. 2001;194(6):863–9.
45. Medzhitov R, Preston-Hurlburt P, Janeway CAJ. A human homologue of the Drosophila Toll protein signals activation of adaptive immunity. Nature. 1997 Jul;388(6640):394–7.
46. Rock FL, Hardiman G, Timans JC, Kastelein RA, Bazan JF. A family of human receptors structurally related to Drosophila Toll. Proc Natl Acad Sci U S A. 1998 Jan;95(2):588–93.
47. Brightbill HD, Libraty DH, Krutzik SR, Yang RB, Belisle JT, Bleharski JR, et al. Host defense mechanisms triggered by microbial lipoproteins through toll-like receptors. Science. 1999 Jul;285(5428):732–6.
48. Trinchieri G, Sher A. Cooperation of Toll-like receptor signals in innate immune defence. Nat Rev Immunol. 2007 Mar;7(3):179–90.
49. Akira S, Uematsu S, Takeuchi O. Pathogen recognition and innate immunity. Cell. 2006 Feb;124(4):783–801.
50. Kawai T, Akira S. The role of pattern-recognition receptors in innate immunity: update on Toll-like receptors. Nat Immunol. 2010 May;11(5):373–84.
51. Jo EK. Mycobacterial interaction with innate receptors: TLRs, C-type lectins, and NLRs. Curr Opin Infect Dis. 2008 Jun;21(3):279–86.
52. Rosenberg PS, Che A, Chen BE. Multiple hypothesis testing strategies for genetic case-control association studies. Stat Med. 2006 Sep;25(18):3134–49.
53. Heldwein KA, Fenton MJ. The role of Toll-like receptors in immunity against mycobacterial infection. Microbes Infect. 2002 Jul;4(9):937–44.
54. Quesniaux V, Fremond C, Jacobs M, Parida S, Nicolle D, Yeremeev V, et al. Toll-like receptor pathways in the immune responses to mycobacteria. Microbes Infect. 2004 Aug;6(10):946–59.
55. Jo EK, Yang CS, Choi CH, Harding C V. Intracellular signalling cascades regulating innate immune responses to Mycobacteria: branching out from Toll-like receptors. Cell Microbiol. 2007 May;9(5):1087–98.
56. Takeuchi O, Sato S, Horiuchi T, Hoshino K, Takeda K, Dong Z, et al. Cutting edge: role of Toll-like receptor 1 in mediating immune response to microbial lipoproteins. J Immunol. 2002 Jul;169(1):10–4.

57. Means TK, Wang S, Lien E, Yoshimura A, Golenbock DT, Fenton MJ. Human toll-like receptors mediate cellular activation by Mycobacterium tuberculosis. J Immunol. 1999 Oct;163(7):3920–7.
58. Henning LN, Azad AK, Parsa KVL, Crowther JE, Tridandapani S, Schlesinger LS. Pulmonary surfactant protein A regulates TLR expression and activity in human macrophages. J Immunol. 2008 Jun;180(12):7847–58.
59. Kawai T, Akira S. Toll-like receptors and their crosstalk with other innate receptors in infection and immunity. Immunity. 2011 May;34(5):637–50.
60. Horsburgh CR Jr, Barry CE 3rd, Lange C. Treatment of tuberculosis. *N Engl J Med*. 2015 Nov 26;373(22):2149–60.
61. Sanyaolu A. Tuberculosis: A Review of Current Trends. Epidemiology International Journal. 2019;3(2).
62. Jnawali HN, Ryoo S. First– and Second–Line Drugs and Drug Resistance. In: Mahboub BH, Vats MG, editors. Tuberculosis [Internet]. Rijeka: IntechOpen; 2013. p. Ch. 10. Available from: https://doi.org/10.5772/54960
63. Padda IS, Reddy KM. Antitubercular medications. In: StatPearls [Internet]. StatPearls Publishing; 2021.
64. Stancil SL, Mirzayev F, Abdel-Rahman SM. Profiling pretomanid as a therapeutic option for tb infection: Evidence to date. Vol. 15, Drug Design, Development and Therapy. Dove Medical Press Ltd; 2021. p. 2815–30.
65. Guler R, Brombacher F. Host-directed drug therapy for tuberculosis. Nat Chem Biol. 2025;748–51.
66. Ulrichs, T. and Kaufmann SH. New insights into the function of granulomas in human tuberculosis. J Pathol. 2006;208(2):261–9.
67. Marakalala, M. J., Raju, R. M., Sharma, K., Zhang, Y. J., Eugenin, E. A., Prideaux, B., …Rubin EJ. Inflammatory signaling in human tuberculosis granulomas is spatially organized. Nat Med [Internet]. 2016;22(5):531–8. Available from: https://doi.org/10.1038/nm.4073
68. Young C, Walzl G, Du Plessis N. Therapeutic host-directed strategies to improve outcome in tuberculosis. Mucosal Immunol [Internet]. 2020;13(2):190–204. Available from: http://dx.doi.org/10.1038/s41385-019-0226-5
69. Lee YJ, Han SK, Park JH, Lee JK, Kim DK, Chung HS, et al. The effect of metformin on culture conversion in tuberculosis patients with diabetes mellitus. Korean J Intern Med. 2018 Sep;33(5):933–40.
70. Singhal A, Jie L, Kumar P, Hong GS, Leow MKS, Paleja B, et al. Metformin as adjunct antituberculosis therapy. Sci Transl Med. 2014 Nov;6(263):263ra159.
71. Kukidome D, Nishikawa T, Sonoda K, Imoto K, Fujisawa K, Yano M, et al. Activation of AMP-activated protein kinase reduces hyperglycemia-induced mitochondrial reactive oxygen species production and promotes mitochondrial biogenesis in human umbilical vein endothelial cells. Diabetes. 2006 Jan;55(1):120–7.
72. Martinez N, Ketheesan N, West K, Vallerskog T, Kornfeld H. Impaired Recognition of Mycobacterium tuberculosis by Alveolar Macrophages From Diabetic Mice. J Infect Dis. 2016 Dec;214(11):1629–37.
73. Lopez-Lopez N, Martinez AGR, Garcia-Hernandez MH, Hernandez-Pando R, Castañeda-Delgado JE, Lugo-Villarino G, et al. Type-2 diabetes alters the basal phenotype of human

macrophages and diminishes their capacity to respond, internalise, and control Mycobacterium tuberculosis. Vol. 113, Memórias do Instituto Oswaldo Cruz. scielo; 2018.
74. Martens GW, Arikan MC, Lee J, Ren F, Greiner D, Kornfeld H. Tuberculosis susceptibility of diabetic mice. Am J Respir Cell Mol Biol. 2007 Nov;37(5):518–24.
75. Restrepo B, Twahirwa M, Rahbar M, Schlesinger L. Phagocytosis via Complement or Fc-Gamma Receptors Is Compromised in Monocytes from Type 2 Diabetes Patients with Chronic Hyperglycemia. PLoS One. 2014 Mar 26;9: e92977.
76. Zhou G, Myers R, Li Y, Chen Y, Shen X, Fenyk-Melody J, et al. Role of AMP-activated protein kinase in mechanism of metformin action. J Clin Invest. 2001 Oct;108(8):1167–74.
77. Lachmandas E, Eckold C, Böhme J, Koeken VACM, Marzuki MB, Blok B, et al. Metformin Alters Human Host Responses to Mycobacterium tuberculosis in Healthy Subjects. J Infect Dis. 2019 Jun;220(1):139–50.
78. Bafica A, Scanga CA, Serhan C, Machado F, White S, Sher A, et al. Host control of Mycobacterium tuberculosis is regulated by 5-lipoxygenase-dependent lipoxin production. J Clin Invest. 2005 Jun;115(6):1601–6.
79. Mayer-Barber KD, Andrade BB, Oland SD, Amaral EP, Barber DL, Gonzales J, et al. Host-directed therapy of tuberculosis based on interleukin-1 and type I interferon crosstalk. Nature [Internet]. 2014;511(7507):99–103. Available from: https://doi.org/10.1038/nature13489
80. Parihar SP, Guler R, Khutlang R, Lang DM, Hurdayal R, Mhlanga MM, et al. Statin therapy reduces the mycobacterium tuberculosis burden in human macrophages and in mice by enhancing autophagy and phagosome maturation. J Infect Dis. 2014 Mar;209(5):754–63.
81. Skerry C, Pinn ML, Bruiners N, Pine R, Gennaro ML, Karakousis PC. Simvastatin increases the in vivo activity of the first-line tuberculosis regimen. Journal of Antimicrobial Chemotherapy [Internet]. 2014 Sep 1;69(9):2453–7. Available from: https://doi.org/10.1093/jac/dku166
82. Lobato LS, Rosa PS, Ferreira J da S, Neumann A da S, da Silva MG, do Nascimento DC, et al. Statins increase rifampin mycobactericidal effect. Antimicrob Agents Chemother. 2014 Oct;58(10):5766–74.
83. Kyrklund C, Backman JT, Kivistö KT, Neuvonen M, Laitila J, Neuvonen PJ. Rifampin greatly reduces plasma simvastatin and simvastatin acid concentrations. Clin Pharmacol Ther [Internet]. 2000 Dec 1;68(6):592–7. Available from: https://doi.org/10.1067/mcp.2000.111414
84. Tobin, D. M., Roca, F. J., Oh, S. F., McFarland, R., Vickery, T. W., Ray, J. P., …Ramakrishnan L. Host genotype-specific therapies can optimize the inflammatory response to mycobacterial infections. Cell [Internet]. 2012;148(3):434–46. Available from: https://doi.org/10.1016/j.cell.2011.12.023
85. Yang JH, Kim KM, Kim MG, Seo KH, Han JY, Ka SO, et al. Role of sestrin2 in the regulation of proinflammatory signaling in macrophages. Free Radic Biol Med. 2015 Jan; 78:156–67.
86. Yang YL, Loh KS, Liou BY, Chu IH, Kuo CJ, Chen HD, et al. SESN-1 is a positive regulator of lifespan in Caenorhabditis elegans. Exp Gerontol. 2013 Mar;48(3):371–9.
87. Wang M, Xu Y, Liu J, Ye J, Yuan W, Jiang H, et al. Recent Insights into the Biological Functions of Sestrins in Health and Disease. Cellular Physiology and Biochemistry. 2018;43(5):1731–41.

88. Lee JH, Budanov A V, Park EJ, Birse R, Kim TE, Perkins GA, et al. Sestrin as a feedback inhibitor of TOR that prevents age-related pathologies. Science. 2010 Mar;327(5970):1223–8.
89. Cordani M, Strippoli R, Sánchez-Álvarez M. Sestrins at the Interface of ROS Control and Autophagy Regulation in Health and Disease. Oxid Med Cell Longev. 2019 May 7;2019.
90. Budanov A V, Shoshani T, Faerman A, Zelin E, Kamer I, Kalinski H, et al. Identification of a novel stress-responsive gene Hi95 involved in regulation of cell viability. Oncogene. 2002 Sep;21(39):6017–31.
91. Kim H, An S, Ro SH, Teixeira F, Jin Park G, Kim C, et al. Janus-faced Sestrin2 controls ROS and mTOR signalling through two separate functional domains. Nat Commun [Internet]. 2015;6(1):10025. Available from: https://doi.org/10.1038/ncomms10025
92. Saxton RA, Knockenhauer KE, Wolfson RL, Chantranupong L, Pacold ME, Wang T, et al. Structural basis for leucine sensing by the Sestrin2-mTORC1 pathway. Science. 2016 Jan;351(6268):53–8.
93. Wolfson RL, Chantranupong L, Saxton RA, Shen K, Scaria SM, Cantor JR, et al. Sestrin2 is a leucine sensor for the mTORC1 pathway. Science. 2016 Jan;351(6268):43–8.
94. Budanov A V, Karin M. p53 target genes sestrin1 and sestrin2 connect genotoxic stress and mTOR signaling. Cell. 2008 Aug;134(3):451–60.
95. Lee JH, Budanov A V, Talukdar S, Park EJ, Park HL, Park HW, et al. Maintenance of metabolic homeostasis by Sestrin2 and Sestrin3. Cell Metab. 2012 Sep;16(3):311–21.
96. Park HW, Park H, Ro SH, Jang I, Semple IA, Kim DN, et al. Hepatoprotective role of Sestrin2 against chronic ER stress. Nat Commun. 2014 Jun; 5:4233.
97. Nogueira V, Park Y, Chen CC, Xu PZ, Chen ML, Tonic I, et al. Akt determines replicative senescence and oxidative or oncogenic premature senescence and sensitizes cells to oxidative apoptosis. Cancer Cell. 2008 Dec;14(6):458–70.
98. Budanov A V, Sablina AA, Feinstein E, Koonin E V, Chumakov PM. Regeneration of peroxiredoxins by p53-regulated sestrins, homologs of bacterial AhpD. Science. 2004 Apr;304(5670):596–600.
99. Shin BY, Jin SH, Cho IJ, Ki SH. Nrf2-ARE pathway regulates induction of Sestrin-2 expression. Free Radic Biol Med [Internet]. 2012;53(4):834–41. Available from: http://www.sciencedirect.com/science/article/pii/S0891584912003619
100. Zhang XY, Wu XQ, Deng R, Sun T, Feng GK, Zhu XF. Upregulation of sestrin 2 expression via JNK pathway activation contributes to autophagy induction in cancer cells. Cell Signal [Internet]. 2013;25(1):150–8. Available from: http://www.sciencedirect.com/science/article/pii/S089865681200246X
101. Shi X, Doycheva DM, Xu L, Tang J, Yan M, Zhang JH. Sestrin2 induced by hypoxia inducible factor1 alpha protects the blood-brain barrier via inhibiting VEGF after severe hypoxic-ischemic injury in neonatal rats. Neurobiol Dis [Internet]. 2016 Nov; 95:111—121. Available from: https://europepmc.org/articles/PMC5010975
102. Kimball SR, Gordon BS, Moyer JE, Dennis MD, Jefferson LS. Leucine induced dephosphorylation of Sestrin2 promotes mTORC1 activation. Cell Signal. 2016 Aug;28(8):896–906.
103. Woo H, Bae S, Park S, Rhee SG. Sestrin 2 Is Not a Reductase for Cysteine Sulfinic Acid of Peroxiredoxins. Antioxid Redox Signal. 2009 Apr 1; 11:739–45.
104. Hwang HJ, Jung T, Choi JH, Lee H, Chung H, Seo JA, et al. Knockdown of sestrin2 increases pro-inflammatory reactions and ER stress in the endothelium via an AMPK

dependent mechanism. Biochimica et Biophysica Acta (BBA) - Molecular Basis of Disease. 2017 Feb 1;1863.
105. Hwang HJ, Kim JW, Chung HS, Seo JA, Kim SG, Kim NH, et al. Knockdown of Sestrin2 Increases Lipopolysaccharide-Induced Oxidative Stress, Apoptosis, and Fibrotic Reactions in H9c2 Cells and Heart Tissues of Mice via an AMPK-Dependent Mechanism. Fröde TS, editor. Mediators Inflamm [Internet]. 2018; 2018:6209140. Available from: https://doi.org/10.1155/2018/6209140
106. Kim MJ, Bae SH, Ryu JC, Kwon Y, Oh JH, Kwon J, et al. SESN2/sestrin2 suppresses sepsis by inducing mitophagy and inhibiting NLRP3 activation in macrophages. Autophagy. 2016 Aug;12(8):1272–91.
107. Ding X, Zhao H, Qiao C. Icariin protects podocytes from NLRP3 activation by Sesn2-induced mitophagy through the Keap1-Nrf2/HO-1 axis in diabetic nephropathy. Phytomedicine. 2022 May 1;99.
108. Han D, Kim H, Kim S, Le QA, Han SY, Bae J, et al. Sestrin2 protects against cholestatic liver injury by inhibiting endoplasmic reticulum stress and NLRP3 inflammasome-mediated pyroptosis. Exp Mol Med. 2022 Mar 1;54(3):239–51.
109. Wang JM, Liu BQ, Li C, Du ZX, Sun J, Yan J, et al. Sestrin 2 protects against metabolic stress in a p53-independent manner. Biochem Biophys Res Commun. 2019 Jun 11;513(4):852–6.
110. Sablina AA, Budanov A V, Ilyinskaya G V, Agapova LS, Kravchenko JE, Chumakov PM. The antioxidant function of the p53 tumor suppressor. Nat Med. 2005 Dec;11(12):1306–13.
111. Papadia S, Soriano FX, Léveillé F, Martel MA, Dakin KA, Hansen HH, et al. Synaptic NMDA receptor activity boosts intrinsic antioxidant defenses. Nat Neurosci. 2008 Apr;11(4):476–87.
112. Wu D, Zhang H, Wu Q, Li F, Wang Y, Liu S, et al. Sestrin 2 protects against LPS-induced acute lung injury by inducing mitophagy in alveolar macrophages. Life Sci [Internet]. 2021;267(December 2020):118941. Available from: https://doi.org/10.1016/j.lfs.2020.118941
113. Scherz-Shouval R, Elazar Z. Regulation of autophagy by ROS: physiology and pathology. Trends Biochem Sci [Internet]. 2011;36(1):30–8. Available from: http://www.sciencedirect.com/science/article/pii/S0968000410001404
114. Eiyama A, Okamoto K. PINK1/Parkin-mediated mitophagy in mammalian cells. Curr Opin Cell Biol. 2015 Apr; 33:95–101.
115. Nakahira K, Haspel JA, Rathinam VAK, Lee SJ, Dolinay T, Lam HC, et al. Autophagy proteins regulate innate immune responses by inhibiting the release of mitochondrial DNA mediated by the NALP3 inflammasome. Nat Immunol. 2011 Mar;12(3):222–30.
116. Maiuri M, Malik SA, Morselli E, Kepp O, Criollo A, Mouchel PL, et al. Stimulation of autophagy by the p53 target gene Sestrin2. Cell Cycle. 2009 Jun 1; 8:1571–6.
117. Hou YS, Guan JJ, Xu HD, Wu F, Sheng R, Qin ZH. Sestrin2 Protects Dopaminergic Cells against Rotenone Toxicity through AMPK-Dependent Autophagy Activation. Mol Cell Biol. 2015 Aug;35(16):2740–51.
118. Bae SH, Sung SH, Oh SY, Lim JM, Lee SK, Park YN, et al. Sestrins activate Nrf2 by promoting p62-dependent autophagic degradation of Keap1 and prevent oxidative liver damage. Cell Metab. 2013 Jan;17(1):73–84.
119. Pankiv S, Clausen TH, Lamark T, Brech A, Bruun JA, Outzen H, et al. p62/SQSTM1 binds directly to Atg8/LC3 to facilitate degradation of ubiquitinated protein aggregates by

autophagy. J Biol Chem [Internet]. 2007 Aug;282(33):24131–45. Available from: http://www.jbc.org/lookup/doi/10.1074/jbc.M702824200
120. Yang K, Xu C, Zhang Y, He S, Li D. Sestrin2 Suppresses Classically Activated Macrophages-Mediated Inflammatory Response in Myocardial Infarction through Inhibition of mTORC1 Signaling. Front Immunol. 2017; 8:728.
121. Ho A, Cho CS, Namkoong S, Cho US, Lee JH. Biochemical Basis of Sestrin Physiological Activities. Trends Biochem Sci [Internet]. 2016;41(7):621–32. Available from: http://dx.doi.org/10.1016/j.tibs.2016.04.005
122. Kovaleva IE, Tokarchuk A V, Zheltukhin AO, Dalina AA, Safronov GG, Evstafieva AG, et al. Mitochondrial localization of SESN2. PLoS One [Internet]. 2020 Apr 14;15(4): e0226862. Available from: https://doi.org/10.1371/journal.pone.0226862
123. Pereira BI, De Maeyer RPH, Covre LP, Nehar-Belaid D, Lanna A, Ward S, et al. Sestrins induce natural killer function in senescent-like CD8+ T cells. Nat Immunol [Internet]. 2020;21(6):684–94. Available from: http://dx.doi.org/10.1038/s41590-020-0643-3
124. Lanna A, Gomes DCO, Muller-Durovic B, McDonnell T, Escors D, Gilroy DW, et al. A sestrin-dependent Erk-Jnk-p38 MAPK activation complex inhibits immunity during aging. Nat Immunol. 2017 Feb 15;18(3):354–63.
125. Krutzik SR, Modlin RL. The role of Toll-like receptors in combating mycobacteria. Semin Immunol. 2004 Feb;16(1):35–41.
126. Ehrt S, Schnappinger D, Bekiranov S, Drenkow J, Shi S, Gingeras TR, et al. Reprogramming of the macrophage transcriptome in response to interferon-gamma and Mycobacterium tuberculosis: signaling roles of nitric oxide synthase-2 and phagocyte oxidase. J Exp Med. 2001 Oct;194(8):1123–40.
127. Saliba AE, C Santos S, Vogel J. New RNA-seq approaches for the study of bacterial pathogens. Curr Opin Microbiol. 2017 Feb; 35:78–87.
128. Forrest ARR, Kawaji H, Rehli M, Kenneth Baillie J, de Hoon MJL, Haberle V, et al. A promoter-level mammalian expression atlas. Nature [Internet]. 2014;507(7493):462–70. Available from: https://doi.org/10.1038/nature13182
129. Noguchi S. Data Descriptor: FANTOM 5 CAGE pro fi les of human and mouse samples. 2017;1–10.
130. Lizio M, Harshbarger J, Shimoji H, Severin J, Kasukawa T, Sahin S, et al. Gateways to the FANTOM5 promoter level mammalian expression atlas. Genome Biol. 2015;16(1):1–14.
131. Peng M, Yin N, Li MO. Sestrins function as guanine nucleotide dissociation inhibitors for rag GTPases to control mTORC1 signaling. Cell [Internet]. 2014;159(1):122–33. Available from: http://dx.doi.org/10.1016/j.cell.2014.08.038
132. Choreño-Parra JA, Bobba S, Rangel-Moreno J, Ahmed M, Mehra S, Rosa B, et al. Mycobacterium tuberculosis HN878 Infection Induces Human-Like B-Cell Follicles in Mice. Journal of Infectious Diseases. 2020 Apr 27;221(10):1636–46.
133. Counoupas C, Pinto R, Nagalingam G, Hill-Cawthorne GA, Feng CG, Britton WJ, et al. Mycobacterium tuberculosis components expressed during chronic infection of the lung contribute to long-term control of pulmonary tuberculosis in mice. NPJ Vaccines. 2016 Sep 15;1.
134. Chen Y, Bharrhan S, Xu J, Sharma T, Wang Y, Salgame P, et al. B cells promote granulomatous inflammation during chronic Mycobacterium tuberculosis infection in mice. PLoS Pathog. 2023 Mar 1;19(3).

135. Muñoz-Elías EJ, Timm J, Botha T, Chan WT, Gomez JE, McKinney JD. Replication dynamics of Mycobacterium tuberculosis in chronically infected mice. Infect Immun. 2005 Jan;73(1):546–51.
136. Csonka C, Páli T, Bencsik P, Görbe A, Ferdinandy P, Csont T, et al. Measurement of NO in biological samples Correspondence LINKED ARTICLES. Br J Pharmacol [Internet]. 2015; 172:1620–32. Available from: http://dx.doi.org/10.1111/bph.2015.172.issue-6
137. CellTiter-Blue ® Cell Viability Assay Instructions for Use of Products G8080, G8081 and G8082 [Internet]. Available from: www.promega.com
138. Noreng S, Ota N, Sun Y, Ho H, Johnson M, Arthur CP, et al. Structure of the core human NADPH oxidase NOX2. Nat Commun. 2022 Dec 1;13(1).
139. Guide U. Agilent Seahorse XFp Real-Time ATP Rate Assay Kit For use with Agilent Seahorse XFp Extracellular Flux Analyzers Agilent Seahorse XFp Real-Time ATP Rate Assay Kit User Guide Notices.
140. Murthy SE, Chatterjee F, Crook A, Dawson R, Mendel C, Murphy ME, et al. Pretreatment chest x-ray severity and its relation to bacterial burden in smear positive pulmonary tuberculosis. BMC Med. 2018 May 21;16(1).
141. Wang M, Xu Y, Liu J, Ye J, Yuan W, Jiang H, et al. Recent Insights into the Biological Functions of Sestrins in Health and Disease. Cellular Physiology and Biochemistry. 2018;43(5):1731–41.
142. Dalina AA, Kovaleva IE, Budanov A V. Sestrins are Gatekeepers in the Way from Stress to Aging and Disease. Vol. 52, Molecular Biology. Pleiades Publishing; 2018. p. 823–35.
143. Dong Z, Lin C, Liu Y, Jin H, Wu H, Li Z, et al. Upregulation of sestrins protect atriums against oxidative damage and fibrosis in human and experimental atrial fibrillation. Sci Rep. 2017 Apr 11;7.
144. Wang M, Liu J, Qin J, Liu M, Feng Y, Shi L, et al. Increased expression of Sestrin2 in human and experimental heart failure [Internet]. Vol. 9, Article in International Journal of Clinical and Experimental Pathology. 2016. Available from: www.ijcep.com/
145. Johnson MR, Behmoaras J, Bottolo L, Krishnan ML, Pernhorst K, Santoscoy PLM, et al. Systems genetics identifies Sestrin 3 as a regulator of a proconvulsant gene network in human epileptic hippocampus. Nat Commun. 2015;6.
146. Khan N, Jajeh F, Khan MI, Mukhtar E, Shabana SM, Mukhtar H. Sestrin-3 modulation is essential for therapeutic efficacy of cucurbitacin B in lung cancer cells. Carcinogenesis. 2017 Feb 1;38(2):184–95.
147. Tao R, Xiong X, Liangpunsakul S, Dong XC. Sestrin 3 protein enhances hepatic insulin sensitivity by direct activation of the mTORC2-Akt signaling. Diabetes. 2015 Apr 1;64(4):1211–23.
148. Ordway DJ, Shang S, Henao-Tamayo M, Obregon-Henao A, Nold L, Caraway M, et al. Mycobacterium bovis BCG-mediated protection against W-Beijing strains of Mycobacterium tuberculosis is diminished concomitant with the emergence of regulatory T cells. Clinical and Vaccine Immunology. 2011 Sep;18(9):1527–35.
149. Glynn JR, Whiteley J, Bifani PJ, Kremer K, Van Soolingen D. Worldwide Occurrence of Beijing/W Strains of Mycobacterium tuberculosis: A Systematic Review. Vol. 8, Emerging Infectious Diseases •. 2002.
150. Caws M, Thwaites G, Stepniewska K, Lan NTN, Duyen NTH, Phuong NT, et al. Beijing genotype of Mycobacterium tuberculosis is significantly associated with human

immunodeficiency virus infection and multidrug resistance in cases of tuberculous meningitis. J Clin Microbiol. 2006;44(11):3934–9.
151. Choreño-Parra JA, Bobba S, Rangel-Moreno J, Ahmed M, Mehra S, Rosa B, et al. Mycobacterium tuberculosis HN878 Infection Induces Human-Like B-Cell Follicles in Mice. Journal of Infectious Diseases. 2020 Apr 27;221(10):1636–46.
152. Gopal R, Monin L, Slight S, Uche U, Blanchard E, A. Fallert Junecko B, et al. Unexpected Role for IL-17 in Protective Immunity against Hypervirulent Mycobacterium tuberculosis HN878 Infection. PLoS Pathog. 2014;10(5).
153. Oricchio E, Katanayeva N, Donaldson MC, Sungalee S, Joyce PP, Béguelin W, et al. Genetic and epigenetic inactivation of SESTRIN1 controls mTORC1 and response to EZH2 inhibition in follicular lymphoma. Sci Transl Med. 2017 Jun 28;9(396).
154. Wang M, Xu Y, Liu J, Ye J, Yuan W, Jiang H, et al. Recent Insights into the Biological Functions of Sestrins in Health and Disease. Vol. 43, Cellular Physiology and Biochemistry. S. Karger AG; 2018. p. 1731–41.
155. Xue R, Zeng J, Chen Y, Chen C, Tan W, Zhao J, et al. Sestrin 1 ameliorates cardiac hypertrophy via autophagy activation. J Cell Mol Med. 2017 Jun 1;21(6):1193–205.
156. Soontornniyomkij V, Soontornniyomkij B, Moore DJ, Gouaux B, Masliah E, Tung S, et al. Antioxidant sestrin-2 redistribution to neuronal soma in human immunodeficiency virus-associated neurocognitive disorders. Journal of Neuroimmune Pharmacology. 2012 Sep;7(3):579–90.
157. Yue F, Cheng Y, Breschi A, Vierstra J, Wu W, Ryba T, et al. A comparative encyclopedia of DNA elements in the mouse genome. Nature. 2014 Nov 20;515(7527):355–64.
158. Dorhoi A, Iannaccone M, Farinacci M, Faé KC, Schreiber J, Moura-Alves P, et al. MicroRNA-223 controls susceptibility to tuberculosis by regulating lung neutrophil recruitment. Journal of Clinical Investigation. 2013 Nov 1;123(11):4836–48.
159. Mishra BB, Rathinam VAK, Martens GW, Martinot AJ, Kornfeld H, Fitzgerald KA, et al. Nitric oxide controls the immunopathology of tuberculosis by inhibiting NLRP3 inflammasome-dependent processing of IL-1β. Nat Immunol. 2013 Jan;14(1):52–60.
160. Zhang G, Zhou B, Li S, Yue J, Yang H, Wen Y, et al. Allele-Specific Induction of IL-1β Expression by C/EBPβ and PU.1 Contributes to Increased Tuberculosis Susceptibility. PLoS Pathog. 2014 Oct 1;10(10).
161. Xue R, Zeng J, Chen Y, Chen C, Tan W, Zhao J, et al. Sestrin 1 ameliorates cardiac hypertrophy via autophagy activation. J Cell Mol Med. 2017 Jun 1;21(6):1193–205.
162. Yang F, Chen R. Sestrin1 exerts a cytoprotective role against oxygen-glucose deprivation/reoxygenation-induced neuronal injury by potentiating Nrf2 activation via the modulation of Keap1. Brain Res. 2021 Jan 1;1750.
163. Garlanda C, Dinarello CA, Mantovani A. The Interleukin-1 Family: Back to the Future. Vol. 39, Immunity. 2013. p. 1003–18.
164. McElvania Tekippe E, Allen IC, Hulseberg PD, Sullivan JT, McCann JR, Sandor M, et al. Granuloma formation and host defense in chronic mycobacterium tuberculosis infection requires PYCARD/ASC but not NLRP3 or caspase-1. PLoS One. 2010;5(8).
165. Walter K, Hölscher C, Tschopp J, Ehlers S. NALP3 is not necessary for early protection against experimental tuberculosis. Immunobiology. 2010 Sep;215(9–10):804–11.
166. Silvério D, Gonçalves R, Appelberg R, Saraiva M. Advances on the Role and Applications of Interleukin-1 in Tuberculosis. Vol. 12, mBio. American Society for Microbiology; 2021.

167. Kleinnijenhuis J, Joosten LAB, van de Veerdonk FL, Savage N, van Crevel R, Kullberg BJ, et al. Transcriptional and inflammasome-mediated pathways for the induction of IL-1β production by Mycobacterium tuberculosis. Eur J Immunol. 2009;39(7):1914–22.
168. Gleeson LE, Sheedy FJ, Palsson-McDermott EM, Triglia D, O'Leary SM, O'Sullivan MP, et al. Cutting Edge: Mycobacterium tuberculosis Induces Aerobic Glycolysis in Human Alveolar Macrophages That Is Required for Control of Intracellular Bacillary Replication . The Journal of Immunology. 2016 Mar 15;196(6):2444–9.
169. Silvério D, Gonçalves R, Appelberg R, Saraiva M. Advances on the Role and Applications of Interleukin-1 in Tuberculosis [Internet]. 2021. Available from: https://journals.asm.org/journal/mbio
170. Guler R, Parihar SP, Spohn G, Johansen P, Brombacher F, Bachmann MF. Blocking IL-1α but not IL-1β increases susceptibility to chronic Mycobacterium tuberculosis infection in mice. Vaccine. 2011 Feb 1;29(6):1339–46.
171. Eislmayr K, Bestehorn A, Morelli L, Borroni M, Vande Walle L, Lamkanfi M, et al. Nonredundancy of IL-1α and IL-1β is defined by distinct regulation of tissues orchestrating resistance versus tolerance to infection. Vol. 8, Sci. Adv. 2022.
172. Zhang G, Zhou B, Li S, Yue J, Yang H, Wen Y, et al. Allele-Specific Induction of IL-1β Expression by C/EBPβ and PU.1 Contributes to Increased Tuberculosis Susceptibility. PLoS Pathog. 2014 Oct 1;10(10).
173. Harris JE, Fernandez-Vilaseca M, Elkington PTG, Horncastle DE, Graeber MB, Friedland JS. IFN' synergizes with IL-1α to up-regulate MMP-9 secretion in a cellular model of central nervous system tuberculosis. The FASEB Journal [Internet]. 2007 Feb 1;21(2):356–65. Available from: https://doi.org/10.1096/fj.06-6925com
174. O'Kane CM, Elkington PT, Jones MD, Caviedes L, Tovar M, Gilman RH, et al. STAT3, p38 MAPK, and NF-κB drive unopposed monocyte-dependent fibroblast MMP-1 secretion in tuberculosis. Am J Respir Cell Mol Biol. 2010 Oct 1;43(4):465–74.
175. Frangogiannis NG. Transforming growth factor–ß in tissue fibrosis. Vol. 217, Journal of Experimental Medicine. Rockefeller University Press; 2020.
176. Toossi Z, Ellner JJ. SHORT ANALYTICAL REVIEW The Role of TGFb in the Pathogenesis of Human Tuberculosis. Vol. 87, CLINICAL IMMUNOLOGY AND IMMUNOPATHOLOGY. 1998.
177. Hernandez-Pando R, Orozco E. H, Arriaga K, Sampieri A, Larriva-Sahd J, Madrid-Marina V. Analysis of the local kinetics and localization of interleukin-1α, tumour necrosis factor-α and transforming growth factor-β, during the course of experimental pulmonary tuberculosis. Immunology. 1997;90(4):607–17.
178. Cumming BM, Addicott KW, Adamson JH, Steyn AJ. Mycobacterium tuberculosis induces decelerated bioenergetic metabolism in human macrophages. 2018; Available from: https://doi.org/10.7554/eLife.39169.001
179. Fagerberg L, Hallstrom BM, Oksvold P, Kampf C, Djureinovic D, Odeberg J, et al. Analysis of the human tissue-specific expression by genome-wide integration of transcriptomics and antibody-based proteomics. Molecular and Cellular Proteomics. 2014 Feb;13(2):397–406.
180. Mapamba DA, Sauli E, Mrema L, Lalashowi J, Magombola D, Buza J, et al. Impact of N-Acetyl Cysteine (NAC) on Tuberculosis (TB) Patients—A Systematic Review. Vol. 11, Antioxidants. MDPI; 2022.

181. Amaral EP, Conceição EL, Costa DL, Rocha MS, Marinho JM, Cordeiro-Santos M, et al. N-acetylcysteine exhibits potent anti-mycobacterial activity in addition to its known anti-oxidative functions. BMC Microbiol. 2016 Oct 28;16(1):1–10.
182. Moosa MS, Maartens G, Gunter H, Allie S, Chughlay MF, Setshedi M, et al. A Randomized Controlled Trial of Intravenous N-Acetylcysteine in the Management of Anti-tuberculosis Drug-Induced Liver Injury. Clinical Infectious Diseases. 2021 Nov 1;73(9): E3377–83.
183. Mahakalkar S, Nagrale D, Gaur S, Urade C, Murhar B, Turankar A. N-acetylcysteine as an add-on to Directly Observed Therapy Short-I therapy in fresh pulmonary tuberculosis patients: A randomized, placebo-controlled, double-blinded study. Perspect Clin Res. 2017 Jul 1;8(3):132–6.
184. Safe IP, Safe IP, Lacerda MVG, Lacerda MVG, Lacerda MVG, Printes VS, et al. Safety and efficacy of N-acetylcysteine in hospitalized patients with HIV-associated tuberculosis: An open-label, randomized, phase II trial (RIPENACTB Study). PLoS One. 2020 Jun 1;15(6 June).

SUPPLEMENTARY INFORMATION

Table S2.1: **Myeloid and Lymphoid Flow Cytometry Antibody panels.**

Fluorochromes	Spleen		Lymph Node		Lung	
	Lymph	Myeloid	Lymph	Myeloid	Lymph	Myeloid
APC	CD62L (Clone MEL-14)	CD11c (Clone HL3)	CD62L (Clone MEL-14)	CD11c (Clone HL3)	CD8 (Clone 53-6.7) CD62L (Clone MEL-14)	CD11c (Clone HL3)
APC-Cy7	NK1.1 (Clone PK136)	CD169 (Clone SER-4)	NK1.1 (Clone PK136)	CD169 (Clone	NK1.1 (Clone PK136)	SiglecF (Clone E5-2440)
PE	CD44 (Clone IM7)	CD8 (Clone 53-6.7)	CD44 (Clone IM7)	CD103 (Clone M290)	CXCR3 (Clone CXCR3-173) CD44(Clone IM7)	CD103 (Clone M290)
PE-Cy7	CXCR5 (Clone 2G8)	F4/80 (Clone BM8)	CXCR5 (Clone 2G8)	F4/80 (Clone BM8)	CD127 (Clone SB/199) CXCR5 (Clone 2G8)	CD64 (Clone X54-5/7)
PerCPCy5.5	CD19 (Clone 1D3)	Ly6C (Clone AL-21)	CD19 (Clone 1D3)	Ly6C (Clone AL-21)	CD103 (Clone M290) CD19 (Clone 1D3)	Ly6C (Clone AL-21)
FITC	PD-1 (Clone 29F.1A12)	Ly6G (Clone 1A8)	PD-1 (Clone 29F.1A12)	Ly6G (Clone 1A8)	PD-1 (Clone 29F.1A12)	Ly6G (Clone 1A8)

A700	CD3 (Clone 500A2)	MHCII (Clone M5/114.15.2)	CD3 (Clone 500A2)	MHCII (Clone M5/114.15.2)	CD3 (Clone 500A2)	MHCII (Clone M5/114.15.2)
Bv786	KLRG1 (Clone 2F1/KLRG1)		KLRG1 (Clone 2F1/KLRG1)		KLRG1 (Clone 2F1/KLRG1)	MerTK (Clone 108928)
BV510	CD8 (Clone 53-6.7)	CD209a (Clone 5H10)	CD8 (Clone 53-6.7)	CD8 (Clone 53-6.7)	CD69 (Clone H1.2F3) CD8 (Clone 53-6.7)	
BV421	CD4 (Clone RM4-5)	CD11b (Clone M1/70)	CD4 (Clone RM4-5)	CD11b (Clone M1/70)	CD4 (Clone RM4-5)	CD11b (Clone M1/70)
Biotin	TCRγd (Clone GL3)		TCRγd (Clone GL3)		TCRγd (Clone GL3)	

Table S2.2: **Murine primer sequences for qRT-PCR analysis**

		Sequence	Annealing temperature
Sesn1	Forward	GCAGCCGTCCCTTCGACAT	57.9 ºC
	Reverse	GATTCCAAGTTCCTCGTCCTGG	58 ºC
Sesn2	Forward	CCACTCTCTGGCCTCCTTTG	57.7 ºC
	Reverse	TCAAAGCCCCCTGAGTTGTT	56.9 ºC
Sesn3	Forward	GCGGAAGGACAAAAGAATCCG	56.5 ºC
	Reverse	TTGTTCGTTCATCCGCCGTA	56.8 ºC
FOXO3	Forward	CTGGGGGAACCTGTCCTATG	57 ºC
	Reverse	TCATTCTGAACGCGCATGAAG	55.9 ºC
Cybb	Forward	GTGGTTGGGGCTGAATGTCT	57.7 ºC
	Reverse	AGTGCTGACCCAAGGAGTTT	56.6 ºC

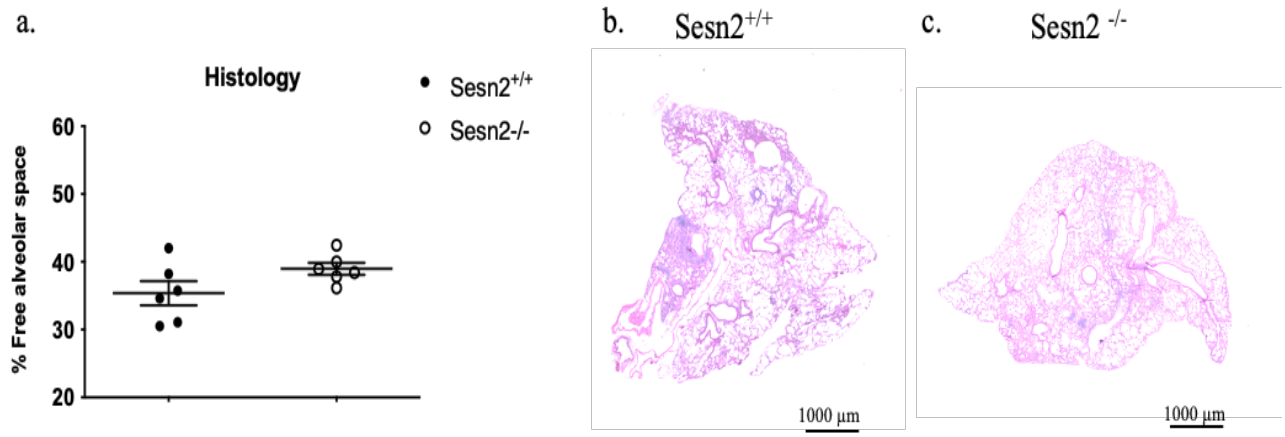

Figure S1: **The deletion of *Sesn2* had no effect on lung tissue pathology after 3-weeks post infection.** Lung samples were collected and fixed in 10% neutral buffered formalin, processed into microscope slides and stained with haematoxylin/eosin. Images were scanned at 20x magnification, a) Quantification of percentage free alveolar space. Representative image of b) *Sesn2*$^{+/+}$ and c) *Sesn2*$^{-/-}$ lung sections. Data are represented as mean ± SEM of n = 6 mice/group. For statistical analysis an unpaired student t-test was used to compare lung tissue pathology in control versus knockout mice.

APPENDIX

Appendix A: Spleen Myeloid Gating Strategy

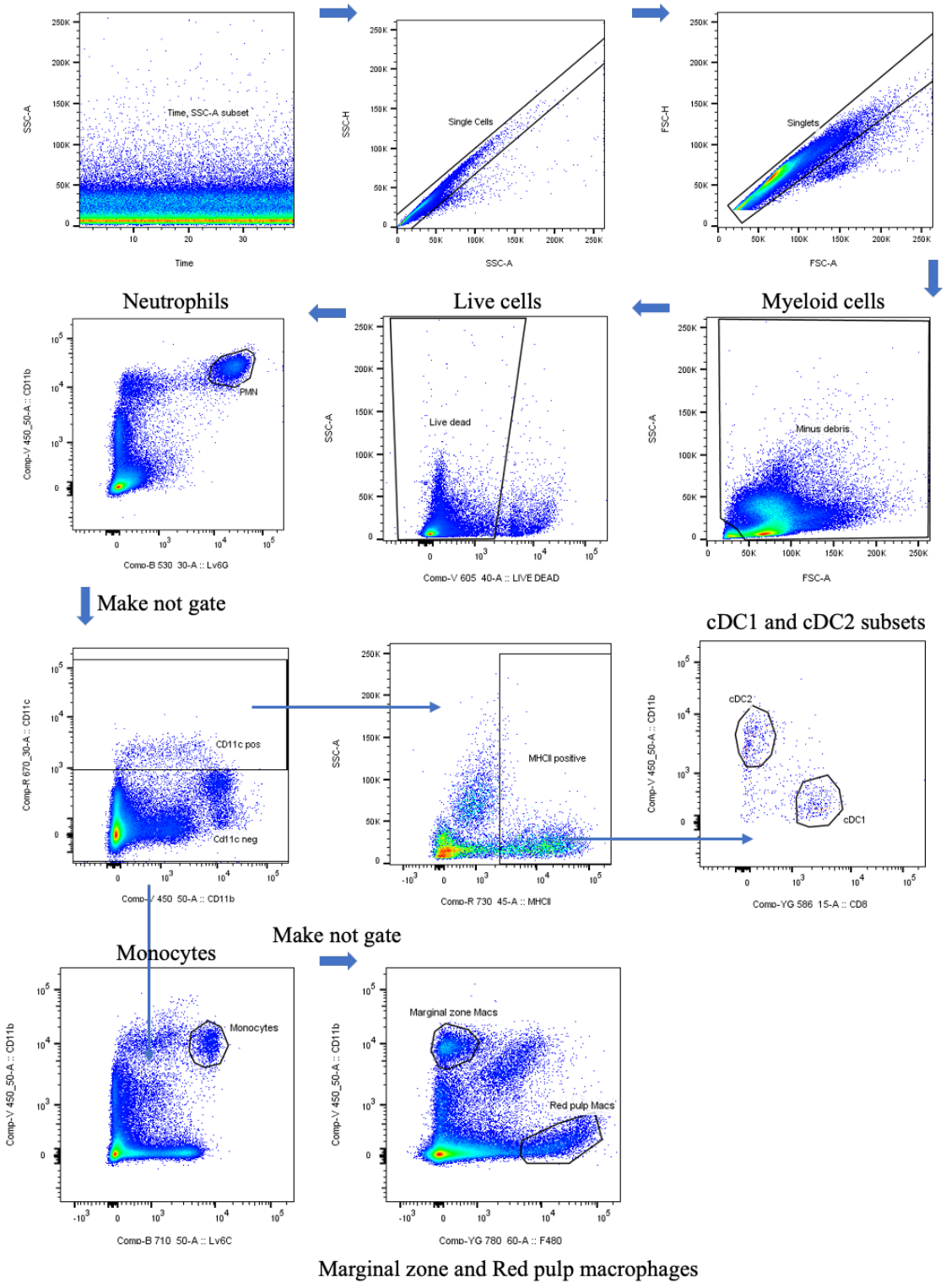

Appendix B: Lung Myeloid Gating strategy

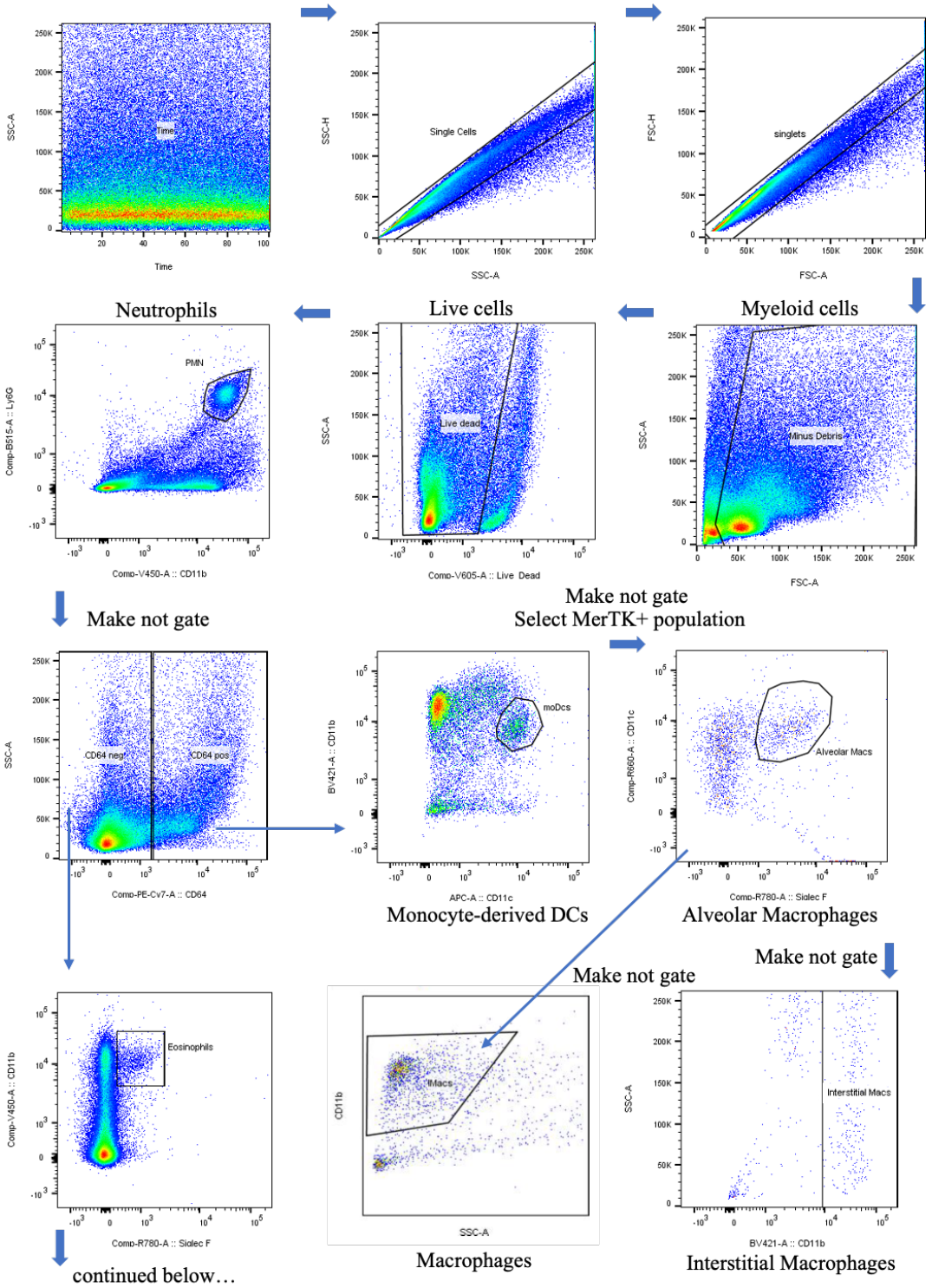

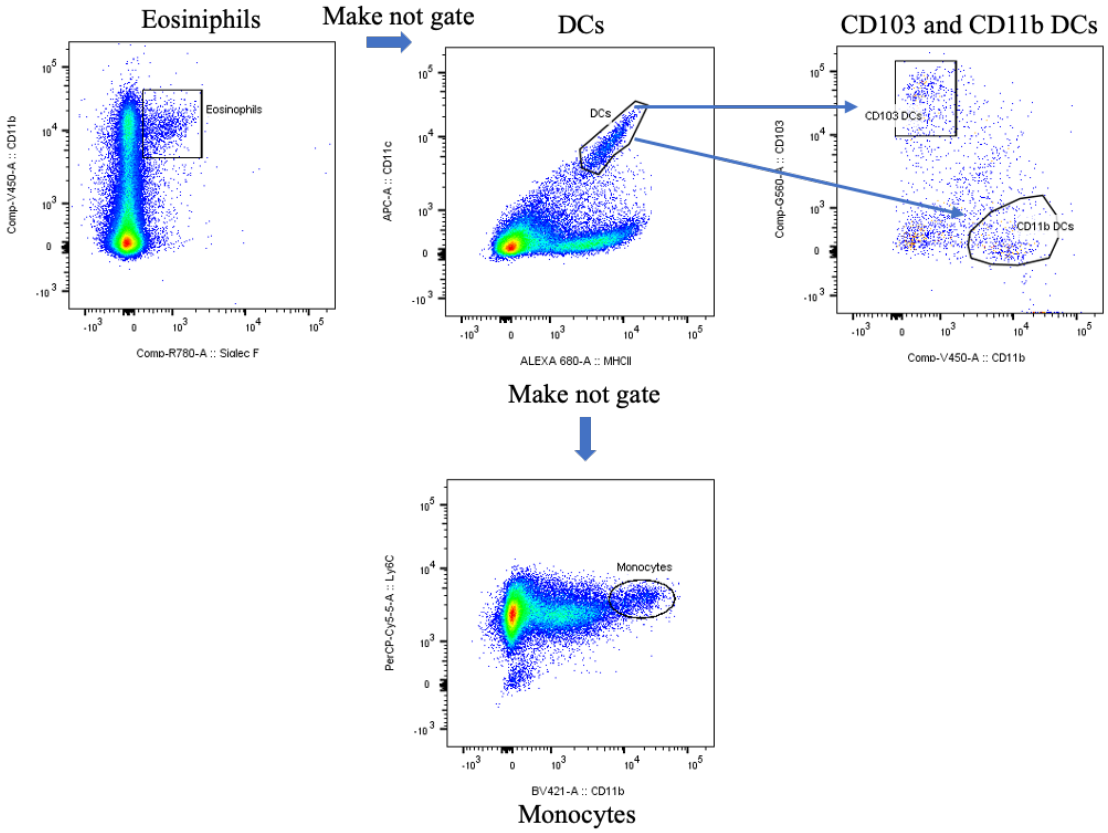
Eosiniphils
Make not gate
DCs
CD103 and CD11b DCs
Eosinophils
Comp-V450-A :: CD11b
Comp-R780-A :: Siglec F
DCs
APC-A :: CD11c
ALEXA 680-A :: MHCII
CD103 DCs
CD11b DCs
Comp-G560-A :: CD103
Comp-V450-A :: CD11b
Make not gate
Monocytes
PerCP-Cy5-5-A :: Ly6C
BV421-A :: CD11b
Monocytes

Appendix C: Lymph Node Myeloid Gating strategy

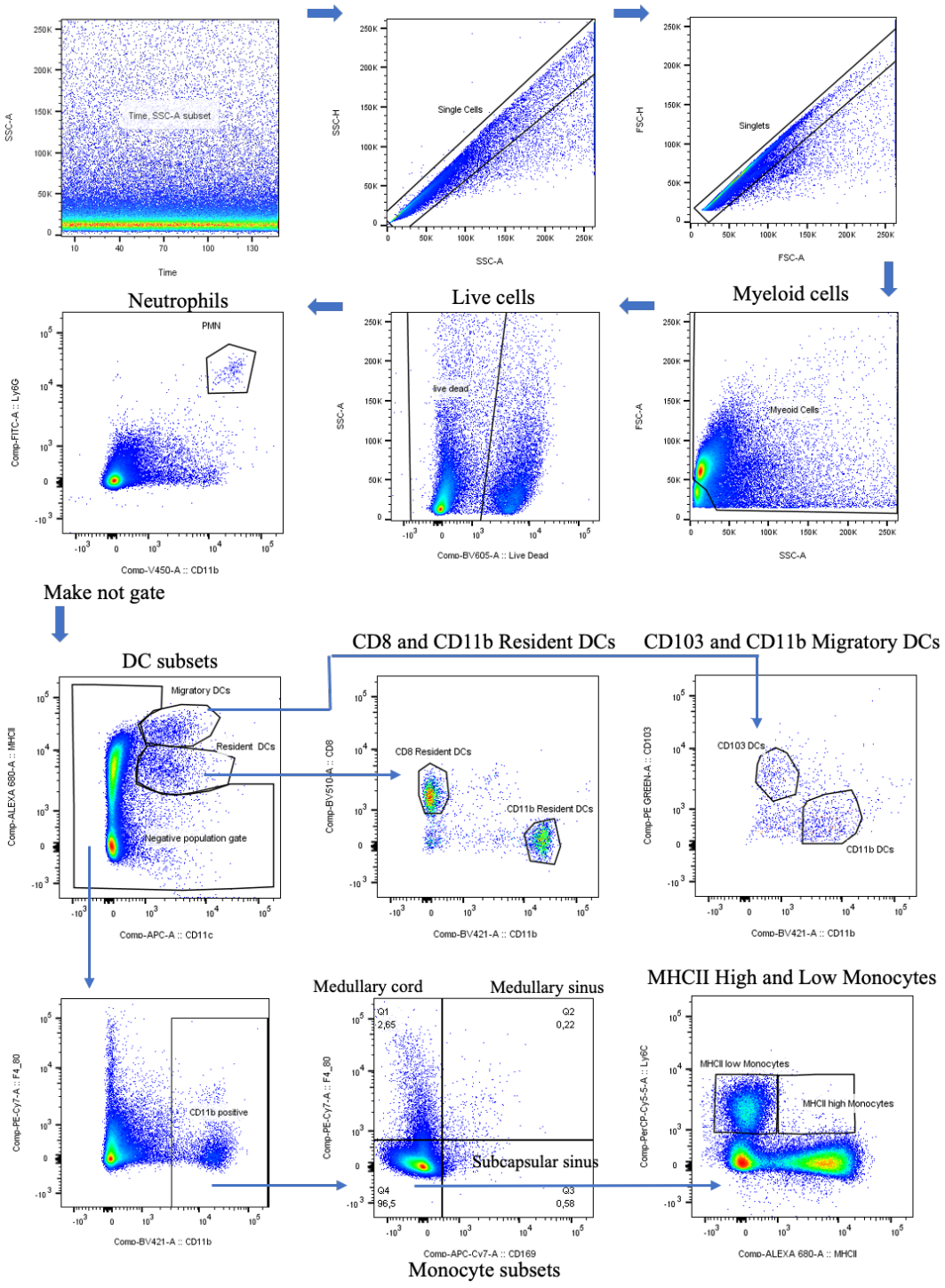

Appendix D: Lung, Lymph Node, Spleen Lymphoid Gating strategy